



“BERNARDINO TELESIO”

School of Science and Technique

PhD Dissertation

Organic Materials of Pharmacological Interest

XXIV cycle (CHIM06)

**MODERN MASS SPECTROMETRIC APPLICATIONS IN
THE STRUCTURE AND FUNCTION EVALUATION OF
ACTIVE PRINCIPLES**

School Director

Prof. Roberto BARTOLINO

Coordinator

Prof. Bartolo GABRIELE

Supervisor

Prof. Giovanni SINDONA

Candidate

Naim MALAJ

Academic Year 2010/2011

To my family

INDEX

List of publications and conference contributes	V
Introduction	1
CHAPTER I	
1 Principles of Liquid Chromatography-Mass Spectrometry Coupling	2
1.1 Introduction	2
1.2 High Performance Liquid Chromatography (HPLC)	3
1.2.1 Chromatographic properties	5
1.3 HPLC Instrumentation	6
1.3.1 Mobile phase reservoirs	7
1.3.2 Pump system	7
1.3.3 Sample injection system	7
1.3.4 The column	8
1.3.5 Detectors	9
1.4 Mass Spectrometry: Principles and Instrumentation	9
1.4.1 Introduction	9
1.4.2 Mass spectrometer components	10
1.4.3 Ion Sources	10
1.4.3.1 Electron Ionization	11
1.4.3.2 Chemical Ionization	13
1.4.3.3 Atmospheric Pressure Chemical Ionization (APCI)	14
1.4.3.4 Electrospray Ionization (ESI)	16
1.4.3.5 Desorption Electrospray Ionization (DESI)	20
1.4.3.6 Direct Analysis in Real Time (DART)	22
1.4.3.7 Matrix-Assisted Laser Desorption Ionization (MALDI)	24

1.5	Mass Analyzers	26
1.5.1	Introduction	26
1.5.2	Linear Quadrupole (Q) Analyzers	30
1.5.3	Ion Trap Analyzers	33
1.5.4	Quadrupole Ion Traps (QIT)	33
1.5.5	Linear Ion Traps (LIT)	34
1.5.6	Time-of-Flight (TOF) Analyzers	35
1.5.6.1	Linear Time-of-Flight Analyzer	37
1.5.6.2	Delayed Pulsed Extraction	38
1.5.6.3	Reflectron Time-of-Flight Analyzers	39
1.5.7	Tandem Mass Spectrometry	41
	References (Chapter I)	44
 CHAPTER II		
2	Recent Ambient Ionization Methods for Mass spectrometry: Paper Spray and Leaf Spray	50
2.1	Introduction	50
2.2	Paper Spray Ionization for Mass Spectrometry (PS-MS)	52
2.3	Leaf Spray Mass Spectrometry (LS-MS)	56
	References (Chapter II)	59
 CHAPTER III		
3	Anticholesterolemic Activity of Brutieridin and Melitidin, Two New Statin-Like Flavonoids Isolated from Bergamot Fruit: Computational and <i>in vivo</i> Approaches	60
3.1	Introduction	60
3.2	Flavonoids: structure, activity and availability	60
3.3	On the Inhibitor Effects of Bergamot Juice Flavonoids Binding to the 3-Hydroxy-3-methylglutaryl-CoA Reductase (HMGR) Enzyme	63
3.4	In vivo anticholesterolemic activity of a bergamot extract enriched with brutieridin and melitidin	69
3.4.1	Introduction	69
3.4.2	Materials and Methods	70

3.4.2.1 Brutieridin/melitidin-enriched bergamot extract	70
3.4.2.2 Animals and diets	70
3.4.2.3 Biochemical estimations	71
3.4.2.4 Statistical analysis	71
3.4.3 Results	71
3.4.3.1 Food intake and body weight gain	71
3.4.3.2 Effects of simvastatin and brutieridin/melitidin-enriched extract on serum and hepatic lipid content	73
3.4.4 Conclusions	74
References (Chapter III)	76
APPENDIX I	79

CHAPTER IV

4 Functional Food from Bergamot Waste Tissues	86
4.1 Introduction	86
4.2 Recycling of industrial essential oil waste: brutieridin and melitidin, two anticholesterolaemic active principles from bergamot albedo	89
4.3 Functional food from bergamot albedo	91
4.4 Isolation of brutieridin and melitidin from bergamot juice by VersaFlash chromatography	94
References (Chapter IV)	97
APPENDIX II	98

CHAPTER V

5 Analysis of Citrus Flavonoids by Paper Spray and Leaf Spray Mass Spectrometry	103
5.1 PS-MS determination of flavonoids from Citrus juices	103
5.1.1 Sample Preparation	104
5.1.2 Instrumentation	104
5.1.3 Results and discussion	105
5.2 Detection of Fraudulent Adulteration of Bergamot Juice	109
5.3 Analysis of Flavonoids from Citrus Albedo by Leaf Spray-Mass Spectrometry	111

5.3.1 Introduction	111
5.3.2 Flavonoids of Citrus albedo by LS-MS	111
References (Chapter V)	114

CHAPTER VI

6 Analysis of Agrochemicals by Leaf Spray Mass Spectrometry	115
6.1 Introduction	115
6.2 Samples	116
6.3 Chemicals	117
6.4 Instrumental conditions	118
6.5 Results and discussion	118
6.6 Conclusions	126
References (Chapter VI)	127

Introduction

The main objective of the present thesis is the evaluation of the biological activity of two new flavonoids, brutieridin and melitidin, isolated from bergamot fruit. The structures of brutieridin and melitidin resemble the active portion of statins, anticholesterolemic drugs widely prescribed in treatment of hypercholesterolemia. Statins bind competitively to the active site of enzyme 3-hydroxy-3-methylglutaryl coenzyme A reductase (HMGR) inhibiting the biosynthesis of cholesterol and consequently lowering its levels in serum. Initially, the ability of brutieridin and melitidin to inhibit the activity of HMGR, in analogy with statins, was examined by a computational approach. Successively, the anticholesterolemic capacity of a bergamot extract enriched with brutieridin and melitidin was tested in hypercholesterolemic rats. In particular, in this latter *in vivo* approach we investigated the effects of this enriched bergamot extract on serum and hepatic total cholesterol, triglycerides, LDL and HDL cholesterol levels. Since rats represent a good model to verify the potential lipid-lowering effects of HMGR inhibitors in preclinical studies, it is expectable that the extract used in this study elicit the same effects in humans.

In other experiments we examined some simple household methods to extract these anticholesterolemic active principles from bergamot albedo. The possibility to extract these active principles using only water as solvent open the door to applications of bergamot albedo for functional food preparations. Therefore, examples of functional foods with anticholesterolemic proprieties prepared from whole or dried bergamot albedo are reported. In addition, we developed a food-compatible chromatographic method to isolate brutieridin and melitidin from bergamot juice which successively may be used for functional food preparations.

Mass spectrometry is a powerful analytical technique with unequalled sensitivity, speed and diversity of its applications. During last two decades, mass spectrometry has progressed rapidly leading to the development of entirely new instruments. The development of new ambient ionization sources represent one of the components of the mass spectrometer with the highest evolution rate. The introduction of new ambient ionization methods made possible to analyze samples directly in their native states, without any sample-preparation. In this context, two recent ambient ionization methods, paper spray and leaf spray, were introduced and applied for direct ambient analysis. The first one was applied for the determination of flavonoids in Citrus juices whereas the latter one was used for fast determination of pesticides in fruit and vegetable tissues.

CHAPTER I

1 Principles of Liquid Chromatography-Mass Spectrometry Coupling

1.1 Introduction

In many analyses, the compound(s) of interest are found as part of a complex mixture and the role of the chromatographic technique is to provide separation of the components of that mixture to allow their identification or quantitative determination. From a qualitative perspective, the main limitation of chromatography in isolation is its inability to provide an unequivocal identification of the components of a mixture even if they can be completely separated from each other. In chromatography, the identification is based on the comparison of the retention characteristics, simplistically the retention time, of an unknown with those of reference materials determined under identical experimental conditions. There are, however, so many compounds in existence that even if the retention characteristics of an unknown and a reference material are, within the limits of experimental error, identical, the analyst cannot say with absolute certainty that the two compounds are the same. Despite a range of chromatographic conditions being available to the analyst, it is not always possible to effect complete separation of all of the components of a mixture and this may prevent the precise and accurate quantitative determination of the analyte(s) of interest.

The role of mass spectrometry lies in the fact that the mass spectra of many compounds are sufficiently specific to allow their identification with a high degree of confidence, if not with complete certainty. If the analyte of interest is encountered as part of a mixture, however, the mass spectrum obtained will contain ions from all of the compounds present and, particularly if the analyte of interest is a minor component of that mixture, identification with any degree of certainty is made much more difficult, if not impossible. Therefore, the combination of the separation capability of chromatography to allow separated (pure) compounds to be introduced into the mass spectrometer with the identification capability of the mass spectrometer is clearly an enormous advantage. The direct coupling of the two techniques is advantageous in many other respects, including the speed of analysis, the convenience, particularly for

the analysis of multi-component mixtures, the reduced possibility of sample loss, the ability to carry out accurate quantitation using isotopically labelled internal standards.

The combination of chromatography and mass spectrometry (MS) is one of the most interesting subjects in the field of analytical chemistry. The coupling of liquid chromatography (LC) to mass spectrometry has not been as simple as for gas chromatography-mass spectrometry (GC-MS), due to the incompatibilities of operation between LC and MS. In fact, in LC the mobile phase is a liquid (often containing significant proportion of water) that is pumped at a high flow rate (typically 1 ml min^{-1}) while the mass spectrometer operates at a very low pressure (10^{-7} - 10^{-5} torr). It was therefore not possible simply to pump the eluate from an HPLC column directly into the source of a mass spectrometer. In order to realize the LC-MS coupling, alternative ionization methods capable to remove the mobile phase and generate gas phase ions, had to be developed. This issue was resolved with the development of interfaces like thermospray (TSP), electrospray (ESI), atmosphere pressure chemical ionization (APCI) etc., that allows the ion generation and solvent evaporation of separated analytes coming from liquid chromatography. Liquid chromatography normally is used for compounds that are not volatile and are not suitable for gas chromatography.

In the following chapter the basic principles of HPLC and MS, as far as they relate to the LC-MS combination, will be discussed. Particular attention will be paid to electrospray and atmospheric pressure chemical ionization interfaces as these are the ones most widely used today, but other older and more recent ionization methods will be described too. The characteristics of common analyzers and the use of MS and tandem mass spectrometry (MS/MS) for identification and quantitation will be described. It should be mentioned that to give a detailed (and the deserved) description of these two techniques, each would require a whole book.

1.2 High Performance Liquid Chromatography (HPLC)

High performance liquid chromatography (HPLC) is the most versatile chromatographic technique that allows the separation, identification, and determination of the chemical components in complex mixtures. The technique is used to separate and determine species in a variety of organic, inorganic, and biological matrixes and, hence, it is used in different disciplines: food, pharmaceutical, environmental, biomedical etc. The separation process is based on the different migration of the components of mixture due to their different affinities for the mobile and the stationary phase. The nature of the stationary and the mobile phases, together with the mode of the transport through the column, is the basis for the classification of chromatographic methods. Therefore, the

types of high-performance liquid chromatography are often classified by separation mechanism or by the polarity of stationary and mobile phases. Based on the stationary and mobile phase polarities, two principal HPLC separation ways are generally distinguished: a) normal phase chromatography and b) reversed phase chromatography. Early work in liquid chromatography was based on highly polar stationary phases and a relatively nonpolar solvent. For historic reasons, this type of chromatography is now called normal-phase chromatography. Normal-phase chromatography can be used for compounds that are too hydrophobic or that are not soluble in water and polar solvents. In normal-phase HPLC, the stationary phase is more polar than the mobile phase. There are a number of stationary phases available for normal-phase chromatography. Silica is the most common of the non-bonded phases and can provide very high selectivity for many applications, but water adsorption by the silica can make reproducible retention times difficult. There are two major types of silica in use. Older less pure silica (type A) have some trace metal content and have highly acidic sites on the surface. Newer type B silica columns are made of high purity silica and have fewer acidic sites and are recommended for separating highly polar or basic compounds. The mobile phase, in normal phase HPLC, consists in a non polar solvent or a binary mixture of solvents (usually hexane, ethyl ether, methyl t-butyl ether, chloroform etc.).

In reversed-phase chromatography, the stationary phase is less polar than the mobile phase (commonly are used solvents such as water, methanol, acetonitrile, or tetrahydrofuran). It has been estimated that more than three quarters of all HPLC separations are currently performed with reversed-phase chromatography [1]. The most widely used columns contain a chemically modified silica stationary phase, with the chemical modification determining the polarity of the column [2]. A very popular reversed-phase stationary phase is one in which a C18 (often C8) alkyl group is bonded to the silica surface. Commercial columns of the same general type (e.g., C18) could differ widely in their separation power among different suppliers. Basic information regarding the specific column provided by the manufacturer, such as surface area, % carbon, and type of bonded phase, usually does not allow prediction of the separation or for the proper selection of columns with similar separation patterns.

The following characteristics could be used for column selection: i) type (monolithic; porous; nonporous); ii) geometry (surface area; pore volume; pore diameter; particle size and shape; etc.); iii) surface chemistry (type of bonded phase; bonding density etc.); iv) type of packing material (silica; polymeric; zirconia; etc). All these characteristics are interrelated. Variations of porosity which include pore diameter can affect both the adsorbent surface area and the bonding density. The type of packing material affects adsorbent surface chemistry. Most geometry-related properties of packing materials are related to the column efficiency and flow resistance: particle size, particle shape,

particle size distribution, packing density, and packing uniformity. Base material with smaller pores has higher surface area. Surface chemistry related properties are mainly responsible for the analyte retention and separation selectivity. However, the quality of an HPLC column is a subjective factor, which is dependent on the types of analytes and even on the chromatographic conditions used for the evaluation of the overall process.

1.2.1 Chromatographic properties

In carrying out a chromatographic separation, an analyst is concerned with whether the components of a mixture can be separated sufficiently for the analytes of interest. The ability to separate successfully the components of a mixture will depend on the performance of the chromatographic system as a whole. The performance may be described in terms of a number of theoretical parameters, although the performance required for a particular analysis will depend on the separation that is required.

The time taken for an analyte to elute from a chromatographic column with a particular mobile phase is termed its retention time, t_{an} . Since this will vary with column length and mobile phase flow rate, it is more useful to use the capacity factor, k' . This relates the retention time of an analyte to the time taken by an unretained compound, i.e. one which passes through the column without interacting with the stationary phase, to elute from the column under identical conditions (t_0). This is represented mathematically by the following equation:

$$k' = \frac{t_{an} - t_0}{t_0}$$

To give adequate resolution in a reasonable analysis time, k' values of between 1 and 10 are desirable.

The separation of two components, e.g. A and B, is termed the selectivity or separation factor (α) and is the ratio of their capacity factors (by convention, $t_B > t_A$ and $\alpha \geq 1$), as shown by the following equation:

$$\alpha = \frac{k'_B}{k'_A} = \frac{t_B - t_0}{t_A - t_0}$$

The separation of two components is of particular importance when one is being determined in the presence of the other and this is defined as the resolution (R), given as follows:

$$R = \frac{t_B - t_A}{0,5(\omega_A + \omega_B)}$$

where w_A and w_B are the peak widths of the detector responses from the two components. These parameters are represented graphically in figure 1.1.

The column performance (efficiency) is measured either in terms of the plate height (H), the efficiency of the column per unit length (L), or the plate number (N), i.e. the number of plates for the column. The mathematical relationships between the number of plates, the retention time of the analyte and the width of the response is shown in the following equations:

$$H = \frac{L}{N} \quad N = 16 \left(\frac{t_A}{w_{0.5}} \right)^2 = 5,54 \left(\frac{t_A}{w} \right)^2$$

The value of N is an indicator of the performance of a chromatographic column, and in general, higher its value is, better will be the column performance.

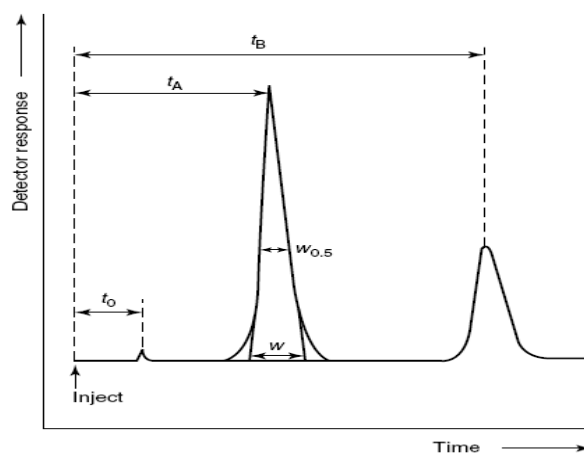
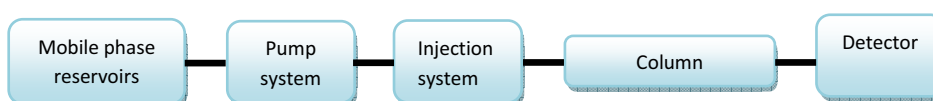


Figure 1.1. Illustration of HPLC parameters: t_0 , retention time of a non-retained component; t_A and t_B , retention times of analytes A and B; w , width of peak at base; $w_{0.5}$, width at half-height [2].

1.3 HPLC Instrumentation

The basic components of an HPLC system include:

- Mobile phase reservoir
- pump
- sample injection
- column
- detector



These components are discussed briefly in the following sections.

13.1 Mobile phase reservoirs

A common HPLC apparatus is equipped with one or more glass reservoirs (> 500 mL of) which contains the solvent used to carry the sample through the system. Provisions are often included to remove dissolved gases and dust from the liquids. The former produce bubbles in the column and thereby cause band spreading; in addition, both bubbles and dust interfere with the performance of most detectors. Degassers may consist of a vacuum pumping system, a distillation system, a device for heating and stirring, or a system for sparging in which the dissolved gases are swept out of solution by fine bubbles of an inert gas that is not soluble in the mobile phase. An elution with a single solvent or a solvent mixture of constant composition is called isocratic elution. In gradient elution, two (and sometimes more) solvents that differ significantly in polarity are used. The ratio of the two solvents is varied in a preprogrammed way during the separation, sometimes continuously and sometimes in a series of steps. Modern HPLC instruments are usually equipped with proportioning valves that introduce liquids from two or more reservoirs at ratios that can be varied continuously.

1.3.2 Pump system

The role of pump(s) is to provide a constant flow of the mobile phase through the system. Most modern pumps allow controlled mixing of different solvents from different reservoirs. The requirements for liquid chromatographic pumps include (1) ability to generate pressures of up to 6000 psi, (2) pulse-free output, (3) flow rates ranging from 0.1 to 10 mL/min, (4) flow reproducibilities of 0.5% relative or better, and (5) resistance to corrosion by a variety of solvents. There are three major types of pumps: the screw-driven syringe type, the reciprocating pump, and the pneumatic or constant-pressure pump. The most widely used types of pumps are the reciprocating pumps. These devices consists of a small cylindrical chamber that is filled and then emptied by the back-and-forth motion of a piston. The pumping motion produces a pulsed flow that must be subsequently damped. Advantages of reciprocating pumps include small internal volume, high output pressure (up to 10,000 psi), ready adaptability to gradient elution, and constant flow rates, which are largely independent of column back-pressure and solvent viscosity.

1.3.3 Sample injection system

A convenient way of introducing a liquid sample into a flowing liquid stream consists of a loop injector (sometimes known as the valve injector) of a nominal volume into which sample is introduced by using a conventional syringe. While the loop is

being filled, mobile phase is pumped, at the desired flow rate, through the valve to the column to keep the column in equilibrium with the mobile phase and maintain chromatographic performance. When injection is required, a rotating switch is moved and the flow is diverted through the loop, thus flushing its contents onto the top of the column. Usually, interchangeable loops are available to provide a choice of sample volumes ranging from 5 to 500 μL . From a quantitative perspective, the way in which the injector functions is crucial to the precision and accuracy which may be obtained. It is usual to fill the loop completely by having a greater volume in the conventional syringe than the loop capacity (excess goes to waste) and it is important to ensure, as much as is possible, that air bubbles are not introduced in place of the sample. New generation HPLC instruments incorporate an autosampler with an automatic injector which can inject continuously variable volumes.

1.3.4 The column

The column is the heart of the HPLC system, the place where the separation of the components of the mixture is realized. Liquid chromatographic columns are usually constructed from stainless steel tubing, although glass or Tygon tubing is sometimes employed for lower pressure applications. Most analytical columns range in length from 5 to 30 cm and have inner diameters of 2 to 5 mm. Column packings typically have particle sizes of 3 to 10 μm . Columns of this type provide 40,000 to 60,000 plates/m. Recently, micro-columns have become available with inside diameters of 1 to 4.6 mm and lengths of 3 to 7.5 cm. These columns, which are packed with 2- 5 μm particles, contain as many as 100,000 plates/m and have the advantage of speed and minimal solvent consumption. This latter property is of considerable importance because the high-purity solvents required for liquid chromatography are expensive to purchase and to dispose of after use. The most common packing for liquid chromatography is prepared from silica particles, which are synthesized by agglomerating submicron silica particles under conditions that lead to larger particles with highly uniform diameters. The resulting particles are often coated with thin organic films, which are chemically or physically bonded to the surface. Other packing materials include alumina particles, porous polymer particles, and ion-exchange resins.

Guard Columns: often, a short guard column is positioned ahead of the analytical column to increase the life of the analytical column by removing particulate matter and contaminants from the injection of crude samples. The composition of the guard-column packing should be similar to that of the analytical column; larger particle size are usually employed to minimize the pressure drop.

1.3.5 Detectors

There are no highly sensitive universal detectors available for all high-performance liquid chromatography applications. Therefore, the detector used will depend on the nature of the sample to be analyzed. The most widely used detectors are based on absorption of ultraviolet or visible radiation. Both photometers and spectrophotometers specifically designed for use with chromatographic columns are available from commercial sources. The former often make use of the 254- and 280-nm lines from a mercury source because many organic functional groups absorb in the region. Deuterium sources or tungsten-filament sources with interference filters also provide a simple means of detecting absorbing species. Some modern instruments are equipped with filter wheels that contain several interference filters, which can be rapidly switched into place. Spectrophotometric detectors are considerably more versatile than photometers and are also widely used in high-performance instruments. Modern instruments use diode-array detectors that can display an entire spectrum as an analyte exits the column. Another detector, which has found considerable application, is based on the changes in the refractive index of the solvent that is caused by analyte molecules. Several electrochemical detectors that are based on potentiometric, conductometric, and voltammetric measurements have also been introduced.

1.4 MASS SPECTROMETRY: Principles and Instrumentation

1.4.1 Introduction

Mass spectrometry is a powerful analytical technique which has both qualitative and quantitative capabilities. The basic principle of mass spectrometry (MS) is to generate ions by any suitable method, to separate these ions by their mass-to-charge ratio (m/z) and to detect them qualitatively and quantitatively by their respective m/z and abundance. The response is a mass spectrum, a two-dimensional representation of signal intensity (ordinate) versus m/z (abscissa). The intensity of a peak, as signals are usually called, directly reflects the abundance of ionic species of that respective m/z ratio which have been created from the analyte within the ion source. The most intense peak of a mass spectrum is called base peak.

Mass spectrometry's characteristics have raised it to an outstanding position among analytical methods: unequalled sensitivity, speed and diversity of its applications. In analytical chemistry, the most recent applications are mostly oriented

towards biochemical problems, such as proteome, metabolome, high throughput in drug discovery and metabolism, and so on. Other analytical applications are routinely applied in pollution control, food control, forensic science, natural products or process monitoring. Other applications include atomic physics, reaction physics, reaction kinetics, geochronology, inorganic chemical analysis, ion–molecule reactions, determination of thermodynamic parameters etc. Mass spectrometry has progressed extremely rapidly during the last two decades. This progress has led to the advent of entirely new instruments. New atmospheric pressure sources were developed, existing analyzers were perfected and new hybrid instruments were realized by new combinations of analyzers leading to the development of new applications.

1.4.2 Mass spectrometer components

All mass spectrometers consists of three principal parts: the ion source, the mass analyzer, and the detector (figure 1.2). Since the mass analyzer and the detector (and some of the ion sources) require low pressure for operation, the instrument also needs a pumping system. Moreover, another system is required to record the signal registered by the detector, a computer (in all modern instruments a computer-based system is used). Although the role of the pumping system and computers are crucial for instrumental conditions (pumps) and data collection/processing (computers), they will not be included in the following discussion because of the lack of important chemical information.

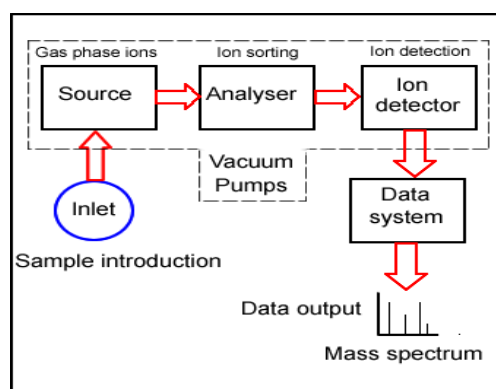


Figure 1.2. Principal building components of all mass spectrometers [3].

1.4.3 ION SOURCES

The role of the ion source in a mass spectrometer is to generate gas phase ions. Analyte atoms, molecules, or clusters are transferred into gas phase and ionized either concurrently or through separate processes. Ions are mainly produced by ionizing a

neutral molecule through electron ejection, electron capture, protonation, deprotonation, adduct formation or by the transfer of a charged species from a condensed phase to the gas phase.

The most important considerations are the internal energy transferred during the ionization process and the physico-chemical properties of the analyte that is ionized. Some ionization techniques are very energetic and cause extensive fragmentation. Other techniques are softer and only produce ions of the molecular species. Electron ionization, chemical ionization and field ionization are only suitable for gas-phase ionization and thus their use is limited to compounds sufficiently volatile and thermally stable. However, a large number of compounds are thermally labile or do not have sufficient vapor pressure. Molecules of these compounds must be directly extracted from the condensed to the gas phase. These direct ion sources exist under two types: liquid-phase ion sources and solid-state ion sources. In liquid-phase ion sources the analyte is in solution. This solution is introduced, by nebulization, as droplets into the source where ions are produced at atmospheric pressure and focused into the mass spectrometer through some vacuum pumping stages. Electrospray (ESI), atmospheric pressure chemical ionization (APCI) and atmospheric pressure photoionization (APPI) sources correspond to this type. In solid-state ion sources, the analyte is in an involatile deposit. It is obtained by various preparation methods which frequently involve the introduction of a matrix that can be either a solid or a viscous fluid. This deposit is then irradiated by energetic particles or photons that desorb ions near the surface of the deposit. These ions can be extracted by an electric field and focused towards the analyzer. Matrix-assisted laser desorption, secondary ion mass spectrometry, plasma desorption and field desorption sources all use this strategy to produce ions.

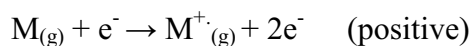
Recently, new ambient ionization methods which allow the analysis of samples in their native state without any previous preparation, have been introduced (DESI, DART, LTP, etc.).

The number of available ion sources is quite large and a concise description of all of them is out of the scope of the present thesis, so in the following sections will be given a brief description of the currently most utilized ionization methods.

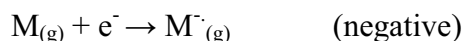
1.4.3.1 Electron Ionization

Electron ionization (EI) was introduced in 1921 by Dempster, who used it to measure lithium and magnesium isotopes [4]. Modern EI sources are, however, based on the design by Bleakney [5] and Nier [6,7]. In EI ionization method, ions are produced by directing an electron beam into a vapor of analyte, at a very low pressure

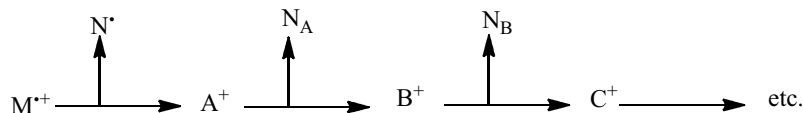
(in the range 10^{-7} – 10^{-5} Torr). A schematic diagram of EI is reported in figure 1.3. Gas phase analytes are introduced directly into the source. The electron beam is created by heating a filament, and the beam is directed through the source and afterwards collected in a trap. Magnets provide for a spiral motion of the electrons so that the path is increased and thus the chance for electron–molecule interactions. Because the electron mass is significantly smaller than any ion mass the latter will not be affected by the magnetic field strength required. The interaction of a highly energetic (70 eV) electron beam with the sample vapor leads to the production of a series of ions related to the chemical properties of the compound(s) under investigation. Upon electron-molecule interaction, one (occasionally more) electron is removed from the analyte creating typically positive radical molecular ions. If the analyte has high electron affinity negative ions can be formed through electron attachment, although this process is not favorable and the utility of negative ion mode is limited:



or



At 70 eV, in a high vacuum, the interaction between electrons and molecules leaves some ions with so much extra internal energy that may be used for further break up (fragmentation) to give ions of smaller mass:



Generally EI leads to a very low intensity molecular ion (often absent and to a series of fragments, generally highly diagnostic from the structural point of view. Some of the fragments (A^{+} , B^{+} , C^{+}) originate from simple bond cleavages, while some others are produced through rearrangement processes. One of the major limitations of EI is that the excess energy imparted to the analyte during electron-analyte interaction may bring about such rapid fragmentation that the molecular ion is not observed in the mass spectrum, making this ionization method not very useful for detection of the molecular ion. This excessive fragmentation can be at some extent reduced by lowering the electron energy, but this may affect and reduce the ionization efficiency, sometimes severely.

What must be emphasized is that EI leads to well reproducible mass spectra. In other words, by different EI sources are obtained practically superimposable spectra (instrument independent) and this is the reason for which many spectrum databases available are based on EI data.

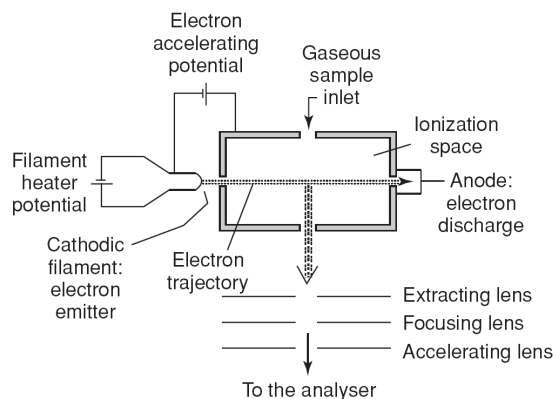
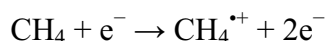


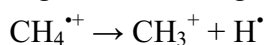
Figure 1.3. Diagram of an electron ionization (EI) source [8].

1.4.3.2 Chemical Ionization

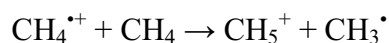
In the previous paragraph we saw that electron ionization (EI) leads to excessive fragmentation of the molecular ion, which sometimes prevents its detection. Chemical ionization (CI), on the other hand, is a technique that produces ions with little excess energy. Thus this technique presents the advantage of yielding a spectrum with less fragmentation in which the molecular species are easily recognized. Chemical ionization (CI) was introduced by Munson and Field in 1966 by allowing a reagent gas into an EI source [9-11]. The pressure is typically 1 torr and the electron beam is more energetic than in EI, typically 500 to 1000 eV. While in EI the analyte is directly ionized by the electron beam, CI is a two-step process, where first reagent gas molecules are ionized by the electron beam and thereafter the reagent gas ions transfer charge to the analyte. Both positive and negative ions of the substance to be analysed will be formed by chemical reactions with ions in this plasma. This causes proton transfer reactions, hydride abstractions, adduct formations, charge transfers, and so on. Originally CI was employed for positive ion analysis, before negative ion analysis was introduced by Hunt et al. in 1976 [12]. The reaction gas is of a type that is nonreactive with itself, but is highly reactive with the sample molecules (methane, isobutane and ammonia are the most used). Initially methane was used to produce stable reagent ions, which in turn react with the analyte forming different types of molecular or fragment ions. The primary reaction with the electrons will be a classical EI reaction:



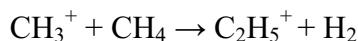
This ion will fragment, mainly through the following reactions:



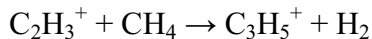
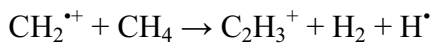
Then it will collide and react with other methane molecules yielding:



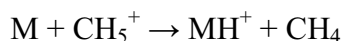
Other ion–molecule reactions with methane will occur:



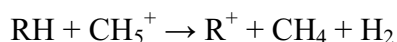
A C_3H_5^+ ion is formed by the following successive reactions:



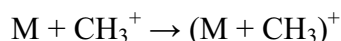
The relative abundance of all these ions will depend on the pressure. Taking CH_5^+ , the most abundant ion, as a reference (100 %), C_2H_5^+ abundance hit the 83% and C_3H_5^+ that of 14 %. Unless it is a saturated hydrocarbon, the sample will mostly react by acquiring a proton in an acid–base type reaction with one of the plasma ions, for example:



A systematic study showed that the main ionizing reactions of molecules containing heteroatoms occurred through acid–base reactions with C_2H_5^+ and C_3H_5^+ . If, however, the sample is a saturated hydrocarbon RH, the ionization reaction will be a hydride abstraction:



Moreover, ion–molecule adduct formation is observed in the case of polar molecules, a type of gas-phase solvation, for example



The ions $(\text{MH})^+$, R^+ and $(\text{M} + \text{CH}_3)^+$ and other adducts of ions with the molecule are termed molecular species or, pseudomolecular ions, and allow the determination of the molecular mass of the molecules in the sample.

The choice of reaction gas depends on application (and ion analysis mode). The advantage of CI over EI is that it is softer so intact molecular ions are easier to obtain. Although most analytes can form positive ions, negative ion formation is selective and can be very efficient, providing very high sensitivity. A disadvantage of CI compared to EI is that the ion source requires cleaning more often.

1.4.3.3 Atmospheric Pressure Chemical Ionization (APCI)

Atmospheric pressure chemical ionization (APCI) was introduced in 1973 by Horning et al. [13-14] and coupled to GC. A year after, corona discharge was introduced for ion generation as well as successful coupling to LC [15-16]. APCI is an ionization technique which uses gas-phase ion–molecule reactions at atmospheric pressure. It is a method analogous to CI where primary ions are produced by corona discharges on a solvent spray. APCI is mainly applied to polar and relatively non-polar compounds with moderate molecular weight up to about 1500 Da and gives generally

mono-charged ions. The principle governing an APCI source is shown in figure 1.4. The analyte in solution from a direct inlet probe or a liquid chromatography eluate at a flow rate between 0.2 and 2 ml min^{-1} , is directly introduced into a pneumatic nebulizer where it is converted into a thin fog by a high-speed nitrogen beam. Droplets are then displaced by the gas flow through a heated quartz tube called a desolvation/vaporization chamber. The heat transferred to the spray droplets allows the vaporization of the mobile phase and of the sample in the gas flow. The temperature of this chamber is controlled, which makes the vaporization conditions independent of the flow and from the nature of the mobile phase. The hot gas (120°C) and the compounds leave this tube. After desolvation, they are carried along a corona discharge electrode where ionization occurs. The ionization processes in APCI are equivalent to the processes that take place in CI but all of these occur under atmospheric pressure. In the positive ion mode, either proton transfer or adduction of reactant gas ions can occur to produce the ions of molecular species, depending on the relative proton affinities of the reactant ions and the gaseous analyte molecules. In the negative mode, the ions of the molecular species are produced by either proton abstraction or adduct formation.

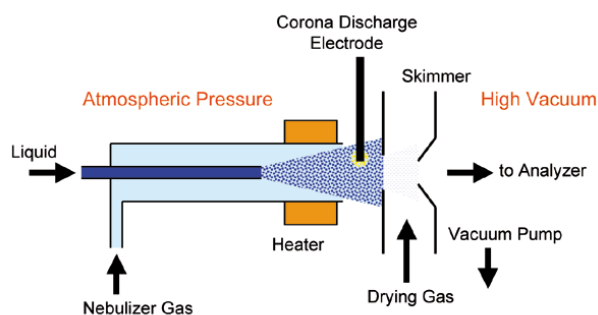


Figure 1.4. Diagram of an APCI source [17].

Generally, the evaporated mobile phase acts as the ionizing gas and reactant ions are produced from the effect of a corona discharge on the nebulized solvent. Typically, the corona discharge forms by electron ionization primary ions such as N_2^{*+} or O_2^{*+} . Then, these ions collide with vaporized solvent molecules to form secondary reactant gas ions. The electrons needed for the primary ionization are not produced by a heated filament, as the pressure in that part of the interface is atmospheric pressure and the filament would burn, but rather using corona discharges or β^- particle emitters. These two electron sources are fairly insensitive to the presence of corrosive or oxidizing gases. As the ionization of the substrate occurs at atmospheric pressure and thus with a high collision frequency, it is very efficient. In the same way, the rapid desolvation and vaporization of the droplets reduce considerably the thermal decomposition of the analyte. The result is production predominantly of ions of the molecular species with

few fragmentations. The ions produced at atmospheric pressure enter the mass spectrometer through a tiny inlet, or through a heated capillary, and are then focused towards the analyser. This inlet must be sufficiently wide to allow the entry of as many ions as possible while keeping a correct vacuum within the instrument so as to allow the analysis. The most common solution to all these constraints consists of using the differential pumping technique on one or several stages, each one separated from the others by skimmers. In the intermediate-pressure region, an effective declustering of the formed ions occurs. APCI has become a popular ionization source for applications of coupled HPLC–MS.

1.4.3.4 Electrospray Ionization

Electrospray ionization (ESI) was first introduced by Dole and coworkers in 1968 [18] and developed and coupled to MS in 1984 by Fenn et al. [19]. ESI is a soft ionization technique that accomplishes the transfer of ions from solution to the gas phase. The generation of ions from the condensed phase into the state of an isolated gas phase ion starts at atmospheric pressure and leads continuously into the high vacuum of the mass analyzer. Another reason for the extraordinary high-mass capability of ESI is found in the characteristic formation of multiply charged ions in case of high-mass analytes. Multiple charging folds up the m/z scale by the number of charges and thus compresses the ions into the m/z range of standard mass analyzers. Nowadays, ESI is the leading member of the group of atmospheric pressure ionization (API) methods and the method of choice for liquid chromatography mass spectrometry coupling (LC-MS). Currently, ESI and MALDI are the most commonly employed ionization methods and they opened doors to the widespread biological and biomedical application of mass spectrometry [20-24].

The electrospray in ESI source is produced by applying a strong electric field, under atmospheric pressure, to a liquid passing through a capillary tube with a weak flux (normally $1\text{--}20\ \mu\text{L}\ \text{min}^{-1}$) [19, 25-27]. The electric field is obtained by applying a difference of potential of $1\text{--}6\ \text{kV}$ between this capillary and the counter-electrode, separated by $0.3\text{--}2\ \text{cm}$, producing electric fields of the order of $10^6\ \text{Vm}^{-1}$ (figure 1.5). This field induces a charge accumulation at the liquid surface located at the end of the capillary, which will break to form highly charged droplets. A gas injected coaxially at a low flow rate allows the dispersion of the spray to be limited in space. These droplets then pass either through a curtain of heated inert gas, most often nitrogen, or through a heated capillary to remove the last solvent molecules.

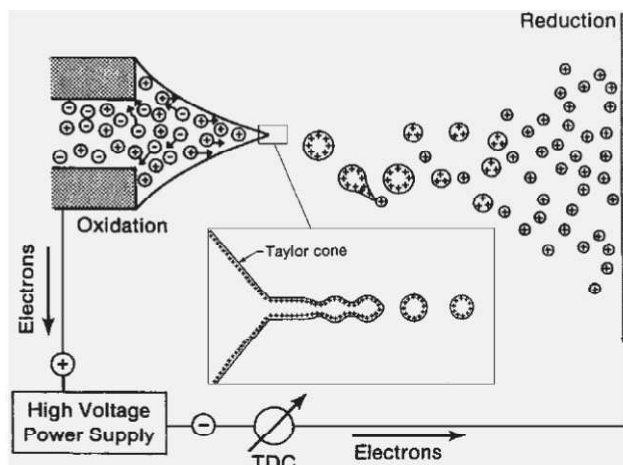


Figure 1.5. Schematic of Taylor cone formation, ejection of a jet, and its disintegration into a fine spray [27].

Mechanism of electrospray generation: The ion formation in ESI can be considered as a three steps process: a) generation of an electrically charged spray; b) solvent evaporation and consequent reduction of the droplets' size; and c) fully desolvated ion formation. To understand the formation of a continuous spray, consider the surface of an ion-containing liquid at the end of an electrically conducting capillary of about 75 μm inner diameter which is held at an electric potential of 3–4 kV with reference to a counter electrode at 1–2 cm distance. At the open end of the capillary (capillary tip) this liquid is exposed to an electric field of about 10^6 V m^{-1} . The electric field causes charge separation in the liquid and finally deformation of the meniscus into a Taylor cone (Taylor for the first time described theoretically this cone formation) [28]. When the critical electric field strength is reached, the Taylor cone instantaneously forms and immediately starts ejecting a fine jet of liquid from its apex towards the counter electrode [29]. The jet carries a large excess of ions of one particular charge sign, because it emerges from the point of highest charge density, i.e., from the cone's tip. However, such a jet cannot remain stable for an elongated period, but breaks up into small droplets. Due to their charge, these droplets are driven away from each other by Coulombic repulsion. Overall, this process causes the generation of a fine spray, and thus gave rise to the term electrospray (figure 1.5).

When a micrometer-sized droplet carrying a large excess of ions of one particular charge sign evaporates some solvent, the charge density on its surface is continuously increased. As soon as electrostatic repulsion exceeds the conservative force of surface tension, disintegration of the droplet into smaller sub-units will occur. The point at which this occurs is known as Rayleigh limit. Originally, it has been assumed that the droplets would then suffer a “Coulomb explosion” repeatedly to generate smaller and smaller microdroplets. While the model of a cascading reduction in size is still valid,

more recent work has demonstrated that the microdroplets do not explode, but eject a series of much smaller microdroplets from an elongated end (figure 1.6) [27, 30, 31]. The ejection from an elongated end can be explained by deformation of the flying microdroplets which have no perfect spherical shape. Thus, the charge density on their surface is not homogeneous, but significantly increased in the region of sharper curvature. The smaller offspring droplets carry off only about 1–2 % of the mass, but 10–18 % of the charge of the parent droplet. This process resembles the initial ejection of a jet from the Taylor cone. The concept of this so-called “droplet jet fission” is not only based on theoretical considerations but was proven by flash microphotographs [31, 32]. The total series of events from the initially sprayed droplet to the isolated ion takes less than one millisecond.

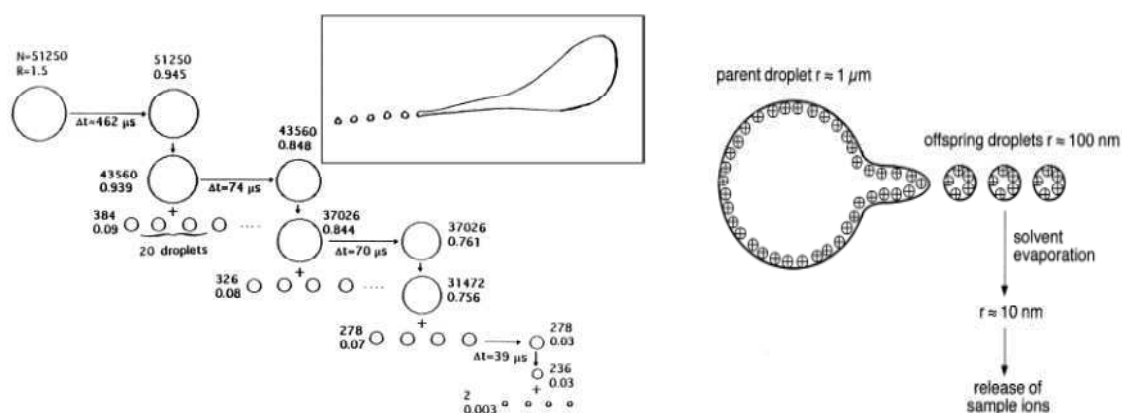


Figure 1.6. Illustration of droplet jet fission. The average number of charges on a droplet, the radii of the droplets (μm), and the timescale of events are assigned. The inset shows a drawing of droplet jet fission based on an actual flash microphotograph [27].

In the past, a couple of other models which describe the electrospray formation were reported. A detailed explanation of these models goes beyond the scope of this thesis and can be found elsewhere [33-34]. Briefly, the elder model of ion formation, known as the charged-residue model (CRM), assumes the complete desolvation of ions by successive loss of all solvent molecules from droplets that are sufficiently small to contain just one analyte molecule in the end of a cascade of Coulomb fissions. The charges (protons) of this ultimate droplet are then transferred onto the molecule. This would allow that even large protein molecules can form singly charged ions, and indeed, CRM is supported by this fact.

Another theory, the ion evaporation model (IEM) [35-36], describes the formation of desolvated ions as direct evaporation from the surface of highly charged microdroplets. Ionic solvation energies are in the range of 3–6 eV, but thermal energy can only contribute about 0.03 eV at 300 K to their escape from solution. Thus, the electric force has to provide the energy needed. It has been calculated that a field of 10^9 V m^{-1} is required for ion evaporation which corresponds to a final droplet diameter of 10 nm

[36]. The IEM corresponds well to the observation that the number of charges is related to the fraction of the microdroplet's surface that a molecule can cover. As the radius diminishes, molecule size and number of droplet charges remain constant; however, the spacing of the surface charges decreases, and thus the increasing charge density brings more charges within the reach of an analyte molecule [37-38]. Flat and planar molecules therefore exhibit higher average charge states than spheric ones.

It is known that ESI spectrum can largely be influenced by the experimental conditions, such as: by the pH of the sprayed solution, the flow of nebulizing or drying gas, and the temperature of these or of a desolvation capillary. In particular, the degree of multiple charging is affected by those parameters, and of course, by the compound class under study. In addition, insufficient spraying conditions (like the use of a nebulizer) can lead to a net lack of protons which reduces the achievable charge state due to the limited number of protons available. In general, the number of charges on a molecule in ESI depends on its molecular weight and on the number of sites available for charge localization, e.g., sites that can be protonated, cationized, or deprotonated. On one hand, this behavior is advantageous as it folds up the m/z scale and makes even extremely large molecules accessible to standard mass analyzers. On the other hand, this produces a confusingly large number of peaks and requires tools to deal with in order to enable reliable mass assignments of unknown samples.

ESI geometries: The originally ESI source introduced by Fenn has been successively modified in order to preserve the source from contamination with non ionized sample material and consequently to enhance its life time. In particular when analytes are accompanied by involatile impurities such as buffer salts used to improve liquid chromatography or organic material as present in blood or urine samples, the deposition of material can cause the rapid breakdown of the ESI interface. Therefore, numerous modifications of spray geometry and skimmer design were developed to circumvent this problem. The principle of such designs is to achieve spatial separation of the deposition site of non-volatilized material and the location of the ion entrance into the mass spectrometer. Such designs include i) spraying off-axis, ii) spraying at some angle up to orthogonal, and iii) guiding the desolvating microdroplets through bent paths. One of the most successful designs of modern commercial ESI interfaces is that of Micromass z-spray interface (figure 1.7).

One of the major limits of ESI is the need for sample pre-purification since the only sample dissolution in a solvent (commonly mixture of water and organic methanol, isopropanol, or acetonitrile) often is not sufficient for a reliable mass spectra acquisition. In fact, analyte signal suppression is a strong inconvenience of ESI and may in practice prevent thorough analysis of complex mixtures if chromatographic separation/purification is not applied.

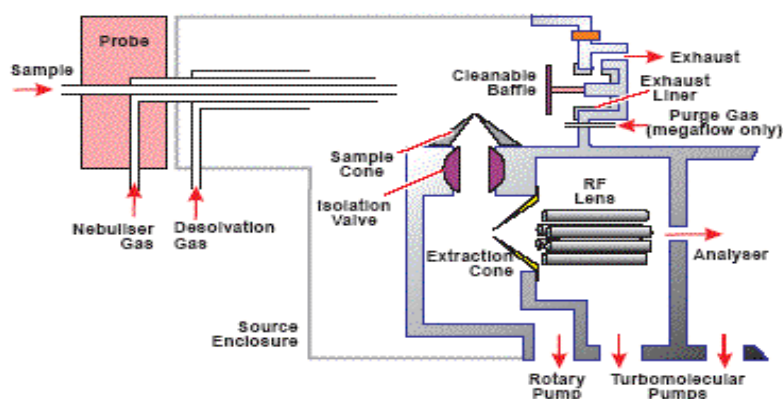


Figure 1.7. Schematic drawing of ESI z-spray interface [39].

A low percentage of formic acid or acetic acid (0,1% v/v) is often added in solvent mixture to assist the protonation of the analyte molecules in the positive ionization mode. In negative ionization mode ammonia solution or a volatile amine is added to aid deprotonation of the analyte molecules.

ESI is an extremely gentle ionization method, accompanied by very little fragmentation of the formed molecular ions. Consequently, weak bonds are often preserved and analysis of intact post-translationally modified peptides/proteins and noncovalently bound complexes, such as protein–ligand complexes, can be successfully performed with ESI-MS.

1.4.3.5 Desorption Electrospray Ionization (DESI)

Desorption electrospray ionization (DESI) is a new ambient ionization method introduced by Cooks and co-workers in 2004 [40]. This direct probe exposure method based on ESI can be used, under ambient conditions, on samples without any previous preparation. The principle is illustrated in figure 1.8. An ionized stream of solvent that is produced by an ESI source is sprayed on the surface of the sample to be analyzed. The interaction of the charged particles with materials on the surface produces gaseous ions of the compounds originally adsorbed to the surface to give mass spectra similar in appearance to conventional ESI mass spectra in that they show mainly peaks corresponding to single- or multi-proton or alkali-ion adducts of the analytes.

The proximity of the spraying device to the sample is important, and can be optimized with simple adjustments while observing the signal of the mass spectrometer. There is some dependence on the angle of incidence that is related to the size of the droplets; large droplets have more momentum and are able to leave the surface at an

angle close to the angle of incidence, whereas smaller droplets are swept along the plane of the surface by the bulk gas flow [41-42].

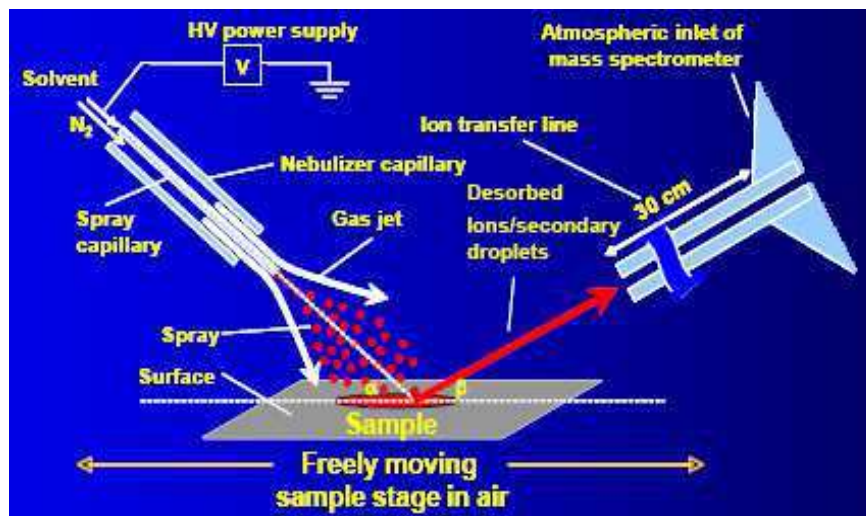


Figure 1.8. DESI ionization scheme [40].

At the microscopic level, the action of the DESI beam of sprayed droplets appears to simulate that of a "power scrubber" in that accumulation of liquid on the surface being analyzed seems to dissolve some of the compounds deposited on the surface, thereby facilitating desorption/ionization during further bombardment of the nascent solution by additional droplets from the sprayer [43]. The ions (possibly trapped in small droplets) emanating from the sample surface are effectively "vacuumed up" by a relatively large capillary through which a high volume rate of air carries the secondary ions (sometimes as far as 3 m) to a skimmer cone for entry into the m/z analyzer [44]. For this reason, the proximity of the entrance to the "sweeper" capillary to the point of impact of the bombarding spray is important. The principal means of ionizing nonvolatile compounds appears first to involve a droplet pick-up scavenging process that takes place during the brief contact time when droplets collide with sample surfaces with the analytes being extracted into the departing droplet. DESI phenomenon causes no damage to polymeric or metallic surfaces, although physical ablation of soft sample material such as biological material does occur [41].

DESI has been used to analyze organic materials from both conductive and insulator surfaces, and for compounds ranging from nonpolar small molecules such as lycopene, the alkaloid coniceine, small drugs, as well as polar compounds such as peptides and proteins; changes in the solution being electrosprayed can be used to ionize particular compounds selectively, including those in biological matrices [40] or in inks for forensic purposes [43]. In another application, DESI was used to characterize the active ingredients in pharmaceutical samples formulated as tablets, ointments, and liquids [45]. DESI has also been used for trace detection of the explosives directly from

a wide variety of surfaces (metal, plastic, paper, polymer), including skin [46-47] without sample preparation or pretreatment. Urinary metabolites [48], peptides [49], proteins [50], as well as intact bacteria [51] have been characterized by DESI.

A variation of the technique, called reactive DESI, uses reactive chemicals in the bombarding droplets [52]. By adding an organic salt (e.g., a phosphonium chloride) to the spraying solution, the bombarding droplets can be used to direct selected chemical modification of the analyte to improve specificity of the analysis. By adding boronic acid to the spraying solution in DESI, it is possible to promote covalent reactions with analytes containing the cis-diol functionality as in some carbohydrates, catecholamines, etc. [53]. Again, such use of the DESI experiment is exceptional in that it keeps unnecessary chemistry and sample preparation out of the mass spectrometer.

A hallmark of the DESI experiment is that the sample is not introduced into the mass spectrometer, only the ions are introduced through the skimmer cone. In this way, there is minimal insult to the m/z analyzer from the materials in the sample matrix that would otherwise contaminate the instrument.

1.4.3.6 Direct Analysis in Real Time (DART)

The direct analysis in real time (DART) ionization method was introduced in 2005 by Cody *et al.* [54]. Similarly to DESI, DART allows direct detection of chemicals on surfaces, in liquids and in gases without the need for sample preparation. All of these analyses take place under ambient conditions in a space just in front of the inlet of the mass spectrometer. The sample is not altered because no exposure to high voltage or to vacuum is required. In the source, a gas such as helium or nitrogen is introduced and submitted to a beam of electrons by applying a high-voltage potential between two electrodes as shown in figure 1.9.

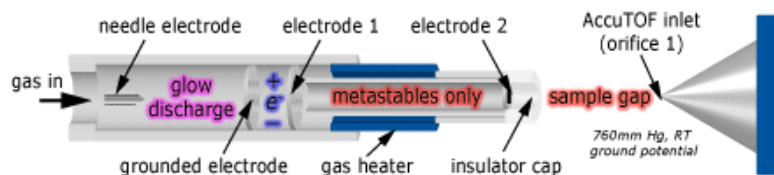


Figure 1.9. DART ionization source operation [55].

Ions, electrons and neutral species with electronic or vibronic excitation are produced. This resulting plasma passes through a series of electrodes designed to remove any charged species, leaving only neutral species that then interact with the sample and the atmosphere. It seems that mainly these excited neutral species produce the ionization of the sample molecules. Several mechanisms involved in ion formation are possible, depending on the polarity and reaction gas, the proton affinity and ionization potential

of the analyte, and presence of additives or dopants. Some of the mechanisms of ion formation in DART have not yet been fully explored. One of these mechanisms involves the use of excited-state species such as metastable helium atoms (2^3S) that have an energy of 19.8 eV. These excited-state species can react with analytes on surfaces to produce molecular ions through a process of Penning ionization. The helium metastables can also react with atmospheric water to produce protonated water clusters $[(\text{H}_2\text{O}_{n-1})\text{H}]^+$ and hydroxyl ions. The presence of dopants will produce adduct ions and, in some cases, increase sensitivity. The ion/molecule reactions between protonated water clusters and analyte molecules can produce protonated molecules of analytes. The system can also produce thermalized electrons to form negative-charge molecular ions. Gases such as N_2 will produce positive-charge molecular ions through Penning ionization. Other ionization systems using a corona discharge in air, as is used by DART, produce nitrogen oxide anions that interfere with the analysis of nitrogen-based explosives. DART can detect ClO_3^- and ClO_4^- ions from sodium perchlorate deposited from solution on a glass rod as well as molecules of volatile solvents such as from an open bottle of acetonitrile 10-20 feet from the ionization source. Various dopants have been used to enhance analyses by the detection of adduct ions like $[\text{M} + \text{NH}_4]^+$ when vapors of NH_4OH are purged through the ion source [54]. Unlike in ESI, alkali adducts are never seen in conjunction with protonated molecules, nor are multiple-charge ions. An important feature of DART is its lack of reliance on sample position in the ionization interface, which is operated at atmospheric pressure (open to the atmosphere) and there is no electric potential between the DART exit and the ion inlet of the mass spectrometer. Ionization takes place without the need for any solvents or sample preparation. Samples can be positioned in the interface while being held by hand i.e. intact fruits have been used for the detection of pesticides on their surfaces [54]. Detection of illicit drugs can be performed by placing a drop of urine on a melting point capillary and then holding the capillary in the DART ionization region. DART can also detect gas-phase molecules at very low concentrations in ambient air. Hundreds of compounds on different surfaces have been tested, many examples concerning mainly explosives on different surfaces, as well as the analysis of blood and urine samples containing drugs.

DART produces relatively simple mass spectra characterized by the presence of two main types of ions of the molecular species: M^{++} or $[\text{M}+\text{H}]^+$ in positive ion mode and $\text{M}^{\bullet-}$ or $[\text{M}-\text{H}]^-$ in negative ion mode. Fragmentation is observed for most of the compounds. These results appear similar to those obtained with DESI, but no multiply charged ions are produced. Consequently, the range of analytes that can be analyzed by DART is less broad than by DESI. Furthermore, DART cannot be used for the spatial analysis of surfaces.

1.4.3.7 Matrix-Assisted Laser Desorption Ionization

Matrix-assisted laser desorption ionization (MALDI) was introduced by Tanaka et al. in 1988 [56] for which in 2002 was awarded with the Nobel Prize in chemistry [57]. However, the routine techniques for MALDI as used today were developed by Karas and Hillenkamp and coworkers [58-60]. In MALDI, the sample is mixed with an organic matrix compound, such as dihydroxybenzoic acid (or other matrixes such as: α -cyano-4-hydroxycinnamic acid, 3,5-dimethoxy-4-hydroxy cinnamic acid, 2-mercapto-benzothiazole), in a convenient solvent to achieve a molar ratio of analyte to matrix of approximately 1:5000. Depending on the application, choice of the matrix compound can be very important. One role of the matrix is to separate the analyte molecules (by dilution) in order to prevent analyte-analyte molecular (or ionic) interactions during the ionization process. The key role of the matrix is in absorbing the radiation, thereby protecting the analyte from radiation damage. However, the matrix is selected not only for its capacity to absorb laser energy absorption, but for solubility characteristics similar to those of the analyte. The high energy density at the spot illuminated by the laser causes a phase transition from solid to gas; the explosive expansion of the localized segment of matrix (containing a trace of the analyte) mostly disperses neutrals, but also some ions, with initial velocities of 400 to 800 msc⁻¹. Interestingly, very little increase in the internal energy of the analyte occurs as there is little or no fragmentation of the analyte, making MALDI one of the soft ionization techniques.

When a solid matrix is to be employed, the sample and matrix are mixed together in an organic or aqueous solvent of mutual solubility. Once the solvent is removed, the matrix and analyte molecules codeposit onto a sample planchet. The mechanism for ionization of the analyte during MALDI is still under investigation [61-64]. Adduct formation by the matrix to the analyte sometimes occurs, especially with α -cyano-4-hydroxycinnamic acid (α -CHCA), although this phenomenon is somewhat analyte-dependent. In some cases, adduct formation by the matrix can be suppressed by adding surfactants to the sample/matrix mixture. The possibility of forming Na⁺ or K⁺ ion adducts of the analyte also exists. In other cases, matrix complexes with sodium and potassium ions can be annoying as they may interfere with detection of low-mass ions of the analyte. On the other hand, because these matrix-alkali ion complexes have been so well characterized, they can be used as internal calibrants of the m/z axis. If desirable, these matrix-alkali ion complexes can be suppressed by adding ammonium salt, such as citrates or phosphates, directly to the MALDI matrix. Use of iodine as a matrix additive has been reported to reduce adduct formation with the matrix, as well as diminish adduct formation with Na⁺ and K⁺.

In general, MALDI is recognized as a soft ionization technique (i.e., there is little, if any, fragmentation of the protonated molecule formed during the MALDI

process). On the other hand, some matrix compounds do promote some fragmentation of the protonated molecule. A more recent study on the influence of the matrix on fragmentation of the analyte during analysis by MALDI reports that bumetamide used alone or in combination with α -cyano-4-hydroxycinnamic acid can significantly promote fragmentation of peptides [65].

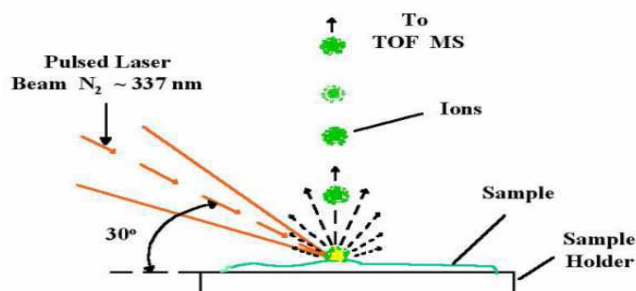


Figure 1.10. Schematic diagram of MALDI [66].

Bursts of radiation at 10 Hz from the laser are focused on the sample probe tip through appropriate optics. A UV laser, based on nitrogen, at 337 nm is most commonly used for MALDI; however, IR lasers have been used in some applications. Because the MALDI process is inherently a pulsed procedure, it is a logical application to use a TOF-MS to analyze the ions formed. Although TOF instruments are most often used for MALDI, ICR and ion trap instruments are being used with greater frequency. An interesting technique for accumulating ions from multiple laser shots, including those from a calibration compound located separate from the analyte, has been reported based on an ICR instrument for improved signal reproducibility and mass accuracy. In addition, certain hybrid instruments, such as the Qq-TOF with orthogonal acceleration, offer special applications or effects, such as the possibility of CID.

One feature of MALDI-MS, making it especially promising for analysis of biological samples, is the ability to detect biomolecules in complex mixtures in the presence of relatively large concentration of salts, buffers, and other species. Because of this ability, MALDI-MS has been utilized to study proteins and peptides in serum, cerebrospinal fluid, blood, tissue extracts, and whole cells [67-70]. Recently, imaging of biological samples/tissues has emerged as a promising diagnostic technique [71-72]. MALDI-MS is extremely sensitive, allowing detection of peptides in the attomole range. In both positive and negative ion mode MALDI mainly generates singly charged ions (somewhat dependent on the matrix), but multiply charged ions are common, especially for high mass proteins, and dimers occur as well. Because of the soft nature of the MALDI method, it is possible to desorb, ionize, and detect large, intact proteins. In many cases it is also possible to detect proteins or peptides intact with post-translational modifications, for example, phosphorylation and glycosylation [73-74].

Long sample preparation is perhaps the most time-consuming aspect and the principal disadvantage of analysis by MALDI MS.

1.5 MASS ANALYZERS

1.5.1 Introduction

Once the gas-phase ions have been produced, they need to be separated according to their masses, which must be determined. The physical property of ions that is measured by a mass analyzer is their mass-to-charge ratio (m/z). Therefore, it should be mentioned that for multiply charged ions the apparent m/z values are fractional parts of their actual masses. The operating pressure of the m/z analyzer is an important parameter. In order to ensure that ions can efficiently traverse the region from the ion source to the ion detector without interference, the mass spectrometer is maintained in a matter-free state, a vacuum. The entire m/z analyzer is operated at a low pressure (high vacuum) of 10^{-5} - 10^{-7} Pa. Once an ion is set in motion, it is important for it to avoid collision with molecules and other neutrals (radicals) or with other ions that could deflect its trajectory, result in collisional activation that could bring about fragmentation, or cause its disappearance due to charge neutralization.

As there are a great variety of ionization sources, several types of mass analyzers have been developed. The separation of ions according to their mass-to-charge ratio can be based on different principles (table 1.1). All mass analyzers use static or dynamic electric and magnetic fields that can be alone or combined. Most of the basic differences between the various common types of mass analyzer lie in the manner in which such fields are used to achieve separation. Each mass analyzer has its advantages and limitations. Analyzers can be divided into two broad classes on the basis of many properties. Scanning analyzers transmit the ions of different masses successively along a time scale. They are either magnetic sector instruments with a flight tube in the magnetic field, allowing only the ions of a given mass-to-charge ratio to go through at a given time, or quadrupole instruments. However, other analyzers allow the simultaneous transmission of all ions, such as the dispersive magnetic analyzer, the TOF mass analyzer and the trapped-ion mass analyzers that correspond to the ion traps, the ion cyclotron resonance or the orbitrap instruments. Analyzers can be grouped on

the basis of other properties, for example ion beam versus ion trapping types, continuous versus pulsed analysis, low versus high kinetic energies.

A new type of mass analyzer, the orbitrap, was introduced on the market in 2005. However, the existing mass analyzers have continued to be improved. Indeed, to overcome the limitations of conventional ion traps, linear ion traps (LITs), which have geometries more closely related to those of quadrupole mass analyzers, have been developed. In the same way, the TOF mass analyzers have been improved significantly with the development of numerous techniques, such as delayed extraction and the reflectron. The TOF mass analyzer requires the ions to be produced in bundles and is thus especially well suited for pulsed laser sources. However, the advent of ion introduction techniques such as orthogonal acceleration allows the analysis of ions from a continuous source with a TOF analyzer. Fourier transform (FT) ion cyclotron resonance spectrometers have shown impressive performances at high masses and high resolution. The new orbitrap mass analyser is capable of similar high performance but has more modest size, complexity and cost.

Another trend in mass analyzer development is to combine different analyzers in sequence in order to increase the versatility and allow multiple experiments to be performed. Triple-quadrupole and more recently hybrid instruments, for instance the quadrupole TOF instrument or the ion trap–FT ion cyclotron resonance mass spectrometer, allow one to obtain a mass spectrum resulting from the decomposition of an ion selected in the first analyzer. The time-dependent decomposition of a selected ion can also be observed in ion cyclotron resonance and ion trap instruments. They allow fragments over several generations (MS^n) to be observed.

The five main characteristics for measuring the performance of a mass analyzer are the mass range limit, the analysis speed, the transmission, the mass accuracy and the resolution. The mass range determines the limit of m/z over which the mass analyzer can measure ions. It is expressed in Th, or in u for an ion carrying an elementary charge, that is $z=1$. The analysis speed, also called the scan speed, is the rate at which the analyzer measures over a particular mass range. It is expressed in mass units per second ($u\ s^{-1}$) or in mass units per millisecond ($u\ ms^{-1}$). The transmission is the ratio of the number of ions reaching the detector and the number of ions entering the mass analyzer. The transmission generally includes ion losses through other sections of the mass analyzer such as electric lenses before and after the analyzer. This should not be confused with the duty cycle. The duty cycle is the proportion of time during which a device or system is usefully operated. For a mass spectrometer, the duty cycle is the part of ions of a particular m/z produced in the source that are effectively analyzed. The duty cycle can be expressed as a ratio or as a percentage. It is not a characteristic of the analyzer but is rather a characteristic of the whole mass spectrometer. Duty cycles differ

between different mass spectrometer designs. But the same mass spectrometer can have different duty cycles because they are also highly dependent on the mode of its operation. For instance, a quadrupole mass spectrometer used in selected ion monitoring mode (i.e. detecting only one specific ion) has a duty cycle of 100 %. But when this mass spectrometer is used in scan mode (i.e. scanning the analyzer to detect an m/z range), the duty cycle of the spectrometer decreases according to the proportion of the total observation time spent for each ion. For a quadrupole mass spectrometer scanning over 1000 amu, the duty cycle is $1/1000=0.1\%$. These parameters are closely associated with the sensitivity of a mass spectrometer. But the sensitivity of an instrument is better described by a factor defined as the mass spectrometer efficiency that takes into account the duty cycle, the transmission of the analyzer and the efficiency of the detector. Mass accuracy indicates the accuracy of the m/z provided by the mass analyzer. It is the difference that is observed between the theoretical m/z ($m_{\text{theoretical}}$) and the measured m/z (m_{measured}). It can be expressed in millimass units (mmu) but is often expressed in parts per million (ppm). Mass accuracy is largely linked to the stability and the resolution of the analyzer. A low-resolution instrument cannot provide high accuracy. The precision obtained on the mass of the analyzed sample depends also on the determination of the centroid of the peak. High mass accuracy has significant applications such as the determination of elemental composition. Last but not least, there is the characteristic of a mass analyzer concerning the resolution or its resolving power. Resolution or resolving power is the ability of a mass analyzer to yield distinct signals for two ions with a small m/z difference. The exact definition of these terms is one of the more confusing subjects of mass spectrometry terminology that continues to be debated. We will use here the definitions proposed by Marshall et al. [75]. Two peaks are considered to be resolved if the valley between them is equal to 10% of the weaker peak intensity when using magnetic or ion cyclotron resonance (ICR) instruments and 50% when using quadrupoles, ion trap, TOF, and so on. If Δm is the smallest mass difference for which two peaks with masses m and $m+\Delta m$ are resolved, the definition of the resolving power R is $R=m/\Delta m$. Therefore, a greater resolving power corresponds to the increased ability to distinguish ions with a smaller mass difference. The resolving power can also be determined with an isolated peak. Indeed, the resolving power is also defined using the peak width Δm at $x\%$ of the peak height. Often x is taken to be 50% and Δm is designated as full width at half maximum (FWHM). The relationship between the two definitions is obvious for two peaks with equal intensities. The resolution full width at $x\%$ of the peak height is equal to the resolution at $2x\%$ for the valley (figure 1.11). It should be noted that with the FWHM definition, the resolving power needed to observe separated peaks could no longer be deduced directly from R . Indeed, as shown in figure 1.11, when two peaks cross at 50% height, the valley is at 100 %. Thus the resolving

power needed to separate them must be higher than the one calculated using the FWHM definition. With Gaussian peak shapes, the FWHM definition of the resolving power gives values which are around double that of those obtained by 10% valley definition. Low resolution or high resolution is usually used to describe analysers with a resolving power that is less or greater than about 10 000 (FWHM), respectively. However, there is no exact definition of the boundary between these two terms.

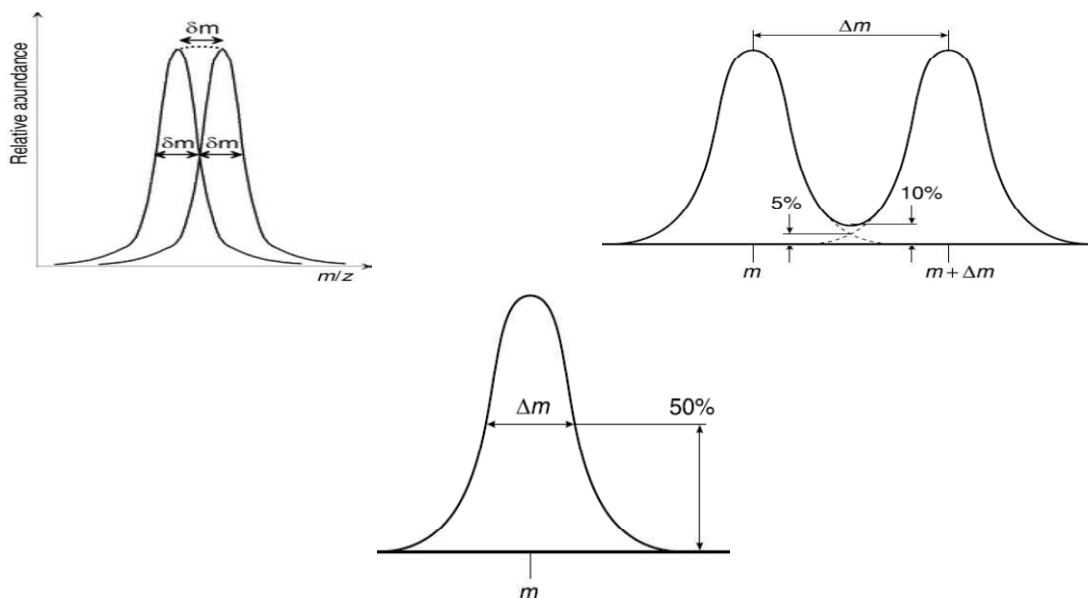


Figure 1.11. If δm is taken at half maximum height, two peaks having a mass difference equal to this width will cross at 50% height. As the valley depth will be two times this height, it will be at 100 %. There is thus no separation.

The description of all the analyzers today commercially available (see table 1.1) goes beyond the scope of this thesis, therefore in the following sections will be discussed the principles of operation of quadrupole, ion trap and time of flight analyzers which have been used during my PhD research activity.

Table 1.1. Common mass spectrometer analyzers

Type	Acronym	Principle
Magnetic sector	B	Deflection of a continuous ion beam; separation by momentum in magnetic field due to Lorentz force
Linear quadrupole	Q	Continuous ion beam in linear radio frequency quadrupole field; separation due to stability of trajectories
Linear quadrupole ion trap (2D LIT)	LIT	Continuous ion beam and trapped ions; storage and eventually separation in linear radio frequency quadrupole field due to stability of trajectories
Quadrupole ion trap (3D QIT)	QIT	Trapped ions; separation in three-dimensional radio frequency quadrupole field due to stability of trajectories
Time-of-flight	TOF	Time dispersion of a pulsed ion beam; separation by time-of-flight
Ion cyclotron resonance	ICR	Trapped ions; separation by cyclotron frequency (Lorentz force) in magnetic field

1.5.2 Linear Quadrupole Analyzers

The quadrupole analyzer is a device which uses the stability of the trajectories in oscillating electric fields to separate ions according to their m/z ratios. The 2D or 3D ion traps are based on the same principle. Quadrupole analyzers are made up of four perfectly parallel rods of circular or, ideally, hyperbolic section. The rod electrodes extend in the z -direction and are mounted in a square configuration (xy -plane), figure 1.12a and b. The pairs of opposite rods are each held at the same potential which is composed of a DC and an AC component.

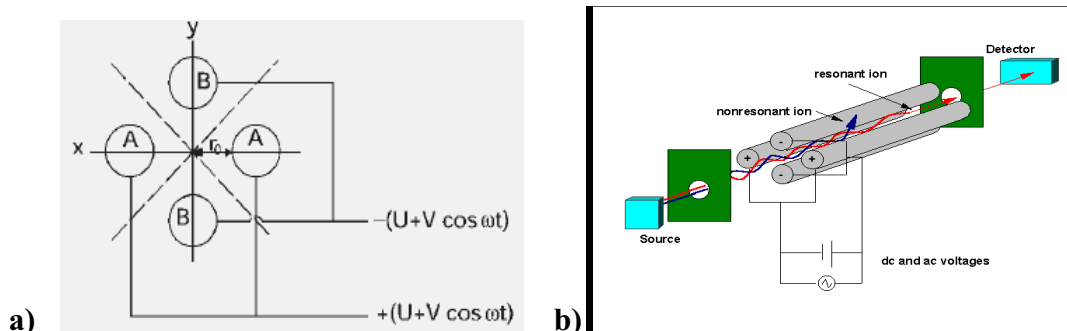


Figure 1.12. (a) Cross section of a quadrupole; (b) quadrupole rods and ion trajectories [76]

As an ion enters the quadrupole assembly in z -direction, an attractive force is exerted on it by one of the rods with its charge actually opposite to the ionic charge. If the voltage applied to the rods is periodic, attraction and repulsion in both the x - and y -directions are alternating in time, because the sign of the electric force also changes periodically in time. If the applied voltage is composed of a DC voltage U and a radiofrequency (RF) voltage V with the frequency ω , the total potential Φ_0 is given by

$$\Phi_0 = U + V \cos \omega t \quad (\text{eq. 1.1})$$

Thus, the equations of the motions are

$$\begin{aligned} \frac{d^2 x}{dt^2} + \frac{e}{m_i r_0^2} (U + V \cos \omega t) x &= 0 \\ \frac{d^2 y}{dt^2} - \frac{e}{m_i r_0^2} (U + V \cos \omega t) y &= 0 \end{aligned} \quad (\text{eq. 1.2})$$

In case of an inhomogenous periodic field such as the above quadrupole field, there is a small average force which is always in the direction of the lower field. The electric field is zero along the dotted lines in figure 1.12a, i.e., along the asymptotes in case of the hyperbolic electrodes. It is therefore possible that an ion may traverse the quadrupole without hitting the rods, provided its motion around the z -axis is stable with limited

amplitudes in the xy -plane. Such conditions can be derived from the theory of the Mathieu equations. Writing eq. 1.2 dimensionless yields

$$\begin{aligned} \frac{d^2 x}{d\tau^2} + (a_x + 2q_x \cos 2\tau)x &= 0 \\ \frac{d^2 y}{d\tau^2} + (a_y + 2q_y \cos 2\tau)y &= 0 \end{aligned} \tag{eq. 1.3}$$

The parameters a and q can now be obtained by comparison with Eq. 1.2:

$$a_x = -a_y = \frac{4eU}{m_i r_0^2 \omega^2}, \quad q_x = -q_y = \frac{2eV}{m_i r_0^2 \omega^2}, \quad \tau = \frac{\omega t}{2} \tag{eq. 1.4}$$

For a given set of U , V and ω the overall ion motion can result in a stable trajectory causing ions of a certain m/z value or m/z range to pass the quadrupole. Ions oscillating within the distance $2r_0$ between the electrodes will have stable trajectories. These are transmitted through the quadrupole and detected thereafter. The path stability of a particular ion is defined by the magnitude of the RF voltage V and by the ratio U/V . By plotting the parameter a (ordinate, time invariant field) versus q (abscissa, time variant field) one obtains the stability diagram of the two-dimensional quadrupole field. This reveals the existence of regions where i) both x - and y -trajectories are stable, ii) either x - or y -trajectories are stable, and iii) no stable ion motion occurs (figure 1.13a) [77]. Among the four stability regions of the first category, region I is of special interest for the normal mass-separating operation of the linear quadrupole (figure 1.13a).

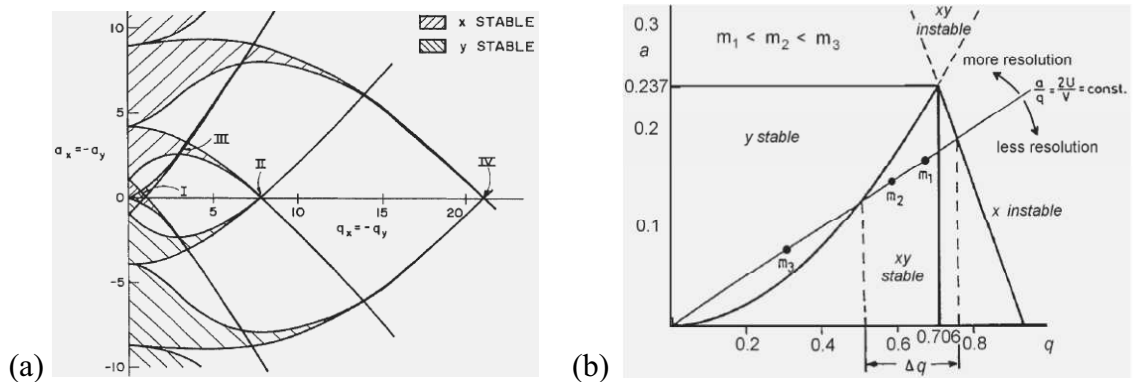


Figure 1.13. (a) Stability diagram for a linear quadrupole analyzer showing four stability regions (I–IV) for x - and y -motion [77]; (b) detail of the upper half of region I of the stability diagram for a linear quadrupole analyzer [78].

If the ratio a/q is chosen so that $2U/V = 0.237/0.706 = 0.336$, the xy -stability region shrinks to one point, the apex, of the diagram (eq. 1.4, figure 1.13b). By reducing a at constant q , i.e., reducing U relative to V , an increasingly wider m/z range can be

transmitted simultaneously. Sufficient resolution is achieved as long as only a small m/z range remains stable, e.g., one specific $m/z \pm 0.5$ for unit resolution. Thus, the width (Δq) of the stable region determines the resolution (figure 1.14). By varying the magnitude of U and V at constant U/V ratio an $U/V = \text{constant}$ linked scan is obtained allowing ions of increasingly higher m/z values to travel through the quadrupole. Hence, quadrupole analyzer acts as a mass filter (the term quadrupole mass filter is widely used). Scanning of any quadrupole means shifting the whole stability diagram along a “scan line”, because each m/z value has its own stability diagram.

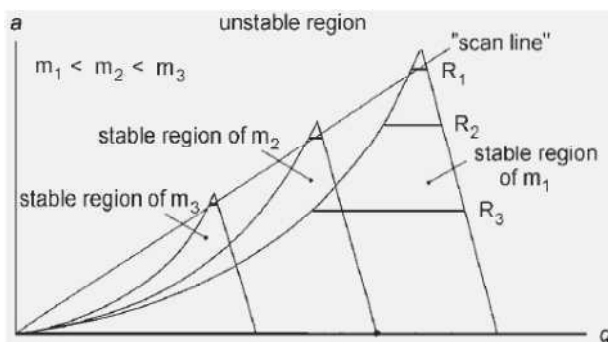


Figure 1.14. Scanning of linear quadrupoles means performing an $U/V = \text{constant}$ linked scan. Resolution is adjusted by variation of the a/q ratio: higher a/q ratio means higher resolution, and is represented by a steeper “scan line”; $R_1 > R_2 > R_3$.

Quadrupole analyzers generally are operated at so-called unit resolution normally restricting their use to typical low resolution applications. The resolution as adjusted by the U/V ratio cannot arbitrarily be increased, but is ultimately limited by the mechanical accuracy with which the rods are constructed and supported ($\pm 10\mu\text{m}$). Above an m/z value characteristic of each quadrupole assembly, any further improvement of resolution can only be achieved at the cost of significantly reduced transmission. High-performance quadrupoles allowing for about 10-fold unit resolution have only recently been developed [79].

The advantages of quadrupoles are that they i) have high transmission, ii) are light-weighted, very compact and comparatively low-cost, iii) have low ion acceleration voltages, and iv) allow high scan speeds, since scanning is realized by solely sweeping electric potentials.

Quadrupoles are analyzers of choice for tandem MS (MS/MS) applications. In fact, triple quadrupole mass spectrometers, QqQ, have become a standard analytical tool for LC-MS/MS applications, in particular when accurate quantitation is desired. To operate triple quadrupole mass spectrometers in the MS/MS mode, Q1 serves as MS1; the intermediate RF-only device, q2, acts as “field-free region” for metastable dissociations or more often as collision cell for collision induced dissociation (CID) experiments, and Q3 is used to analyze the fragment ions exiting from q2. Typically, the

mass selected ions emerging from Q1 are accelerated by an offset of some ten electronvolts into q2 where the collision gas (N₂, Ar) is provided at a pressure of 0.1–0.3 Pa. Careful optimization of all parameters allows major improvements of CID efficiency and resolution to be made. If MS/MS is not intended, either Q1 or Q3 may be set to RF-only mode, thereby reducing its function to that of a simple flight tube with ion-guiding capabilities. The instrument then behaves as though it was a single quadrupole mass spectrometer. In triple quadrupole instruments Q1 and Q3 are operated independently as MS1 and MS2, respectively, making MS/MS a straightforward matter. The experimental setups for different scanning options (product ion, precursor ion, and neutral loss) are reported later in the section of tandem mass spectrometry.

1.5.3 Ion Trap Analyzers

An ion trap is a device that uses an oscillating electric field to store ions. The ion trap works by using an RF quadrupolar field that traps ions in two or three dimensions. Therefore, ion traps can be classified into two types: the 3D ion trap or the 2D ion trap. Historically, the first ion traps were 3D ion traps. They were made up of a circular electrode, with two ellipsoid caps on the top and the bottom that creates a 3D quadrupolar field. These traps were also named quadrupole ion traps (QITs) or Paul ion traps. Besides 3D ion traps, 2D ion traps have also been developed. They are based on a four rod quadrupole ending in lenses that reflect ions forwards and backwards in that quadrupole. Therefore, in these 2D ion traps, which are also known as linear ion traps (LITs), ions are confined in the radial dimension by means of a quadrupolar field and in the axial dimension by means of an electric field at the ends of the trap.

1.5.4 Quadrupole Ion Traps (QIT)

The quadrupole ion trap (QIT), known as 3D quadrupole ion trap (3D QIT), mass spectrometer uses a three-dimensional quadrupole electric field to store ions of multiple m/z values in concentric three-dimensional orbitals as opposed to filtering out ions of all m/z values except those of a selected value from an ion beam. These concentric 3D orbitals can be visualized as layers of an onion with ions of the lowest stored m/z value composing the outer layer and ions of successively higher m/z values occupying orbitals of progressively shorter radii. The QIT consists of two end-cap electrodes that are electrically isolated from either side of a ring electrode (figure 1.15). This three-dimensional device has a hyperbolic cross-sectional surface, which is consistent with those used in quadrupole technology.

Conceptually, a 3D ion trap can be imagined as a quadrupole bent in on itself in order to form a closed loop. The inner rod is reduced to a point at the centre of the trap, the outer rod is the circular electrode, and the top and bottom rods make up the caps. The overlapping of a direct potential with an alternative one gives a kind of '3D quadrupole' in which ions of all masses are trapped on a 3D trajectory (figure 1.15). The inventors, Paul and Steinwedel [80], proposed the use of this ion trap as a mass spectrometer by applying a resonant frequency along z to expel the ions of a given mass. In quadrupole instruments, the potentials are adjusted so that only ions with a selected mass go through the rods. Ions of different masses are present together inside the trap, and are expelled according to their masses so as to obtain the spectrum. As the ions repel each other in the trap, their trajectories expand as a function of the time. To avoid ion losses by this expansion, care has to be taken to reduce the trajectory. This is accomplished by maintaining in the trap a pressure of helium gas which removes excess energy from the ions by collision. This pressure hovers around 10^{-3} Torr.

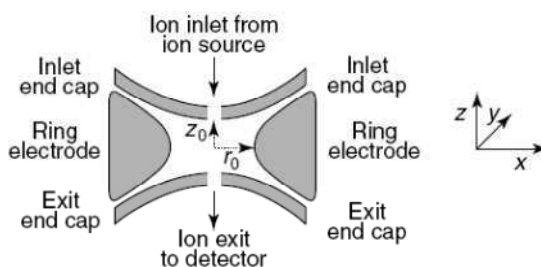


Figure 1.15. Schematic view of a 3D ion trap, and direction of the x , y and z coordinates [8].

As is the case with quadrupole instruments, a potential Φ_0 , the sum of a direct and an alternative potential, could be applied to the caps, and $-\Phi_0$ to the circular electrode. However, in most commercial instruments, Φ_0 is applied only to the ring electrode. In both cases, the resulting field must be seen in three dimensions. Here again, a mathematical analysis using the Mathieu equations allows us to locate areas in which ions of given masses have a stable trajectory. These areas may be displayed in a diagram as a function of U , the direct potential, and of V , the amplitude of the alternative potential. The areas in which the ions are stable are those in which the trajectories never exceed the dimensions of the trap, z_0 and r_0 . The detailed mathematical relations which govern the 3D ion trap operation goes beyond the aim of this thesis.

1.5.5 Linear Ion Traps (LIT)

The linear ion trap (LIT), also known as the 2D ion trap, is an analyzer based on the four-rod quadrupole ending in lenses that repel the ions inside the rods, and thus at positive potentials for positive ions, and vice versa [81]. In these traps, ions are confined

in the radial dimension by means of a quadrupolar field and in the axial dimension by means of an electric field at the ends of the trap. Once in the LIT, the ions are cooled by collision with an inert gas and fly along the z axis between the end electrodes while simultaneously oscillating in the xy plane owing to the application of an RF-only potential on the rods. The rods are furthermore often divided into three segments. Application of an additional DC voltage to the end parts of the quadrupole also allows the ions to be trapped. This can be used either without end electrodes or together with these electrodes. These voltages repel the ions inside the linear trap, and this repulsion is higher when the ions are closer to the ends. Ions are thus repelled towards the centre of the quadrupole if the same repelling voltages are applied at each end. Thus, the ion cloud will be squeezed at the centre of the quadrupole if the applied voltages are symmetrically applied, but can be located at closer to one end if the repelling voltage at that end is smaller. One great advantage of LITs in comparison with QIT is a more than 10-fold higher ion trapping capacity. Furthermore, this higher trapping capacity is combined with the ability to contain many more ions before space charge effects occur owing to both a greater volume of the trap and a focusing along the central line rather than around a point. Even with 20 000 trapped ions, well resolved mass spectra can be obtained without any space charge effects in 2D ion traps, whereas more than 500 trapped ions in 3D traps induce space charge effects. Another common advantage is the higher trapping efficiency. Indeed, a trapping efficiency of more than 50% is achieved when ions are injected into the 2D ion trap from an external source, while this trapping efficiency is only 5% for the 3D ion trap. Both of these advantages increase the sensitivity and the dynamic range. Ions trapped within an LIT can be mass selectively ejected either along the axis of the trap (axial ejection) or perpendicular to its axis (radial ejection).

All the operations of a 3D ion trap can be applied in a LIT, but LIT also shares similar limitations, for example MS/MS is limited to fragmentation scans. Thus precursor ion scan or neutral loss scan that are available with triple quadrupole instruments cannot be used on ion traps.

1.5.6 Time-of-Flight Analyzers

The construction of a time-of-flight (TOF) analyzer has been reported in 1946 by Stephens [82]. Soon, other groups shared Stephens' concept and increasingly useful TOF instruments were constructed [83-84]. These first generation TOF instruments were designed for gas chromatography-mass spectrometry (GC-MS) coupling and their performance was poor as compared to modern TOF analyzers, but the specific

advantage of TOF over the competing magnetic sector instruments was the rate of spectra per second they were able to deliver. In GC-MS the TOF analyzer soon became superseded by linear quadrupole analyzers and it took until the late 1980s for their revival [85-86], the success of pulsed ionization methods, especially of matrix-assisted laser desorption/ionization (MALDI), made it possible. MALDI generated a great demand for a mass analyzer ideally suited to be used in conjunction with a pulsed ion source and capable of transmitting ions of extremely high mass up to several 10^5 u [59]. Since then, the performance of TOF instruments has tremendously increased and TOF analyzers were adapted for use with other ionization methods and are now even strong competitors to the well-established quadrupolar and magnetic sector instruments in many applications.

The principle of TOF is quite simple: ions of different m/z are dispersed in time during their flight along a field-free drift path of known length. Provided all the ions start their journey at the same time or at least within a sufficiently short time interval, the lighter ones will arrive earlier at the detector than the heavier ones. This demands that they emerge from a pulsed ion source which can be realized either by pulsing ion packages out of a continuous beam or more conveniently by employing a true pulsed ionization method. In the following section will be discussed the basic principles of TOF instruments, focusing particularly on ion velocity and ion time of flight.

Independently from the ionization method, the electric charge q of an ion of mass m_i is equal to an integer number z of electron charges e , and thus $q = ez$. The energy uptake E_{el} by moving through a voltage U is given by the relation:

$$E_{el} = qU = ezU$$

Thereby, the former potential energy of a charged particle in an electric field is converted into kinetic energy E_{kin} , i.e., into translational motion: $E_{el} = ezU = 1/2m_iv^2 = E_{kin}$.

Assuming the ion was at rest before, which is correct in a first approximation, the velocity attained is obtained by rearranging the previous equation:

$$v = \sqrt{\frac{2ezU}{m_i}} \quad (\text{eq. 1.5})$$

Hence, the ion velocity, v , is inversely proportional to the square root of mass. From here, we can calculate the time for an ion of unknown m/z to travel a distance s after having been accelerated by a voltage U . The relationship between velocity and time t needed to travel the distance s is:

$$t = \frac{s}{v} \quad (\text{eq. 1.6})$$

which upon substitution of v with eq. 1.6 becomes

$$t = \frac{s}{\sqrt{\frac{2ezU}{m_i}}} \quad (\text{eq. 1.7})$$

This equation gives the time needed for the ion to travel the distance s at constant velocity, i.e., in a field-free environment after the process of acceleration has been completed. Rearrangement of eq. 1.7 reveals the relationship between the instrumental parameters s and U , the experimental value of t and the ratio m_i/z

$$\frac{m_i}{z} = \frac{2eUt^2}{s^2} \quad (\text{eq. 1.8})$$

From eq. 18 the time to drift through a fixed length of field-free space is proportional to the square root of m_i/z :

$$t = \frac{s}{\sqrt{2eU}} \sqrt{\frac{m_i}{z}} \quad (\text{eq. 1.9})$$

and thus, the time interval Δt between the arrival times of ions of different m/z ions is proportional to

$$s \left(\sqrt{\frac{m_i}{z_1} - \frac{m_i}{z_2}} \right)$$

The proportionality of time-of-flight to the square root of m/z causes Δt for a given $\Delta m/z$ to decrease with increasing m/z : under otherwise the same conditions Δt per 1 u is calculated as 114 ns at m/z 20, 36 ns at m/z 200, and just 11 ns at m/z 2000. Therefore, the realization of a time-of-flight mass analyzer depends on the ability to measure short time intervals with sufficient accuracy. At this point it becomes clear that the performance of the early TOF analyzers – among other reasons – suffered also from the too slow electronics of their time.

As the charge z increases, charge state $z > 1$, the numerical value of m/z is reduced, i.e., the ion will be detected at lower m/z than the corresponding singly-charged ion of the same mass. According to eq. 1.9, the time-of-flight is reduced by a factor of 1.414 (the square root of 2) for doubly-charged ions which is the same time-of-flight as for a singly-charged ion of half of its mass. Accordingly, the time-of-flight is reduced by a factor of 1.732 (the square root of 3), for triply-charged ions corresponding to a singly-charged ion of one third of its mass.

1.5.6.1 Linear Time-of-Flight Analyzer

In this geometry of TOF analyzers, ions formed are continuously extracted and accelerated by a voltage U . When leaving the acceleration region, the ions should possess equal kinetic energies. They drift down a field-free flight path in the order of 1–2 m and finally hit the detector. Such an instrumental setup where the ions are travelling on a straight line from the point of their creation to the detector is called linear TOF (figure 1.16).

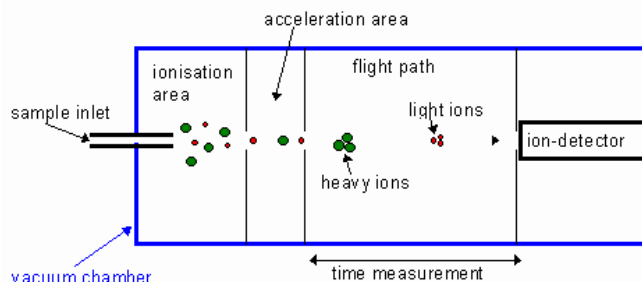


Figure 1.16. Scheme of a linear TOF analyzer [87].

The transmittance (that leads to very high sensitivity) of a linear TOF analyzer approaches 90 % because ion losses are solely caused by collisional scattering due to residual gas or by poor spatial focusing of the ion source. With a sufficiently large detector surface located in not a too large distance from the ion source exit, a very high fraction of the ions will be collected by the detector.

The most important drawback of the linear TOF analyzers was their poor mass resolution. Mass resolution is affected by factors that create a distribution in flight times among ions with the same m/z ratio. These factors are the length of the ion formation pulse (time distribution), the size of the volume where the ions are formed (space distribution), the variation of the initial kinetic energy of the ions (kinetic energy distribution), and so on (figure 1.17). This situation is substantially improved with the development of two techniques: the delayed pulse extraction and the reflectron (electrostatic mirror). The electronics and more particularly the digitizers, the stability of power supplies, space charge effects and mechanical precision can also affect the resolution and the precision of the time measurement.

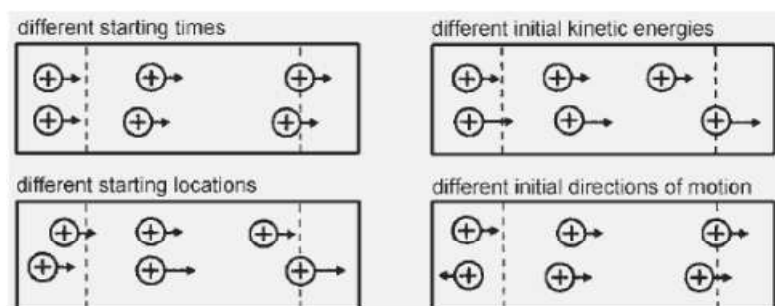


Figure 1.17. Effects of initial time, space, and kinetic energy distributions on mass resolution in TOF-MS [88].

1.5.6.2 Delayed Pulsed Extraction

To reduce the kinetic energy spread among ions with the same m/z ratio leaving the source, a time lag or delay between ion formation and extraction can be introduced. The ions are first allowed to expand into a field-free region in the source and after a certain delay (hundreds of nanoseconds to several microseconds) a voltage pulse is

applied to extract the ions outside the source. This mode of operation is referred to as delayed pulsed extraction to differentiate it from continuous extraction used in conventional instruments. The ions formed in the source using the continuous extraction mode are immediately extracted by a continuously applied voltage. The ions with the same m/z ratio but with different kinetic energy reach the detector at slightly different times, resulting in peak broadening. In the delayed pulsed extraction mode, the ions are initially allowed to separate according to their kinetic energy in the field-free region. For ions of the same m/z ratio, those with more energy move further towards the detector than the initially less energetic ions. The extraction pulse applied after a certain delay transmits more energy to the ions which remained for a longer time in the source. Consequently, the initially less energetic ions receive more kinetic energy and join the initially more energetic ions at the detector. So, delayed pulsed extraction corrects the energy dispersion of the ions leaving the source with the same m/z ratio and thus improves the resolution of the TOF analyzer.

1.5.6.3 Reflectron Time-of-Flight Analyzers

Another way to improve mass resolution is to use an electrostatic reflector, called a reflectron. It creates a retarding field that acts as an ion mirror by deflecting the ions and sending them back through the flight tube. The term reflectron time-of-flight (ReTOF) analyzer is used to differentiate it from the linear time-of-flight (LTOF) analyzer. The simplest type of reflectron, which is called a single-stage reflectron, consists usually of a series equally spaced grid electrodes or more preferably ring electrodes connected through a resistive network of equal-value resistors. The reflectron is situated behind the field-free region opposed to the ion source. The detector is positioned on the source side of the ion mirror to capture the arrival of ions after they are reflected. There are two common methods of positioning the detector. It may be coaxial with the initial direction of the ion beam. This detector has a central hole to transmit the ions leaving the source. However, the most common instrument geometry has the detector off-axis with respect to the initial direction of the ion beam. Indeed, adjusting the reflectron at a small angle in respect to the ions leaving the source allows the detector to be positioned adjacent to the ion source.

The reflectron corrects the kinetic energy dispersion of the ions leaving the source with the same m/z ratio, as shown in figure 1.18. Indeed, ions with more kinetic energy and hence with more velocity will penetrate the reflectron more deeply than ions with lower kinetic energy. Consequently, the faster ions will spend more time in the reflectron and will reach the detector at the same time than slower ions with the same m/z . Although the reflectron increases the flight path without increasing the dimensions

of the mass spectrometer, this positive effect on the resolution is of lower interest than its capability to correct the initial kinetic energy dispersion.

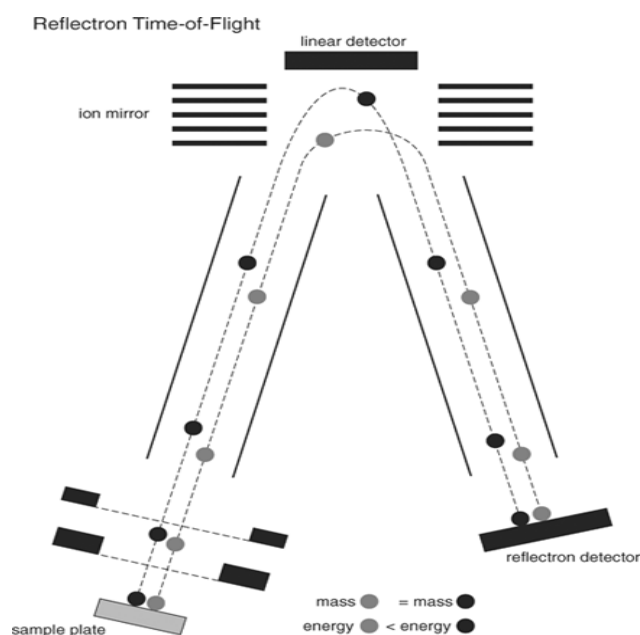


Figure 1.18. Scheme of reflectron TOF analyzer.

The ability of the ReTOF to compensate for the initial energy spread of ions largely increases the resolving power of TOF instruments. However, the reflectron increases the mass resolution at the expense of sensitivity and introduces a mass range limitation. While a typical continuous extraction TOF instrument in linear mode cannot resolve isotopic patterns of analytes above about m/z 500, it will do when operated in reflector mode. At substantially higher m/z , the ReTOF still fails to resolve isotopic patterns, even though its resolution is still better than that of a linear TOF analyzer.

The main advantages of TOF instruments are: i) in principle, the m/z range is unlimited, ii) from each ionizing event, e.g., a single laser shot in MALDI, a complete mass spectrum is obtained within several tens of microseconds; iii) the transmission of a TOF analyzer is very high, giving rise to high sensitivity; iv) the construction of a TOF instrument is comparatively straightforward and inexpensive; and v) recent instruments allow for accurate mass measurements and tandem MS experiments.

1.5.7 Tandem Mass Spectrometry

Tandem mass spectrometry, abbreviated MS/MS, is any general method involving at least two stages of mass analysis, either in conjunction with a dissociation process or in a chemical reaction that causes a change in the mass or charge of an ion. In the most common tandem mass spectrometry experiment a first analyzer is used to isolate a precursor ion which then undergoes, spontaneously or by some activation, a fragmentation to yield product ions and neutral fragments. A second spectrometer (analyzer) analyses the product ions. It is possible to increase the number of steps: select ions of a first mass, then select ions of a second mass from the obtained fragments, and finally analyze the fragments of these last selected ions. This is labelled as an MS/MS/MS or MS³ experiment. The number of steps can be increased to yield MSⁿ experiments (where *n* refers to the number of generations of ions being analysed).

Basically, a tandem mass spectrometer can be conceived in two ways: performing tandem mass spectrometry in space by the coupling of two physically distinct instruments, or in time by performing an appropriate sequence of events in an ion storage device. Thus, there are two main categories of instruments that allow tandem mass spectrometry experiments: i) tandem mass spectrometers in space and ii) in time.

Common space instruments have two mass analyzers, allowing MS/MS experiments to be performed. A frequently used instrument of this type uses quadrupoles as analyzers. The QqQ configuration indicates an instrument with three quadrupoles where the second one, indicated by a lower case q, is the reaction region. It operates in RF-only mode and thus acts like a lens for all the ions. Other instruments combine electric and magnetic sectors (E and B) or E, B and qQ, thus electric and magnetic sectors and quadrupoles. TOF instruments with a reflectron, or a combination of a quadrupole with a TOF instrument (QqTOF), are also used. To obtain higher order MSⁿ spectra would require *n* analyzers to be combined, increasing the complexity and thus also the cost of the spectrometer. Furthermore, successive analyzers can be arranged in any number, but because the fraction of ions transmitted at each step is low, the practical maximum is three or four analyzers in the case of beam instruments.

Besides this spatial separation method using successive analyzers, tandem mass spectrometry can also be achieved through time separation with a few analyzers such as ion traps, orbitrap and FTICR, programmed so that the different steps are successively carried out in the same instrument. The maximum practical number of steps for these instruments is seven to eight. In these instruments the proportion of ions transmitted is high, but at each step the mass of the fragments becomes lower and lower. A significant difference between the two types of trapping instruments is that in the ion trap mass

spectrometers, ions are expelled from the trap to be analyzed. Hence they can be observed only once at the end of the process. In FTMS, they can be observed nondestructively, and hence measured at each step in the sequential fragmentation process.

MS/MS scan modes: The four main scan modes available using tandem mass spectrometry are represented in figure 1.19, using the symbolism proposed by Cooks et al. [89].

- Product ion scan (daughter scan) consists of selecting a precursor ion (or parent ion) of a chosen mass-to-charge ratio and determining all of the product ions (daughter ions) resulting from collision-induced-dissociation (CID). If reactive gas is used in the collision cell, collision-activated-reaction (CAR) products are observed. When only fragment ions are produced, this scan mode is also referred to as 'fragment ion scan'.
- Precursor ion scan (parent scan) consists of choosing a product ion (or daughter ion) and determining the precursor ions (or parent ions). This method is called 'precursor scan' because the 'precursor ions' are identified. This scan mode cannot be performed with time-based mass spectrometers. This scan requires the focusing of the second spectrometer on a selected ion while scanning the masses using the first spectrometer. All of the precursor ions that produce ions with the selected mass through reactions or fragmentations thus are detected.
- Neutral loss scan consists of selecting a neutral fragment and detecting all the fragmentations leading to the loss of that neutral. As in the case of the precursor ion scan, this scan mode is not available with time-based mass spectrometers. This scan requires that both mass spectrometers are scanned together, but with a constant mass offset between the two. Thus, for a mass difference a , when an ion of mass m goes through the first mass spectrometer, detection occurs if this ion has produced a fragment ion of mass $(m-a)$ when it leaves the collision cell.
- Selected reaction monitoring (SRM) consists of selecting a fragmentation reaction. For this scan, both the first and second analyzers are focused on selected masses. There is thus no scan. The method is analogous to selected ion monitoring in standard mass spectrometry. But here the ions selected by the first mass analyzer are only detected if they produce a given fragment, by a selected reaction. The absence of scanning allows one to focus on the precursor and fragment ions over longer times, increasing the sensitivity as for selected ion monitoring, but this sensitivity is now associated with a high increase in selectivity.

Note that precursor or neutral loss scans are not possible in time separation analyzers. The product ion scan is the only one available directly with these mass spectrometers. However, with these instruments, the process can be easily repeated over several ion generations. Thus time-based instruments easily allow MSⁿ product ion spectra to be obtained. Therefore, the MSⁿ is very valuable way to obtain structural information from ions that represent the intact molecule produced by soft ionization techniques such as ESI and APCI.

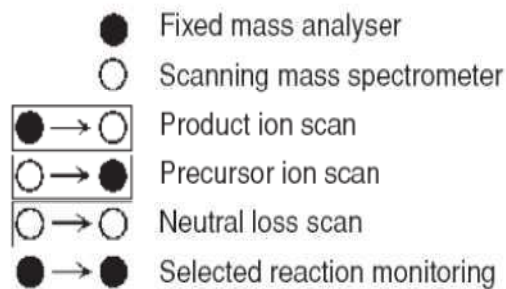


Figure 1.19. Symbolism proposed by Cooks *et al.* for the easy representation of various scan modes [89].

References

1. Skoog D. A., West D. M., Holler F. J., Crouch S. R., Fundamentals of analytical chemistry, 8th edition, Thomson Brooks/Cole, USA, 2004.
2. Robert E. Ardrey, Liquid Chromatography – Mass Spectrometry: An Introduction, 2003, John Wiley & Sons, Ltd., England.
3. <http://www.hull.ac.uk/chemistry/masspec3/principlesofms.html>
4. Dempster A. J., Positive Ray Analysis of Lithium and Magnesium. *Phys. Rev.*, 18, 1921, 415–422.
5. Bleakney W., *Phys. Rev.*, 34, 1929, 157.
6. Nier A. O., A Mass Spectrometer for Routine Isotope Abundance Measurements. *Rev. Sci. Instrum.*, 11, 1940, 212–216.
7. Nier A. O., A Mass Spectrometer for Isotope and Gas Analysis. *Rev. Sci. Instrum.*, 18, 1947, 398–411.
8. de Hoffmann E., Stroobant V., Mass Spectrometry: Principles and applications, 3rd edition, John Wiley & Sons Ltd, 2007, England.
9. Munson M. S. B. and Field F. H., Chemical Ionization Mass Spectrometry, General Introduction, *J. Am. Chem. Soc.*, 1966, 88, 2621–2630.
10. Field F. H., The Early Days of Chemical Ionization: A Reminiscence, *J. Am. Soc. Mass Spectrom.*, 1990, 1, 277–283.
11. Munson B., Development of Chemical Ionization Mass Spectrometry. *Int. J. Mass Spectrom.*, 2000, 200, 243–251.
12. Hunt D. F., Stafford G. C., Crow F. W. and Russell J. W., Pulsed Positive Negative Ion Chemical Ionization Mass Spectrometry, *Anal. Chem.*, 1976, 48, 2098–2104.
13. Horning E. C., Horning M. G., Carroll D. I., Dzidic I. and Stillwell R. N., New Picogram Detection System Based on a Mass Spectrometer with an External Ionization Source at Atmospheric Pressure, *Anal. Chem.*, 1973, 45, 936–943.
14. Carroll D. I., Dzidic I., Stillwell R. N., Horning M. G. and Horning E. C., Subpicogram Detection System for Gas Phase Analysis Based upon Atmospheric Pressure Ionization (API) Mass Spectrometry, *Anal. Chem.*, 1974, 46, 706–710.
15. Horning E. C., Carroll D. I., Dzidic I., Haegele K. D., Horning M. G. and Stillwell R. N., Liquid Chromatograph-Mass Spectrometer-Computer Analytical

- Systems: A Continuous-Flow System Based on Atmospheric Pressure Ionization Mass Spectrometry, *J. Chromatogr. A*, 1974, 99, 13–21.
16. Carroll D. I., Dzidic I., Stillwell R. N., Haegele K. D. and Horning E. C., Atmospheric Pressure Ionization Mass Spectrometry. Corona Discharge Ion Source for Use in a Liquid Chromatograph-Mass Spectrometer-Computer Analytical System, *Anal. Chem.*, 1975, 47, 2369–2373.
 17. <http://commons.wikimedia.org/wiki/File:Apci.gif>
 18. Dole M., Mack L. L., Hines R. L., Mobley R. C., Ferguson L. D. and Alice M. B., Molecular Beams of Macro ions, *J. Chem. Phys.*, 1968, 49, 2240–2249.
 19. Yamashita M. and Fenn J. B., Electrospray Ion Source: Another Variation on the Free-Jet Theme, *J. Phys. Chem.*, 1984, 88, 4451–4459.
 20. Rossi D.T., Sinz M.W., *Mass Spectrometry in Drug Discovery*, Marcel Dekker, 2002, New York.
 21. Schalley C.A., *Modern Mass Spectrometry*, Springer, 2003, New York.
 22. Siuzdak G., *The Expanding Role of Mass Spectrometry in Biotechnology*, MCC Press, 2003, San Diego.
 23. Roboz J., *Mass Spectrometry in Cancer Research*, 1st edition, CRC Press, 1999, Boca Raton.
 24. Chapman J. R., *Mass Spectrometry of Proteins and Peptides*, Humana Press, 2000, Totowa.
 25. Yamashita M. and Fenn J. B., *Phys. Chem.*, 1988, 88, 4671.
 26. Ikonomou M. G., Blades A. T. and Kebarle P., *Anal. Chem.*, 1990, 62, 957.
 27. Kebarle P., Tang L., From Ions in Solution to Ions in the Gas Phase - the Mechanism of ESI-MS, *Anal. Chem.* 1993, 65, 972A-986A.
 28. Taylor G. I., Disintegration of water drops in an electric field, *Proc. R. Soc. A.*, 1964, 280, 383–397.
 29. Wilm M. S., Mann M., Electrospray and Taylor-Cone Theory, Dole's Beam of Macromolecules at Last?, *Int. J. Mass Spectrom. Ion Proc.*, 1994, 136, 167-180.
 30. Cole R. B., Some Tenets Pertaining to ESIMS, *J. Mass Spectrom.*, 2000, 35, 763-772.
 31. Gomez A., Tang K., Charge and Fission of Droplets in Electrostatic Sprays, *Phys. Fluids* 1994, 6, 404-414.
 32. Duft D., Achtzehn T., Müller R., Huber B.A., Leisner T., Coulomb Fission. Rayleigh Jets From Levitated Microdroplets, *Nature*, 2003, 421, 128.
 33. Felitsyn N., Peschke M., Kebarle P., Origin and Number of Charges Observed on Multiply-Protonated Native Proteins Produced by ESI, *Int. J. Mass Spectrom.*, 2002, 219, 39-62.

34. Kauppila T. J., Kotiaho T., Kostianen R. and Bruins A. P., *J. Am. Soc. Mass Spectrom.*, 2004, 15, 203.
35. Iribarne J. V., Thomson B. A., On the Evaporation of Small Ions From Charged Droplets, *J. Chem. Phys.*, 1976, 64, 2287- 2294.
36. Thomson B.A., Iribarne J.V., Field-Induced Ion Evaporation From Liquid Surfaces at Atmospheric Pressure, *J. Chem. Phys.*, 1979, 71, 445-4463.
37. Fenn J. B., Ion Formation From Charged Droplets: Roles of Geometry, Energy, and Time, *J. Am. Soc. Mass Spectrom.* 1993, 4, 524-535.
38. Fenn J. B., Rosell J., Meng C. K., In ESI, how much pull does an ion need to escape its droplet prison?, *J. Am. Soc. Mass Spectrom.*, 1997, 8, 1147-1157.
39. http://www.chemistry.nmsu.edu/Instrumentation/Waters_ElectoSpray.html
40. Takats Z., Wiseman J., Gologan B. and Cooks R. G., Mass spectrometry sampling under ambient conditions with desorption electrospray ionization, *Science*, 2004, 306, 471-3.
41. Venter A., Sojka P. E. and Cooks R. G., Droplet Dynamics and Ionization Mechanisms in Desorption Electrospray Ionization Mass Spectrometry, *Analytical Chemistry*, 2006, 78 (24), 8549-8555.
42. Takats Z., Wiseman J. M. and Cooks R. G., Ambient MS by DESI: Instrumentation, mechanisms and applications in forensics, chemistry, and biology, *J. Mass Spectrom.*, 2005, 40, 1261-1275.
43. Ifa D. R., Gumaelius L. M., Eberlin L. S., Manicke N. E. and Cooks R. G., Forensic analysis of inks by imaging DESI mass spectrometry, *Analyst*, 2007, 132 (5), 461-467.
44. Cooks R. G., Ouyang Z., Takats Z. and Wiseman J. M., Ambient Mass Spectrometry, *Science*, 2006, 311 (5767), 1566-1570.
45. Chen H, Talaty N. N., Takats Z. and Cooks R. G., Desorption Electrospray Ionization Mass Spectrometry for High-Throughput Analysis of Pharmaceutical Samples in the Ambient Environment, *Analytical Chemistry*, 2005, 77 (21), 6915-6927.
46. Justes D. R., Talaty N., Cotte-Rodriguez I. and Cooks R. G., Detection of explosives on skin using ambient ionization MS, *Chem. Commun.*, 2007, 21, 2142-2144.
47. Cotte-Rodriguez I., Takats Z., Talaty N., Chen H. and Cooks R. G., DESI of Explosives on Surfaces: Sensitivity and Selectivity Enhancement by Reactive DESI, *Anal. Chem.*, 2005, 77, 6755-6764.
48. Pan Z., Gu H., Talaty N., Chen H., Shanaiah N., Hainline B. E., Cooks R. G. and Raftery O., Principal component analysis of urine metabolites detected by NMR

- and DESI-MS in patients with inborn errors of metabolism, *Analytical and Bioanalytical Chemistry*, 2007, 387 (2), 539-549.
49. Kaur-Atwal G., Weston D. J., Green P. S., Crosland S., Bonner P. L. R. and Creaser C. S., Analysis of tryptic peptides using DESI combined with ion mobility spectrometry/mass spectrometry, *RCM*, 2007, 21, 1131-1138.
 50. Shin V. S., Drolet B., Mayer R., Dolence K. and Basile F., DESI-MS of Proteins, *Anal. Chem.*, 2007, 79, 3514-3518.
 51. Song V., Talaty N., Tao W. A., Pan Z. and Cooks R. G., Rapid ambient mass spectrometric profiling of intact, untreated bacteria using DESI, *Chem. Commun*, 2007, 1, 61-63.
 52. Sparrapan R., Eberlin L. S., Haddad R., Cooks R. G., Eberlin M. N. and Augusti R., Ambient Eberlin reactions via desorption electrospray ionization mass spectrometry, *Journal of Mass Spectrometry*, 2006, 41(9), 1242-1246.
 53. Chen H., Cotte-Rodriguez I. and Cooks R. G., cis-diol functional group recognition by reactive desorption electrospray ionization (DESI), *Chemical Communications*, 2006, 6, 597-599.
 54. Cody R. B., Laramée J. A. and Durst H. D., Versatile New Ion Source for the Analysis of Materials in Open Air under Ambient Conditions, *Anal. Chem.*, 2005, 77, 2297-2302.
 55. <http://www.jeolusa.com/PRODUCTS/AnalyticalInstruments/MassSpectrometers/AccuTOFDART/AccuTOFDARTTechnology/tabid/449/Default.aspx>
 56. Tanaka K., Waki H., Ido H., Akita S. and Yoshida T., Protein and polymer analysis up to m/z 100 000 by laser ionization time-of-flight mass spectrometry, *Rapid Commun. Mass Spectrom.* 1988, 2, 151-153.
 57. Tanaka K., The Origin of Macromolecule Ionization by Laser Irradiation (Nobel Lecture), *Angew. Chem. Int. Ed.*, 2003, 42, 3861-3870.
 58. Karas M., Bachmann O., Bahr U. and Hillenkamp., Matrix-Assisted Laser Desorption Ionization Mass Spectrometry, *Int. J. Mass Spec. Ion Proc.*, 1987, 78, 53-68.
 59. Karas M. and Hillenkamp F., Laser Desorption of Proteins with Molecular Masses Exceeding 10,000 Daltons, *Anal. Chem.*, 1988, 60, 2299-2301.
 60. Karas M., Bahr U. and Giessman U., MALDI-MS, *Mass Spectrom. Rev.*, 1991, 10, 335-357.
 61. Knochenmuss R., A Quantitative Model of UV MALDI Including Analyte Ion Generation, *Anal. Chem.*, 2003, 75, 2199-2207.
 62. Kruger R. and Karas M., Formation and fate of ion pairs during MALDI analysis: anion adduct generation as an indicative tool to determine ionization processes, *J. Am. Soc. Mass Spectrom.*, 2002, 13, 1218-26.

63. Zenobi R., Knochenmuss R., Ion formation in MALDI MS, *Mass Spectrom. Rev.*, 1999, 17, 337-366.
64. Oreisewerd K., Berkenkamp S., Leisner A., Rohlfing A. and Menzel C., Fundamentals of MALDI mass spectrometry with pulsed infrared lasers, *Int. J. Mass Spectrom.*, 2003, 226, 189-209.
65. Lavine G., and Allison J., Bumetanide as a matrix for prompt fragmentation MALDI and demonstration of prompt fragmentation/PSD MALDI MS, *J. Mass Spectrom.*, 1999, 34: 741-8.
66. <http://www.psrc.usm.edu/mauritz/maldi.html>
67. Westman A., Nilsson C. L. and Ekman R., Matrix-Assisted Laser Desorption/Ionization Time-of-Flight Mass Spectrometry Analysis of Proteins in Human Cerebrospinal Fluid, *Rapid Commun. Mass Spectrom.*, 1998, 12, 1092–1098.
68. Haag A. M., Chaiban J., Johnston K. H. and Cole R. B., Monitoring of Immune Response by Blood Serum Profiling Using Matrix-Assisted Laser Desorption/Ionization Time-of-Flight Mass Spectrometry, *J. Mass Spectrom.*, 2001, 36, 15–20.
69. Gobom J., Kraeuter K. O., Persson R., Steen H., Roepstorff P. and Ekman R., Detection and Quantification of Neurotensin in Human Brain Tissue by Matrix-Assisted Laser Desorption/Ionization Time-of-Flight Mass Spectrometry, *Anal. Chem.*, 2000, 72, 3320–3326.
70. Krishnamurthy T. and Ross P. L., Rapid Identification of Bacteria by Direct Matrix-Assisted Laser Desorption/Ionization Mass Spectrometric Analysis of Whole Cells, *Rapid Commun. Mass Spectrom.*, 1996, 10, 1992–1996.
71. Cornett D. S., Reyzer M. L., Chaurand P. and R. M. Caprioli, MALDI Imaging Mass Spectrometry: Molecular Snapshots of Biochemical Systems, *Nat. Meth.*, 2007, 4, 828–833.
72. McDonnell L. A. and Heeren R. M. A., Imaging Mass Spectrometry, *Mass Spectrom. Rev.*, 2007, 26, 606–643.
73. Annan R. S. and Carr S. A., Phosphopeptide Analysis by Matrix-Assisted Laser Desorption Time-of-Flight Mass Spectrometry, *Anal. Chem.*, 1996, 68, 3413–3421.
74. Lennon J. J. and Walsh K. A., Locating and Identifying Posttranslational Modifications by In-Source Decay During MALDI-TOF Mass Spectrometry, *Protein Sci.*, 1999, 8, 2487–2493.
75. Marshall, A. G., Hendrickson, C. L. and Shi, S. D. H., *Anal. Chem.*, 2002, 74, 253A–9A.
76. <http://www.files.chem.vt.edu/chem-ed/ms/quadrupo.html>

77. Dawson, P. H., Quadrupole Mass Analyzers: Performance, Design and Some Recent Applications, *Mass Spectrom. Rev.* 1986, 5, 1-37.
78. Paul, W., Electromagnetic Traps for Charged and Neutral Particles, *Nobel Prize Lectures in Physics*, 1993, 601-622.
79. Liyu Y., Amad M. H., Winnik W. M., Schoen A. E., Schweingruber H., Mylchreest I., Rudewicz P. J., Investigation of an Enhanced Resolution Triple Quadrupole Mass Spectrometer for High-Throughput LC-MS/MS Assays, *Rapid Commun. Mass Spectrom.* 2002, 16, 2060-2066.
80. Paul, W. and Steinwedel, H. S., 1960, US Patent 2939952.
81. Douglas D. J., Frank A. J. and Mao D., Linear ion traps in mass spectrometry, *Mass Spectrom. Rev.*, 2005, 24, 1–29.
82. Stephens W. E., A Pulsed Mass Spectrometer With Time Dispersion, *Phys. Rev.* 1946, 69, 691.
83. Wolff M. M., Stephens W. E., A Pulsed Mass Spectrometer With Time Dispersion, *Rev. Sci. Instrum.*, 1953, 24, 616-617.
84. Wiley W. C., McLaren I. H., Time-of-Flight Mass Spectrometer With Improved Resolution, *Rev. Sci. Instrum.*, 1955, 26, 1150-1157.
85. Guilhaus M., The Return of Time-of-Flight to Analytical Mass Spectrometry, *Adv. Mass Spectrom.* 1995, 13, 213-226.
86. Guilhaus M., Mlynski V., Selby D., Perfect Timing: TOF-MS, *Rapid Commun. Mass Spectrom.* 1997, 11, 951-962.
87. <http://www.kore.co.uk/tutorial.htm>
88. Cotter, R. J., Time-of-Flight Mass Spectrometry for the Analysis of Biological Molecules. *Anal. Chem.* 1992, 64, 1027A-1039A.
89. Schwartz J. C., Wade A. P., Enke C. G. and Cooks, R. G., Systematic delineation of scan modes in multidimensional mass spectrometry, *Anal. Chem.*, 1990, 62, 1809–18.

CHAPTER II**2 Recent Ambient Ionization Methods for Mass spectrometry:
Paper Spray and Leaf Spray****2.1 Introduction**

The development and the successive commercial availability of atmospheric pressure ionization sources, such as electrospray ionization, has given greater flexibility within mass spectrometric analysis, and has overcome a number of issues in bridging the gap between the prepared sample and its introduction into the mass spectrometer vacuum system. ESI has allowed analysis of a wide range of compounds present in solution phase, relying upon solvent evaporation and charge-driven transfer into a free gas-phase ion population, which can be sampled by the vacuum system of the mass spectrometer. Particularly in the context of liquid chromatographic (LC) separations, the ability to introduce an MS-compatible LC eluent stream was revolutionary. However, it soon became evident that sample preparation prior to introduction, for example purification with solid phase extraction (SPE) and liquid chromatography (LC), was required for complex samples and pure analytes still required dissolution in a suitable solvent for sample introduction.

Alternative approaches for sample ionization in the condensed phase, using matrix-assisted laser desorption ionization (MALDI) have also been utilized widely to increase the range of sample types, functionalities and molecular weights amenable to mass spectrometric detection. Extensive sample preparation is required for MALDI in the form of dissolving the sample in a suitable solvent, spotting together or coating with an energy absorbing matrix solution, prior to spotting a small volume onto a target plate, usually placed inside the vacuum housing of the mass spectrometer. Therefore, ESI, MALDI and all the traditional atmospheric pressure ionization (API) sources, such as atmospheric pressure chemical ionization (APCI) and atmospheric pressure photo

ionization (APPI) etc., still require extensive sample-preparation steps before the sample can be dissolved in or coated with a specially selected suitable matrix that is amenable to and required by the analytical system.

With the introduction of desorption electrospray ionization (DESI) and direct analysis in real time (DART), for the first time, it became possible to analyze samples directly in their native condition, bypassing most elements of the analytical system and transferring ions into the mass spectrometer without any sample-manipulation or sample-preparation steps. Ambient desorption ionization techniques, in a single operational step, successfully bridged the gap between the ambient environment, where condensed phase samples are present, and the vacuum system, where analysis takes place. The development of DESI created an awareness of the potential of open ambient environment analysis and sparked a new sub-field in MS. The novelty of this concept is demonstrated by the rapid introduction of 15 new methods just in three years (2005-2008), summarized and described accurately by Cooks et al. [1]. Boundaries between techniques can be somewhat blurred, and some instances have arisen where very similar techniques have received rather disparate names or acronyms, or indeed have been renamed.

The distinction between atmospheric pressure ionization and ambient ionization is vital in gaining clearer understanding of the impact of these new methods. Whilst ambient ionization methods often have operational commonality with atmospheric pressure ionization, techniques that fall strictly under the ambient ionization group display a number of basic characteristics: namely the direct analysis of untreated samples or objects in the open environment, while largely maintaining the native condition and spatial integrity of the sample. Here, analyte ions derived from the sample, but not the whole sample itself, are transferred into the mass spectrometer. These rapid techniques offer unprecedented flexibility in sample analysis in the open environment, often remote from the mass spectrometer, and have made a significant impact on the world of analytical science. A more recent overview of the ambient ionization methods in MS field and their impact in analytical sciences can be found in a critical review prepared by Weston D. J. [2].

The more established ambient ionization techniques like DESI and DART were described in chapter I (paragraphs 1.4.3.5 and 1.4.3.6, respectively). Here instead, will be given a detailed description and the impact on modern analytical science of two new ambient ionization techniques, paper spray (PS) and leaf spray (LS), introduced respectively in 2010 and 2011 by Cooks group.

2.2 Paper Spray Ionization for Mass Spectrometry (PS-MS)

Paper spray is a recently developed ambient ionization method for direct mass spectrometric analysis of complex mixtures [3]. In PS experiments the paper is cut to a sharp triangular tip (1-10 cm long, 0.5-5 cm base width), a small volume of solvent (<10 micro liter) is added and a high voltage (2-5 kV) is applied to generate charged gas phase ions for mass spectrometry. The tip of paper is held usually 0,3-1 cm from mass spectrometer inlet (figure 2.1).

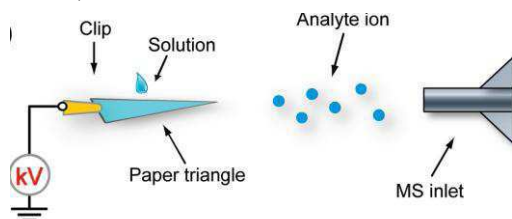


Figure 2.1. Schematic illustration of paper spray for MS analysis [4].

In PS, samples can be loaded in different ways: i) liquid samples can be loaded onto the triangle paper without any pretreatment and sprayed directly as the voltage is applied; ii) samples can be preloaded on paper, allowed to get dried and the successive solvent addition and the high voltage application induce a spray of charged droplets at the tip of the triangle, iii) samples can first be transferred from surfaces using the paper as a wipe and then spraying it as in ii); iv) for applications where paper chromatography is used, components of the mixture can first be separated on paper, and the separated components can be analyzed by PS-MS (simply cutting a triangle of paper containing the desired component). Pneumatic assistance is not required to transport the analyte and the experiments are done in the open lab environment, holding the tip of the paper triangle about >3 mm from mass spectrometer inlet. Ions of a wide variety of compounds, including small organic compounds, peptides, and proteins were detected operating in the above conditions (i-iv) [3-4,6]. The use of paper to generate electrospray was reported previously by Fenn [5], but no further investigations about its applicability were done.

Although some other porous materials potentially could also be used for spray ionization, the commercial availability at low cost and the ease of fabrication and chemical modification of paper make it a superior candidate for producing sample cartridges that have multiple functions for simple sample treatment and ionization. Paper, typically made from cellulose, is a hydrophilic porous material that can hold a certain amount of liquid. Wet paper is conductive, and the network of cellulose offers microchannels for liquid (including dissolved analyte) transport. Presumably the high electric potential applied between the paper triangle and MS inlet generates an electric field that induces a charge that accumulates at the apex of the paper triangle. Similar to

electrospray, the Coulombic force breaks the liquid to form charged droplets, which undergo subsequent desolvation processes to generate dry ions. Taylor cone at the tip was observed when examined under a microscope; the mist of fine droplets generated were observed under strong illumination [3]. The Taylor cone and the spray typically disappear after about few minutes of spraying, presumably because of the loss of solution via the spray as well as the evaporation of solvent. The mechanism of spray generation, in the positive and negative ion modes, is not fully clear and require further investigations.

In order to evaluate the influence of paper on PS performance, Liu et al. [4] used six types of commercially available paper as a substrate for paper spray ionization: four filter papers of different pore sizes, glass fiber paper, and chromatography paper. Filter papers and the chromatography paper were made from cellulose, while the glass fiber paper was made from glass microfiber. Paper triangles of the same dimensions were cut from these materials, and a 10 μ L methanol/water solution containing cocaine (200 ng/mL) was added to each in order to record the mass spectra. Each type of paper showed different chemical background containing peaks of various intensities which were attributed to the additives used in the paper industry, either as part of the formulation or as process contaminants. The poorest performance was observed for glass fiber paper for which the total intensity was 2 orders of magnitude lower than any of the others and for which the cocaine peak could not be identified. The highest quality spectrum with the highest *S/N* value for cocaine was obtained with chromatography paper. These findings indicate that the choice of paper is critical and may affect the results of the analysis.

In another set of analysis was investigated the positioning tolerance, as an important factor for judging the ease of use of an ionization source. It was found that accurate positioning is not required for implementation of paper spray since a stable high intensity can be obtained with the paper tip positioned anywhere in an area of about 5x10 mm (*x* by *y*) respect the inlet of mass spectrometer (figure 2.2).

The performance of paper spray for the analysis of real samples which involve complex matrices such as raw and dried biological fluids has been examined as well. The monitoring of drugs in whole blood is of critical importance in therapeutic drug development and clinical disease treatment as well as in forensic applications. Storing blood samples as dried blood spots on paper is a common procedure of sample storage for neonatal screening [8], and recently it has also been explored for the analysis of therapeutic drugs. Dried blood spots on paper can be stored for years before analysis, without special storage conditions. The analysis of whole blood using traditional mass spectrometric methods typically requires the removal of the blood cells and further separation/purification processes to clean the plasma.

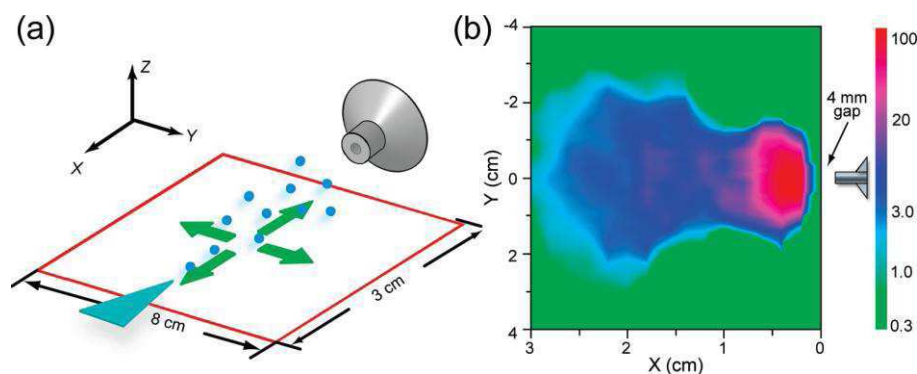


Figure 2.2. Tolerance of paper spray ionization to position of the paper tip, using a cocaine solution (10 μL methanol/water, 200 ng/mL) and chromatography paper. A paper triangle was mounted on a 2D moving stage and was moved 8 cm in the y-direction and 3 cm in the x-direction with a 2 mm increment for each step. (a) Illustration of the spatial movement of the paper tip. (b) 2D contour plot showing the relative intensity of m/z 304 (cocaine) as a function of the paper tip location on the x-y plane [4].

Therefore, using paper spray, direct MS analysis of the therapeutic drugs in blood can be achieved easily by wetting the paper with methanol/water solution without any sample preparation. In fact, Cooks and co-workers developed methods for analyzing therapeutic and illicit drugs from dried blood spots. The detailed procedure for analysis of dried blood spots using paper spray is as follows: 1) 0.4 μL of whole blood spiked with a therapeutic drug is directly applied to the center of a triangle of paper; 2) it is allowed to dry in air for about 1 min to form a dried sample spot with a diameter of about 2 mm; 3) a small volume ($<10 \mu\text{L}$) of solvent (usually methanol/water 1:1, v/v) is then applied near the base of the paper triangle; 4) apply the voltage (3-5 kV) and acquire the MS spectra in MS or MS/MS mode. This protocol was used to detect the atenolol (a blocker drug used in cardiovascular disease) spiked in bovine blood samples. A S/N ratio of about 4 was achieved with MS analysis of atenolol in dried blood spots at an original concentration of 1 $\mu\text{g/mL}$ (400 pg absolute analyte amount), while a much better S/N could be achieved at much lower concentrations with MS/MS analysis, for instance, at 50 ng/mL (20 pg absolute). Use of an internal standard, such as a deuterated drug compound added to the blood sample, allowed good quantitation (RSD $<5\%$ for imatinib) of the drug concentrations in whole blood samples. Figure 2.3 shows the photographs of the dried blood spot after 1 min of spray time; presumably most of the blood cells remained on the paper, while the drug and other molecules dissolved in methanol/water were carried to the paper tip and released in the spray. The same procedure was tested and applied successfully for the analysis of illicit drugs in undiluted urine samples.

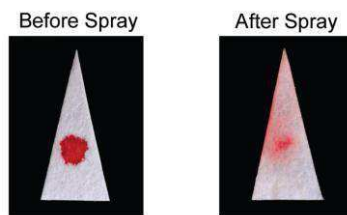


Figure 2.3. Photographs of PS before and after analysis of dried blood spots containing a therapeutic drug (atenolol) [4].

Development of the paper spray MS analysis of dried sample spots provides a new means for direct characterization of biofluids without sample preparation and consequently without a need for human intervention during the analysis process. This should have a significant impact on the implementation of MS technologies for clinical analysis in laboratories as well as at point-of-care facilities.

PS was used also for food analysis purposes. 10 μL cola drink were dropped on the paper and sprayed operating in both polarities. In the positive mode, the peak due to protonated caffeine was found to dominate the mass spectrum, due to the high concentration of caffeine (100 $\mu\text{g}/\text{mL}$) in this drink. In the negative mode, benzoate ion, from potassium benzoate (a food preservative) and acesulfame anion from acesulfame potassium (an artificial sweetener) could be identified easily by MS/MS analysis.

Paper spray ionization can also be used for the analysis of surfaces by wiping the surface of interest with a paper triangle, adding solvent, and applying a high voltage. Small amounts (pictogram range,) of cocaine, heroin and explosives have been detected in areas of 1 cm^2 to many cm^2 by MS/MS [3]. This approach of sample collection by paper wiping followed by analysis using paper spray was also adapted for fast analysis of agrochemicals on fruits.

For analysis of target analytes which have relatively low ionization efficiencies and relatively low concentrations in mixtures, derivatization is often necessary to provide adequate sensitivity in the analysis. In paper spray, online derivatization can also be implemented by using methanol/water solutions containing reagents appropriate for targeted analytes. If the reagents to be used are stable on paper, they may also be added onto the paper when the paper triangles and the sample cartridges are fabricated, long before they are used to load and analyze the samples.

One unique feature of paper spray is the low consumption of sample as well as consumables required for the analysis, a feature which is particularly suitable for on-site clinical analysis. In fact, it has been demonstrated that paper spray can also be used for direct analysis of biological tissues. Less than 1 μL of tissue sample is enough for direct detection of hormones, lipids etc. without any sample pretreatment [7]. This method can be coupled with tissue biopsy as a point-of-care medical test to probe the chemical information of biological tissues.

Paper is an important medium in chemical separations, and this feature can be incorporated into a version of the PS experiment which utilizes separation by chromatography on paper. The components of the mixture can first be separated on paper, and the separated components can be analyzed by MS simply cutting a triangle of paper containing the desired separated component and applying the voltage on triangle's base.

The above examples indicating the good performance of paper spray, its simplicity of use (respect the consolidated ionization techniques), the non necessity of sample pretreatment, low volumes of solvent needed etc. make it a potential candidate for its diffusion in analytical laboratories.

2.3 Leaf Spray Mass Spectrometry (LC-MS)

Leaf spray (LS) is a new ambient ionization method for mass spectrometry introduced this year by Cooks et al. for direct analysis of plant tissues [9]. It is a version of paper spray with the difference that leaf spray uses the plant tissue itself to generate gas phase ions for mass spectrometry instead of using paper as substrate for sample loading. Hence, no other ionization device or support is needed since the vegetal tissue acts simultaneously as an ionization source and as the sample. In leaf spray experiments, plant tissues are cut to a sharp triangular tip (1-3 cm long, <1 cm base width, and < 5 mm of thickness) and sprayed directly. It should be pointed out that any other geometry containing a sharp tip work well and the choice of triangular shape is only due to the easiness of sharp tip formation. Plant tissues which have natural tips (e.g., sprouts or plants with needles) can be used directly, hence cutting is not necessary. As the high voltage is applied to the base of the plant tissue tip, held 0,3-1 cm from mass spectrometer inlet, and a small volume of solvent (1-2 μL) is added directly on tissue, signals will appear in mass spectrum indicating the formation of charged gas phase ions. Plant tissues which are naturally sufficiently juicy (high water content) do not require solvent addition at all (figure 2.4). However, small volumes of solvent added (1-2 μL) to the tissue triangle often show higher signal intensities, better S/N ratios and sometimes richer signal mass spectra.

The spray duration goes from 1 to several minutes depending on the volume of solvent added and the juiciness of the vegetal tissue. This spray duration is sufficient to perform full scan, tandem mass spectrometry (MS/MS) and exact mass experiments.

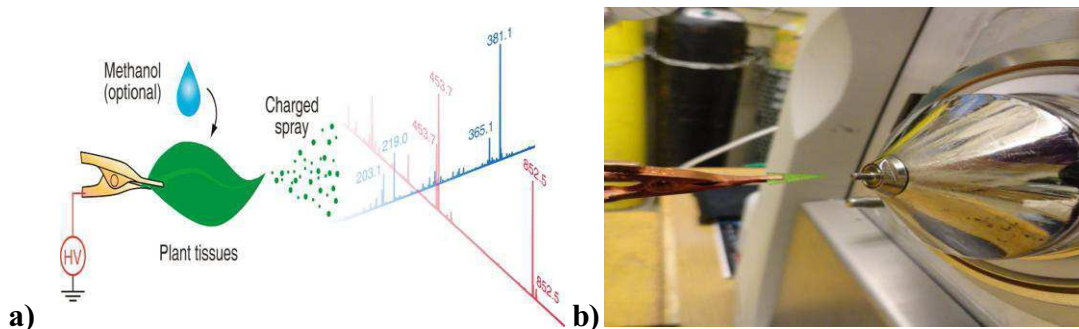


Figure 2.4. Leaf spray operation mode. Tissues which do not have a natural sharp tip are cut to a triangle and held by a high voltage copper clip in front of the inlet of a mass spectrometer. (a) scheme of LS ionization of a leaf with natural tip; b) LS photograph of a triangular tip cut from cucumber peel [10].

The leaf spray is not limited only to leaf material, as one may be misled by its name, but any other part of plant including root, stem, flower, fruit, and seed can be used. In fact, several compounds could be analyzed directly from these plant parts (potato, onion, cabbage, ginger, cranberry, ginkgo, arabidopsis thaliana etc.) without sample preparation, except that small triangle sharp point cut when necessary. The variety of compounds detected range from, amino acids, alkaloids, flavonols, carbohydrates, organic acids, fatty acids, and phospholipids.

Another feature of LS is the possibility of *in vivo* experiments. In fact, the plant may be brought to the mass spectrometer (e.g., potted plants) or (ii) the mass spectrometer can be brought to the plant. We have already seen the former one, which is more traditional, and the second one was demonstrated using a Mini 10.5 mass spectrometer. The mass spectrum was acquired using a standard leaf spray protocol on tomato leaf and was perfectly overlapped with that obtained *on site* with Mini 10.5 mass spectrometer [9].

LS may also be used to monitor seasonal variations of chemicals during plant/fruit development.

Besides fresh and living plant tissue, leaf spray works very well on dehydrated plant tissues provided spray solvent is applied. Wetting the dried green tea leaves with methanol and then spraying them directly, in positive mode, permitted the detection of several compounds (choline, caffeine and the potassium adducts of glucose and sucrose). In negative ion mode, on the other hand, were detected a series of phytochemicals, most of which were identified as flavan-3-ols.

Leaf spray is not suited to high spatial resolution imaging analysis on plant tissues as are probe based MS methods. However, it does give useful information about the distribution of chemicals in different parts of a plant. Besides the speed, simplicity, and sensitivity achieved in identifying endogenous compounds in plants, direct

monitoring of metabolic processes in plants using this approach (LS-MS) may become possible.

The choice of solvent used to realize the direct ionization of chemicals from drier samples is expected to have a selective role on the classes of compounds to be extracted and analyzed from the same sample. Liu et al. [9], tested a series of organic solvents with different polarity and dielectric constants: methanol, dichloromethane, hexanes, acetonitrile, acetone, and chloroform gave significantly different spectra from peanuts when the above spray solvents were used. The spectra acquired using methanol, acetone, and acetonitrile look similar, but different solvents polarities cause some differences in relative efficiencies of extraction and ionization.

References

1. Venter A., Nefliu M., Cooks R. G., Ambient desorption ionization mass spectrometry, *Trends in Analytical Chemistry*, 2008, 27, 284-290.
2. Weston D. J., Ambient ionization mass spectrometry: current understanding of mechanistic theory; analytical performance and application areas, *Analyst*, 2010, 135, 661–668.
3. He Wang, Jiangjiang Liu, R. Graham Cooks, and Zheng Ouyang, *Angew. Chem. Int. Ed.* 2010, 49, 877–880.
4. Jiangjiang Liu, He Wang, Nicholas E. Manicke, Jin-Ming Lin, R. Graham Cooks, and Zheng Ouyang, *Analytical Chemistry*, 2010, 82, 2463-2471.
5. Fenn, J. B. U.S. Patent 6,297,499, 2001.
6. Nicholas E. Manicke, QianYang, He Wang, Sheran Oradua, Zheng Ouyang, R. Graham Cooks, *International Journal of Mass Spectrometry*, 300, Issues 2-3, 2011, 123-129.
7. Wang H., Manicke N. E., Yang Q, Zheng L, Shi R, Cooks R. G., Ouyang Z., Direct Analysis of Biological Tissue by Paper Spray Mass Spectrometry, *Anal. Chem.*, 2011, 83, 1197–1201.
8. Azzari Ch., la Marca G., Resti M., Neonatal screening for severe combined immunodeficiency caused by an adenosine deaminase defect: A reliable and inexpensive method using tandem mass spectrometry, *J. Allergy Clin. Immunol.*, 2011, 127, 1394-1399.
9. Liu J., Wang H, Cooks R. G., Ouyang Z., Leaf Spray: Direct Chemical Analysis of Plant Material and Living Plants by Mass Spectrometry, *Anal. Chem.* 2011, 83, 7608–7613.
10. Malaj N., Ouyang Z., Sindona G., Cooks R.G., Analysis of agrochemicals by direct vegetable tissue spray mass spectrometry, Turkey Run Analytical Chemistry Conference, Marshall, IN, USA, 30/9/2011-1/10/2011.

CHAPTER III

Anticholesterolemic Activity of Brutieridin and Melitidin, Two New Statin-Like Flavonoids Isolated from Bergamot Fruit: Computational and *in vivo* Approaches

3.1 Introduction

In this chapter will be presented the results of two studies aiming the determination of biological activity of two new flavonoids, brutieridin and melitidin, isolated from bergamot fruit. In the first part will be given a short introduction of flavonoids, with particular attention on flavonoids of bergamot fruit. After that, results of a computational study that was performed in order to determine the ability of brutieridin and melitidin to inhibit the activity of HMGR enzyme will be shown. Then, in the last part of this chapter are reported and discussed results of an *in vivo* study carried out in order to determine the anticholesterolemic activity of a bergamot extract enriched with brutieridin and melitidin.

3.2 Flavonoids: structure, activity and availability

Flavonoids are a large class of plant secondary metabolites which share a characteristic structural phenolic moiety. In fact, the skeleton of all members of this family is composed of two aromatic rings (commonly indicated as ring A and B), which are connected through a hetero-cycle (known as ring C), as shown in figure 3.1.

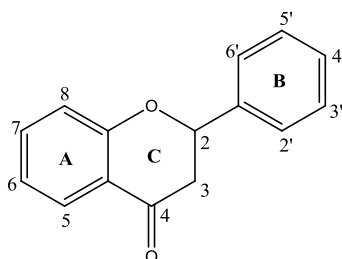


Figure 3.1. Flavonoid skeleton.

Flavonoids may be found as glycosylated derivatives or as aglycones (the forms lacking the sugar moieties). The relatively large number of flavonoids reported is a result of the many different combinations that are possible between polyhydroxylated aglycones

with sugars, usually mono- and di-glycosides. The most common sugar moieties include: glucose, rhamnose, galactose, arabinose, xylose and rutinose. When the site of glycosilation is on one of the hydroxyl groups of aglycone, members are called *O*-glycosides. The most diffused members of this group are those with the sugar moiety bound to the aglycone hydroxyl group at C-7, or in some cases, at the C-3. In addition to these *O*-glycosides, *C*-glycosides (compounds with sugar moieties bound at one of the C-atoms of A, B or C rings) have also been reported in various plants. Di-glycosylated members, are further distinguished between rutinoides (rhamnosyl- α -1,6 glucose linkage) and neohesperidosides (rhamnosyl- α -1,2 glucose linkage), based on the site where rhamnose is linked to glucose (figure 3.2).

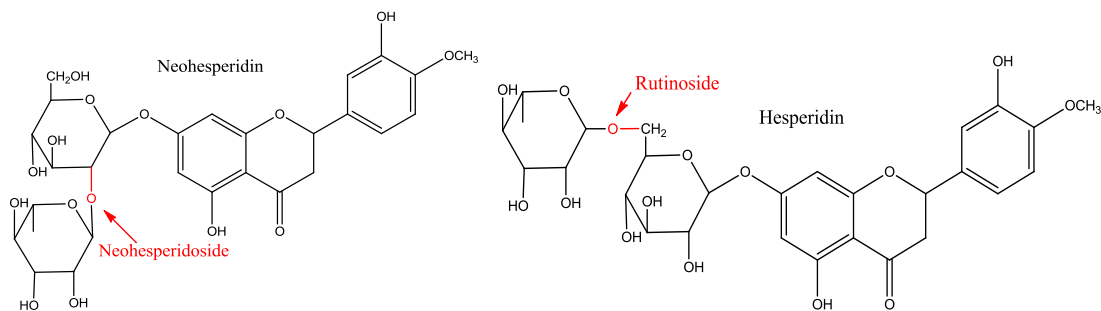


Figure 3.2. Neohesperidoside and rutinoides isomers of di-glycosylated flavonoids.

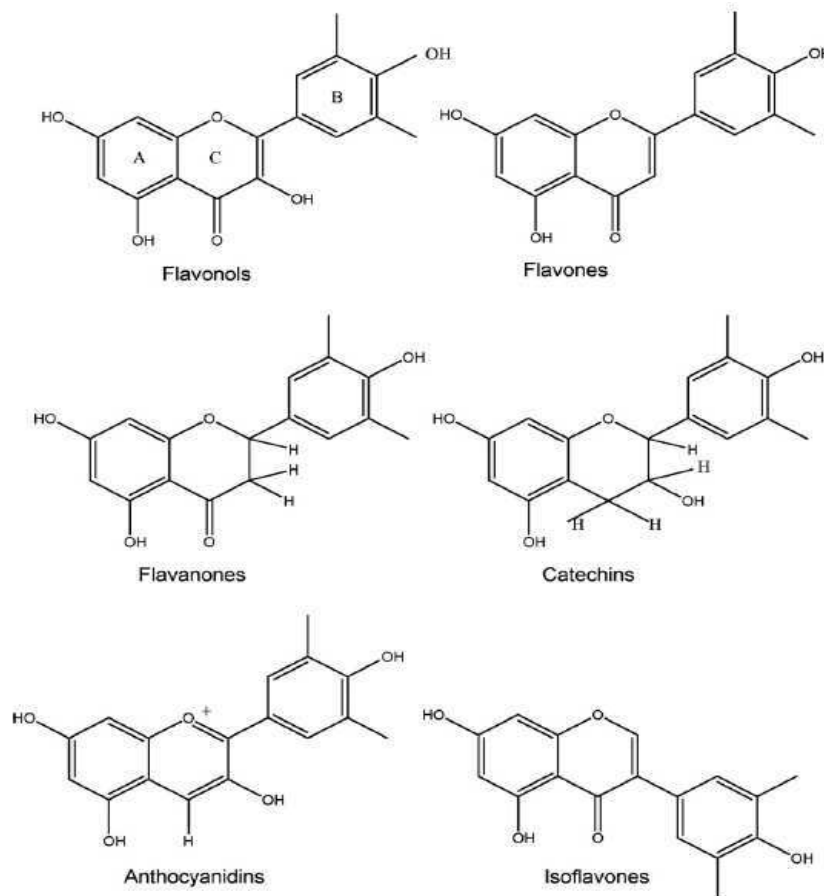


Figure 3.3. Six classes of flavonoids.

According to their molecular structures, flavonoids are divided into six classes: flavones, flavanones, flavonols, isoflavones, anthocyanidins and catechins (or flavanols) (figure 3.3).

All the members are, with few exceptions, plant metabolites deriving from the shikimate pathway and the phenylpropanoid metabolism [1]. They have been indicated to have several health benefits [2]. Flavonoids show a strong antioxidant and radical scavenging activity [3-6] and appear to be associated with reduced risk for certain chronic diseases [7-8], the prevention of some cardiovascular disorders [9-10] and certain kinds of cancerous processes [11-12]. Flavonoids exhibit also antimicrobial [13], and anti-inflammatory activities [14], beneficial effects on capillary fragility (diosmin complex) [15] and antiulcer [16] properties. It should be mentioned that most of the above statements are based on *in vitro* studies, and only a few *in vivo* evidences of the above positive proprieties are confirmed [17]. The mechanism of action is largely unknown [18], probably because most of the studies are focused on *in vitro* tests sometimes using doses much higher than those of humans intake. However, some epidemiological studies have shown an inverse association between risk and intake level of some particular flavonoids, further clinical trials are needed to assess a more precise correlation between the level of flavonoids consumption and human health benefits.

Flavonoids are frequently found in fruits, vegetables and cereals [19-22]. Over the past few years investigations into flavonoids from dietary sources have rapidly increased probably as a consequence of commercials about their health benefits [23-24]. Therefore, in market currently are present lot of products commercialized as food supplements whose active ingredients are plant extracts (fruits, roots, leaves etc.) containing high amounts of flavonoids.

Citrus fruits (orange, mandarin, grapefruit, lemon, bergamot, lime etc.) stand out among the most common flavonoid-rich dietary sources. Glycosylated flavanones and flavones are the most abundant flavonoids in all Citrus fruits. In some of the members of Citrus, low concentrations of aglycones are detected too. Another group of compounds classified as polymethoxyflavones (PMFs) are sometimes found especially in commercial Citrus juices. They are components of the essential oils fraction – flavedo of Citrus peels [25]. Therefore hand-squeezed juices do not contain detectable traces of this class of compounds [26] but commercial juices are rich in PMFs because of the contamination during the industrial processing of fruits to produce juice. The flavonoid composition (and the abundance of each flavonoid) in Citrus juices is variable through the species of Citrus. In table 3.1 are reported the flavonoids identified in hand-squeezed juices of orange, lemon and bergamot fruits.

Calabrian folk medicine has considered, since the introduction of the plant in the middle of XVIII century, bergamot juice as a natural answer to the control of

cholesterol level in blood. These important properties have always been associated to the effect of flavonoids, such as naringin, neoeriocitrin and neohesperidin, present in the order of several hundreds of ppm and to other minor species such as rhoifolin, neodiosmin etc. present at smaller extent. The association of anticholesterolemic activity to flavonoid content lacks of any scientific support. In fact, it can not be possible to explain why other citrus fruits, containing the same species, do not exhibit the healing effect traditionally associated to bergamot.

Table 3.1. Flavonoid composition of hand-squeezed juices of orange, lemon and bergamot fruits.

Orange juice (<i>C. sinensis</i>)		Lemon juice (<i>C. limon</i>)	Bergamot juice (<i>C. bergamia</i> Risso)
Flavanones	Flavones		
Didymin	6,8-di-C-Glu-Apigenin	Eriocitrin	Brutieridin
Eriocitrin	6,8-di-C-Glu-Diosmetin	Hesperidin	Melitidin
Hesperidin	Diosmin	Flavones	Naringin
Narirutin	Neodiosmin	6,8-di-C-Glu-Apigenin	Neoeriocitrin
Neoeriocitrin	Rhoifolin	6,8-di-C-Glu-Diosmetin	Neohesperidin
Poncirin	Isorhoifolin	Diosmin	Poncirin
Neoeriocitrin	Polymethoxyflavones	7-O-Rut-Luteolin	Flavones
Aglycones	Heptamethoxyflavone	Aglycones	6,8-di-C-Glu-Apigenin
Taxifolin	Nobiletin	Luteolin	6,8-di-C-Glu-Diosmetin
Acacetin	Sinensetin		Diosmin
	Tangeretin		Neodiosmin
			Rhoifolin

3.3 On the Inhibitor Effects of Bergamot Juice Flavonoids Binding to the 3-Hydroxy-3-methylglutaryl-CoA Reductase (HMGR) Enzyme

Bergamot (*Citrus bergamia* Risso) is a genus Citrus fruit member belonging to the family of Rutaceae, subfamily of Esperidea. It is a very sensitive plant that has found its natural habitat in a narrow zone in the province of Reggio Calabria (Italy). The fruit flavedo (external part of the peel) is the only tissue of bergamot used in industry as a source of essential oils. In fact, it is widely used in cosmetic industry (for production of perfumes, body lotions, soaps), in pharmaceutical industry (for production of solutions with antiseptic and antibacterial proprieties) the same as in food industry (used as aroma source for production of sweets and liquors). Bergamot juice and albedo (the white tissue between flavedo and the pulp), on the other hand, have no important industrial applications, and are actually waste products. Recently, bergamot fruit has attracted some attention because of its remarkable content in flavonoids [22, 27-28], in

particular way, since Sindona et al. reported the presence of two new flavonoids in bergamot juice, identified and isolated by LC-MS, MS/MS and NMR methods [29-30].

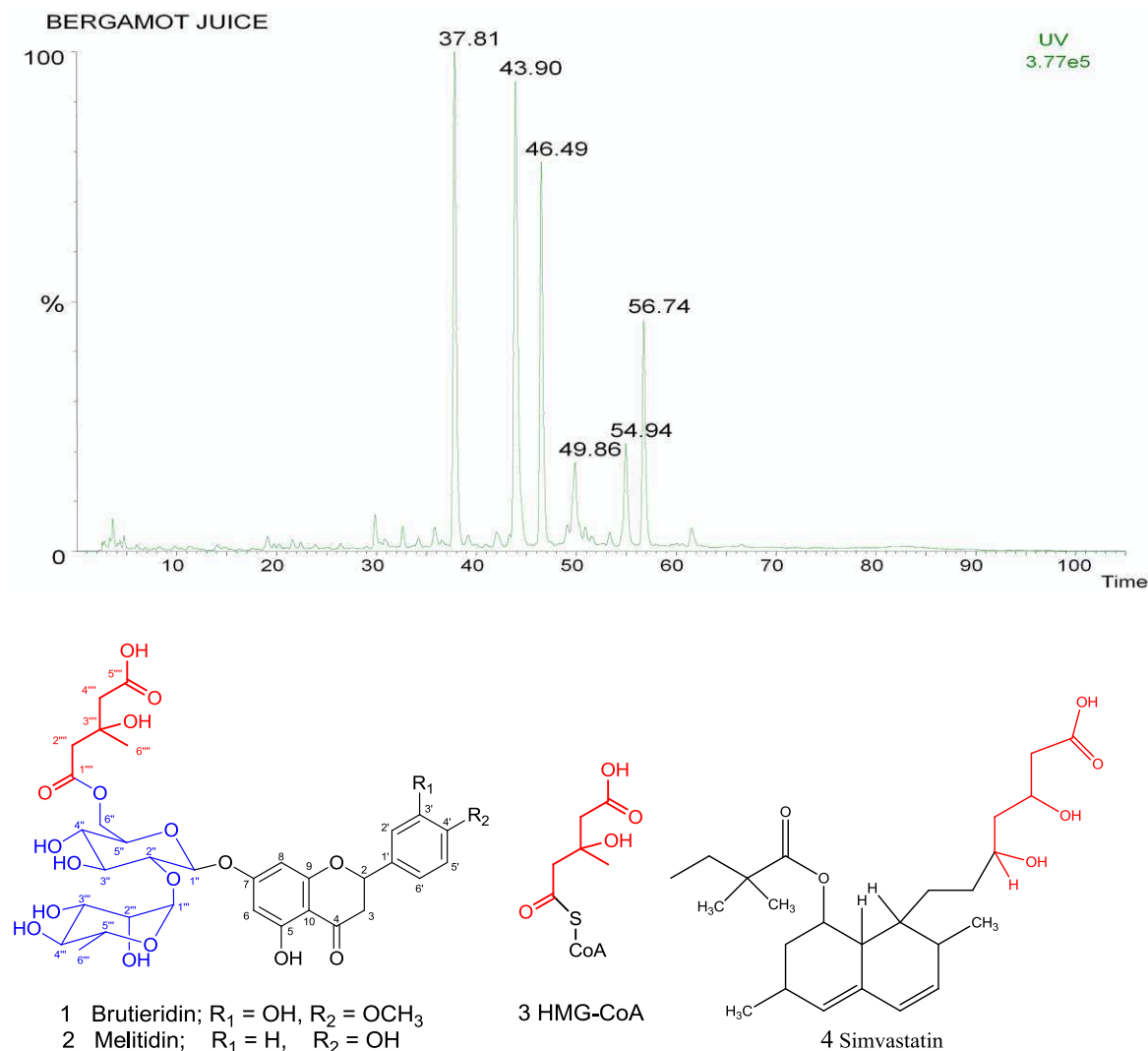


Figure 3.4. Top: UV Chromatogram of bergamot juice: neoeriocitrin (rt 37,81), naringin (rt 43,90), neohesperidin (rt 46,49), neodiosmin (rt 49,86), melitidin (rt 54,94), brutieridin (rt 56,74); Bottom: Structures of brutieridin and melitidin (1 and 2 respectively), and those of HMG's substrate (3) and inhibitor (4). The active HMG moiety is reported in red.

These two new flavonoids, named *brutieridin* (hesperetin 7-(2''- α -rhamnosyl-6''-(3''''-hydroxy-3''''-methylglutaryl)- β -glucoside)) and *melitidin* (naringenin 7-(2''- α -rhamnosyl-6''-(3''''-hydroxy-3''''-methylglutaryl)- β -glucoside)) (figure 3.4) are present in bergamot juice in concentration ranges of approximately 300-500 and 150-300 ppm, respectively.

If we look at the chemical structure of brutieridin, other than the typical aglycone (hesperetin) and the diglycoside (neohesperidoside), there is present a moiety (in red) 3-hydroxy-3-methylglutaric acid (HMG), unusual for flavonoids (1 in figure 3.4). The same HMG moiety is also present in the structure of melitidin (2 in figure

3.4). This HMG moiety is structurally very similar with the substrate of enzyme HMGR (3 in figure 3.4) and with the active portion of its inhibitor drugs, called statins (4 in figure 3.4). Cholesterol is biosynthesized via *mevalonate pathway* in which the key enzyme 3-hydroxy-3-methylglutaryl-CoA reductase (HMGR) catalyzes the conversion of substrate 3-hydroxy-3-methylglutaryl-CoA to mevalonate (figure 3,5), a rate limiting step in whole cholesterol biosynthesis (and all other mevalonate-dependent isoprenoids).

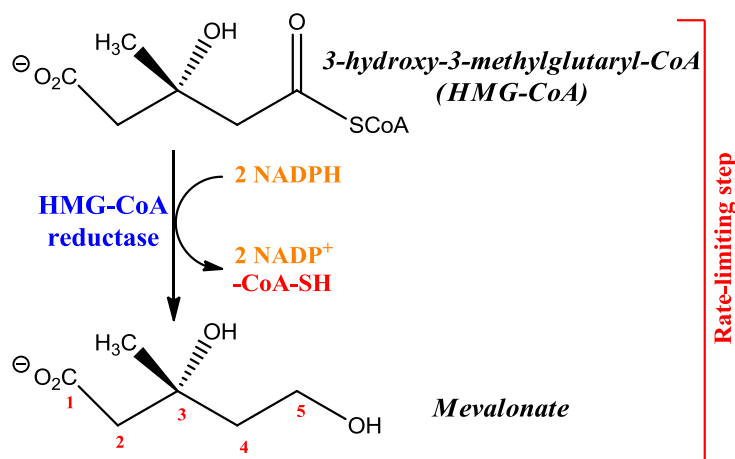


Figure 3.5. The reaction catalyzed by HMGR (and the target of anticholesterolemic drugs- statins).

Therefore, the inhibition of the activity of this enzyme leads to the block of the cholesterol biosynthesis and for this reason it has been indicated as the principal point for non physiological regulation of high blood cholesterol levels. In fact, statins bind competitively to the HMGR active site inhibiting the substrate binding [31-34]. Therefore, blocking the activity of HMGR, statins are able to lower the serum levels of cholesterol. They compete with natural substrate HMG-CoA for the active site of HMGR and are prescribed widely in treatment of hypercholesterolemia.

Being that the structures of brutieridin and melitidin resembles the active portion of statins, we performed a computational study in order to investigate their ability to inhibit HMGR activity. Density Functional Theory (DFT) was applied in order to investigate the interactions of the two new compounds with the active site of the human HMGR enzyme and to have insights on their inhibitory capacity. For purpose of comparison, it was examined even the behavior of simvastatin (4 in figure 3.4) which is an excellent HMGR inhibitor.

The model cluster used to simulate the active site of HMGR enzyme was built starting from the 2.33 Å X-ray structure of human HMGR in complex with simvastatin inhibitor (pdb code = 1HW9) [35]. It was reproduced by considering the five Glu559,

Leu562, Lys735, Leu853 and Ala856 residues and the six Arg590, Val683, Ser684, Asp690, Lys691 and Lys692 residues belonging to the chain A and B of the protein, respectively. Another simple model was used to simulate the *brutieridin/melitidin* statin-like molecules. It consists of a phenyl ring for the flavanone moiety representation and only one sugar molecule, in order to reduce the computational efforts. Simvastatin was considered as such.

The B3LYP optimized structure of the complex between simvastatin and HMGR active site model cluster is illustrated in the figure 3.6a. The minimum energy structure is characterized by several hydrogen bonds as well as hydrophobic interactions. This bonding network obtained through B3LYP computations is in good agreement with that observed in the experimental crystal structure of simvastatin-HMGR complex [34,35], figure 3.7. The binding energy in protein-like environment, was computed to be 47.8 kcal/mol indicating that the binding is energetically favoured, further contributing to the inhibition process.

The B3LYP optimized structure of the complex between brutieridin/melitidin and HMGR active site model cluster is depicted in the figure 3.6b.

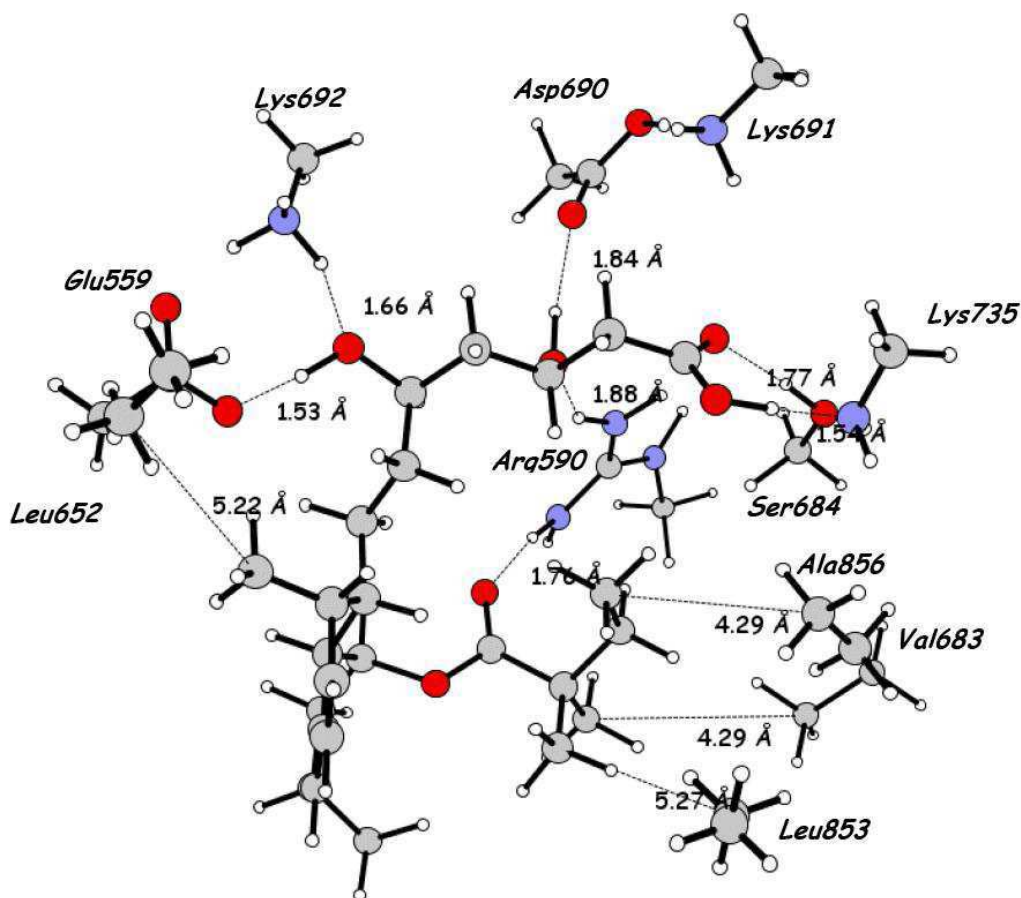


Figure 3.6 (a) (continue)

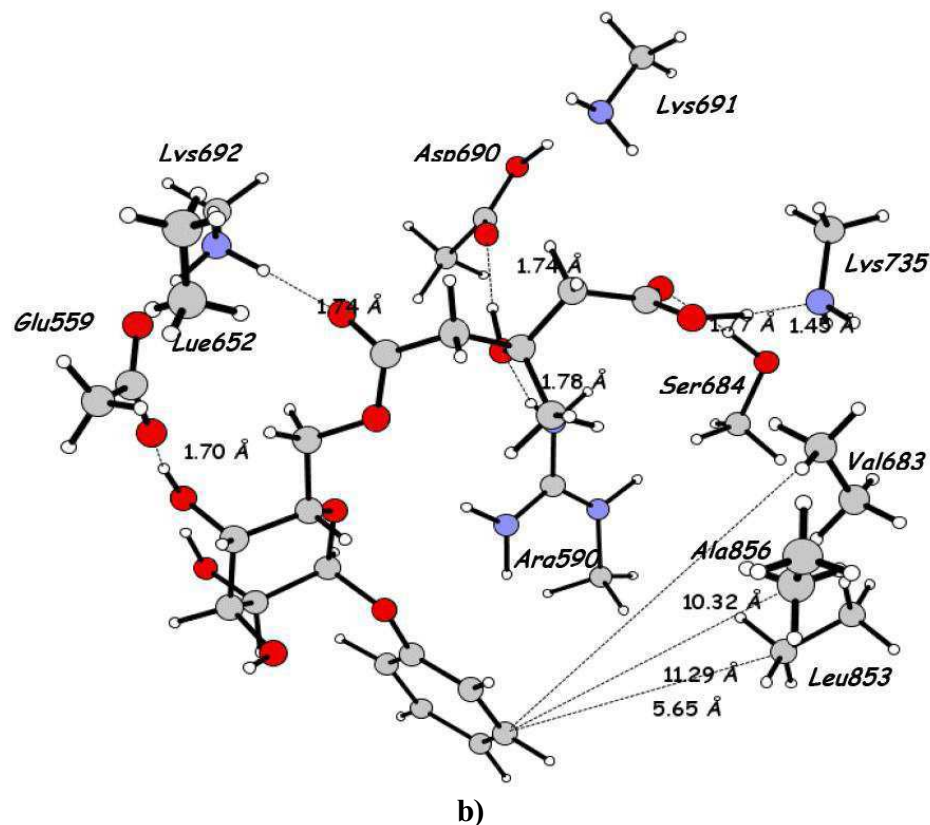


Figure 3.6. a) Interactions of simvastatin-HMGR active site complex; b) interactions of brutieridin/melitidin-HMGR active site complex.

Most of the non covalent bonds found for the binding of simvastatin to HMGR active site are involved in the formation of the complex between brutieridin/melitidin and HMGR enzyme. The B3LYP binding energy in the protein-like medium was computed to be 49.6 kcal/mol. This value is comparable and slightly higher than those exhibited by simvastatin.

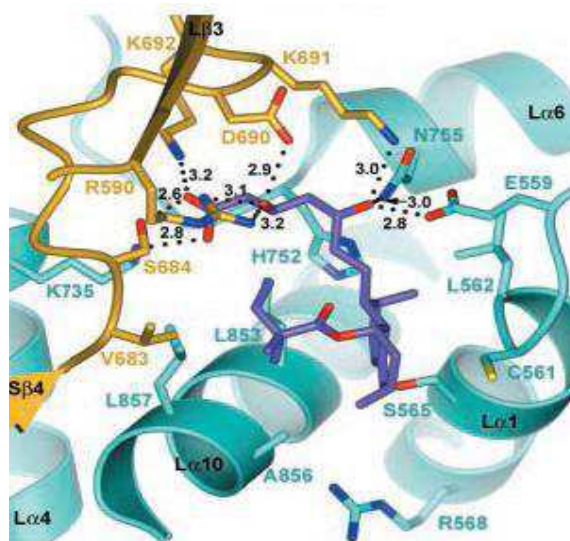


Figure 3.7. X-ray structure of complex simvastatin-HMGR, as reported by references 34-35.

The interactions obtained from computations for the complex HMGR-simvastatin overlap perfectly with the X-ray experimental results obtained for the same complex of HMGR-simvastatin. This is a confirmation of a correct approach used in our computational study. Moreover, the interactions of our compounds in HMGR-brutieridin/melitidin complex are similar with those observed for the complex HMGR-simvastatin. Therefore, the analog interactions and binding energies (respect simvastatin-HMGR complex) in the protein-like medium indicate that brutieridin and melitidin are good candidates to perform the inhibition of HMG-CoA reductase *in vivo*. These findings support the folk medicine indicating bergamot juice able to lower blood cholesterol level, and can be the starting point for other confirmatory studies and bergamot exploitation as a source of anticholesterol compounds. Further details are reported in Appendix I, at the end of this chapter.

3.4 *In vivo* anticholesterolemic activity of a bergamot extract enriched with brutieridin and melitidin *

3.4.1 Introduction

The risk of atherosclerosis and coronary heart disease (CHD) is higher in individuals with elevated concentrations of plasmatic low-density lipoprotein (LDL) [36]. LDLs are a type of lipoproteins that transport cholesterol and triglycerides to extra-hepatic tissues. LDLs are commonly referred as the "bad cholesterol" lipoproteins, in opposition to high-density lipoproteins HDLs, which are frequently referred as "good cholesterol" since their action is to carry the cholesterol back to liver. High levels of LDL cholesterol and triglycerides in serum, accompanied by a reduced HDLs concentration, are associated with an elevated risk of coronary artery diseases [37]. Cholesterol is an essential molecule in many animals, including humans, but is not required in the mammalian diet because cells can synthesize it starting from acetyl-CoA and through mevalonate pathway. The 3-Hydroxy-3-methylglutaryl-CoA reductase (HMGR) is an endoplasmic reticulum bound enzyme that catalyzes, during endogenous cholesterol synthesis, the conversion of HMG-CoA into mevalonate (figure 3.5) [38]. Inhibition of HMGR, the rate-limiting enzyme in cholesterol biosynthesis, has been proven to be one of the most effective approaches for lowering plasma LDL and reducing cardiovascular event rates [39]. As part of a compensatory mechanism to cholesterol depletion in the liver, inhibition of HMGR ultimately leads to the increased production of LDL receptors (LDLR) and subsequent clearance of LDL from systemic circulation [40].

The HMGR inhibitors (statins) are a very effective class of drugs for reducing LDL concentrations. Although statins are the most widely prescribed HMGR inhibitors, the occurrence of adverse side effects (myopathy, liver function abnormalities and statin-associated memory loss) is not a rare event in many patients [41-43]. In this context, the identification of new compounds from natural sources, with anticholesterolemic properties but with no side effects, would be of great interest in order to overcome the disadvantages mentioned above.

The previous computational results (paragraph 3.3) and *in vitro* kinetic results (unpublished data from our lab) clearly indicated the capabilities of brutieridin and melitidin to inhibit the activity of HMGR and consequently to induce the reduction of serum cholesterol.

* Manuscript in preparation for publication.

Now, we have designed the present *in vivo* study, to investigate the effect of a brutieridin/melitidin-enriched bergamot extract on levels of triglycerides (TGs), HDL, LDL and total cholesterol (TC), in hypercholesterolemic rat serum and liver. We compare the anti-cholesterolemic effects of brutieridin/melitidin-enriched bergamot extract with a commercial statin drug, simvastatin. We are also investigating the molecular mechanism elicited by bergamot extract measuring the hepatic gene and protein expression of HMGR, LDLs receptor (LDLR) and FASN in hypercholesterolemic-fed rats, but these experiments are still in progress, therefore, no data will be shown here.

3.4.2 Materials and Methods

3.4.2.1 Brutieridin/melitidin-enriched bergamot extract

The composition of bergamot extract used in this study was as follows: brutieridin 40%; melitidin 20%; all other bergamot phenolic fraction 40%. This brutieridin/melitidin-enriched-extract was obtained from bergamot juice from which were removed partially neoeriocitrin, neohesperidin, naringin and neodiosmin and isolated the fraction containing brutieridin and melitidin by VersaFlash chromatography (more details are reported in chapter 4, paragraph 4.4).

3.4.2.2 Animals and diets

Male Wistar strain rats, weighing about 150 g each, were purchased from Charles River (Lecco, Italy). All of the animal experiment protocols followed the institutional guidelines of the Italian Ministry of Health for Animal Care (D.M. 116/1992). Animals were housed 1 rat per cage in an air conditioned room with a 12 h light/dark cycle and with *ad libitum* access to food and water. Before the experiment, all the animals were allowed to stabilize by being fed with regular rodent chow, then randomly divided into four groups of (n) animals each:

- Group I (H) received the hypercholesterolemic diet (5% of cholesterol) for 3 weeks (hypercholesterolemic controls).
- Group II (H+S) received the hypercholesterolemic diet (5% of cholesterol) for 3 weeks; from the 2nd to the 3rd week, each rat was administered by gavage with simvastatin (20 mg/kg bw/day).
- Group III (H+B) received the hypercholesterolemic diet (5% of cholesterol) for 3 weeks; from the 2nd to the 3rd week, each rat was administered by gavage with water-dissolved brutieridin/melitidin-enriched bergamot extract (60 mg/kg bw/day).

- A group of regular-fed rats was taken under evaluation as a control to verify the induced hypercholesterolemia.

Both, the regular and the hypercholesterolemic diets were supplied by Charles River (Lecco, Italy).

During the experiment, rats were weighed daily and the 24 h food consumption was recorded. At the end of the study, the animals were decapitated and blood samples were collected in EDTA-treated tubes, centrifuged at 2500g for 15 min and the serum was separated and stored at -20°C until analyzed; liver was excised and immediately frozen in liquid nitrogen, then stored at -80°C until used.

3.4.2.3 Biochemical estimations

The levels of total cholesterol and triglycerides (serum and hepatic) were measured by standard enzymatic assays (Chematil Srl, Salerno, Italy) or HPLC after total lipid extraction, while high-density lipoproteins (HDLs) cholesterol and low-density lipoproteins (LDLs) cholesterol in serum were measured by direct enzymatic assays, respectively from Biogemina srl (Catania, Italy) and Intermedical srl (Naples, Italy). The liver samples were treated as described by Giudetti et al. [44]. Briefly, an aliquot of 10 mg protein sample was saponified with alcoholic KOH for 90 min at 85–90 °C followed by 5×5 mL extractions with petroleum ether. The extract was then evaporated and the residue dissolved in 2-propanol was used for HPLC determinations.

3.4.2.4 Statistical analysis

All data are presented as average \pm SD for the number of experiments indicated in each case. Data were analyzed by Student's t-test using the GraphPAD Prism4 software (GraphPad Software, USA). Differences were considered statistically significant at $P < 0.05$ level.

3.4.3 Results

3.4.3.1 Food intake and body weight gain

The data on food intake and body weight are summarized in figures 3.8 and 3.9. In figure 3.8 it is reported the daily food intake during the whole study period for each group of rats. No significant differences of food intake between untreated (H) and simvastatin (H+S) or enriched-bergamot extract (H+B) treated groups were observed.

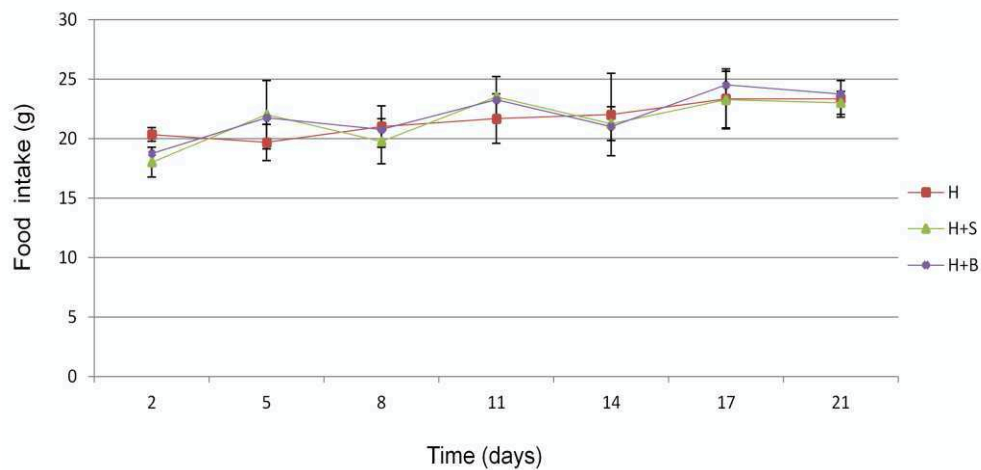


Figure 3.8. Daily food intake for each group of rat over the entire experiment period. Rats in the hypercholesterolemic (H) group were fed by a 5% enriched cholesterol diet. Rats in the H+S and H+B groups were fed with the same 5% enriched cholesterol diet and treated with simvastatin (H+S) 20 mg/kg bw/day and bergamot extract (H+B) 60 mg/kg bw/day respectively, starting from the end of the 2nd week. Values represent the mean \pm SD of the daily chow intake for each rat.

In figure 3.9 is reported the body weight change of each rat group over the study period. As can be observed, the body weight increased in all groups during the study period, without significant differences in weight within the same group nor between the different groups. The livers excised from each rat groups were not significantly different in weight from those of the normal diet fed rats (data not shown). These observations indicate that the diet and treatments used in these studies were well tolerated in rats, given that no physical alterations, body weight loss or food intake reduction occurred over the period of the study.

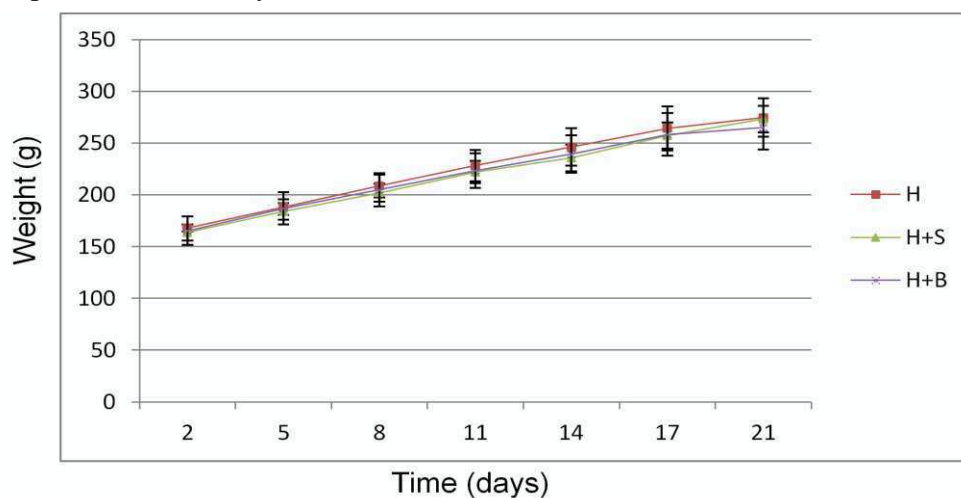


Figure 3.9. Body weight changes over the study period for each group of rat. All rats gained significant weight over the study period regardless of the group and did not show significant differences in function of treatment received. Values represent the mean \pm SD of the daily weight for each rat respect to the group.

3.4.3.2 Effects of simvastatin and brutieridin/melitidin-enriched extract on serum and hepatic lipid content

In serum, groups treated with simvastatin (H+S) and with brutieridin/melitidin-enriched bergamot extract (H+B) exhibited a significant decrease of total cholesterol respect to the untreated hypercholesterolemic group (H) of about 27% and 20%, respectively (figure 3.10). Regarding the LDL cholesterol, a significant reduction was measured in H+S (-34%) and H+B (-40%) groups. HDL cholesterol, on the other hand, was found to be higher in the H+B treated rat group (+20%), while no significant increase was observed for the H+S treated group (+2,5%), respect to the H control group.

In liver, it was observed a significant reduction in total cholesterol content of 11% for simvastatin treated rats (H+S) and a higher reduction, of 35%, for (H+B) enriched bergamot extract treated group (figure 3.11).

Plasmatic lipoproteins transport cholesterol and triglycerides, therefore many HMGR inhibitors have shown to contribute also in decreasing plasmatic triglycerides levels [46]. In order to investigate this feature in our model, we measured the serum and hepatic triglycerides content, demonstrating that the serum ones were lower in simvastatin (H+S) and bergamot extract (H+B) treated rats, respect to the untreated group, of about -32% and -20% respectively (experiments on liver TGs are still in progress).

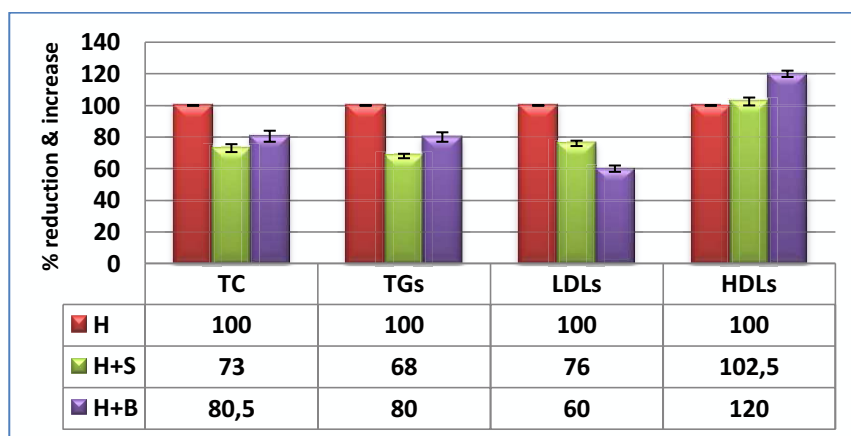


Figure 3.10. Effects of simvastatin and brutieridin/melitidin-enriched bergamot extract administration on rat serum total cholesterol (TC), LDL and HDL associated cholesterol and triglycerides (TGs). Hypercholesterolemic rat group (H) was used as control in all the experiments. Serum lipid levels of H+S and H+B rat groups were measured and plotted as percentage (%) decrease or increase respect to the H group. Results are mean values of three measurements for each lipid class and rat group.

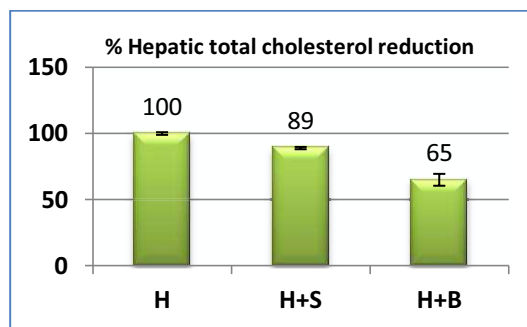


Figure 3.11. Effects of simvastatin and brutieridin/melitidin-enriched bergamot extract administration on hepatic total cholesterol (TC) (experiments on triglyceride (TGs) determination still under progress). TC content measured on rat groups H+S and H+B was plotted as percentage (%) decrease respect to the hypercholesterolemic control group (H). Each value is representative of three measurements.

3.4.4 Conclusions

As shown in figure 3.9, no significant difference amongst groups has been found, thus both hypercholesterolemic diet, drug treatment (H+S) and bergamot extract (H+B) seems to be well tolerated by rats. In simvastatin (H+S) treated rat, it was observed a decrease of TC, TGs, and LDLs in serum whereas no significant HDL level variation was observed. In groups of rats treated with brutieridin/melitidin-enriched bergamot extract, the levels of TC and TGs were found also decreased, even though in a lower extent respect to the simvastatin treated group. The ability of brutieridin/melitidin-enriched extract in decreasing LDL levels in hypercholesterolemic rat serum resulted to be higher respect to the simvastatin-treated group and, moreover, it comes together with another clinically very important effect, which is represented by a significant increase in HDLs levels (figure 3.10). These outcomes clearly indicate that the brutieridin/melitidin-enriched bergamot extract is able to produce a similar effect to that of simvastatin in reducing serum TC, TGs and LDLs, and is more effective in increasing the HDL serum levels. Therefore, these findings confer to the bergamot extract enriched with brutieridin and melitidin the peculiarity of hypocholesterolemic controlling agent. The serum TC and TGs levels depend on the biosynthesis, which mainly occurs in liver, and their subsequent release in blood as free or lipoproteins associated forms. For this reason, we also investigated their hepatic levels and we found a decrease in TC (TGs data are not completed yet) in simvastatin treated rat hepatocytes and, as well, in the bergamot treated group in a surprisingly higher extent, suggesting that the hepatic biosynthesis of cholesterol seems to be regulated/affected by our treatment. These observations led us to deduce that the observed decreased lipidic content in plasma may be affected by the decrease in TC synthesis and secretion by

liver, especially in form of LDLs, which transport most of the cholesterol and TGs contents and which we also found decreased in rat serum. It must be outlined also that the observed drop in LDLs serum levels is accompanied by an increase of HDLs contents in bergamot extract treated rat group, whereas simvastatin did not show this positive effect in our model. The latter peculiarity represents a favorable event, given that HDLs are able to picking up cholesterol from peripheral tissues or cells and carries it back to liver, where they are readily catabolized; for this reason they lower the blood and extrahepatic cholesterol content contributing to decrease the atherosclerosis-associated diseases risk. Additionally, the changes in serum and hepatic lipid contents caused by drug and enriched bergamot extract supplementation led us to wonder whether the levels of the hepatic key enzymes involved in cholesterol and TGs metabolism have been also affected. At this purpose we addressed our attention to the HMGR, LDLR and FASN genes transcription, using real time PCR experiments. These part of experiments are currently in progress.

In conclusion, the results reported here suggest that the daily supplementation with brutieridin/melitidin-enriched bergamot extract is able to reduce significantly the TC, TGs and LDL cholesterol in a similar extent to simvastatin treatment, and increases the HDLs blood levels. Literature data showed that rat represent a good model to verify the potential lipid-lowering effects of HMGR inhibitors in preclinical studies [47], thus we are hopeful that brutieridin/melitidin-enriched bergamot extract used in this study may elicit the same effects in man.

References

1. Stafford H. A., *Flavonoid Metabolism*, CRC, Boca Raton, FL, 1990, 1–59.
2. Hooper L., Cassidy A., A review of the health care potential of bioactive compounds. *J. Sci. Food Agric.* 2006, 86, 1805–1813.
3. Pietta P. G., Flavonoids as antioxidants, *J. Nat. Prod.*, 2000, 63, 1035–1042;
4. Prior R. L., Antioxidant and prooxidant behavior of flavonoids: structure-activity relationships, *Free Radic. Biol. Med.*, 1997, 22, 749–760.
5. Burda S., Oleszek W., Antioxidant and antiradical activities of flavonoids, *J. Agric. Food Chem.* 2001, 49, 2774–2779.
6. Rice-Evans C., Flavonoid antioxidants, *Curr. Med. Chem.*, 2001, 8, 797–807.
7. Drewnowski A., Gomez-Carneros C., Bitter taste, phytonutrients, and the consumer: a review, *Am. J. Clin. Nutr.* 2000, 72, 1424–1435.
8. Kris-Etherton P. M., Lefevre M., Beecher G. R., Gross M. D., Keen C. L., Etherton T. D., Bioactive compounds in nutrition and health-research methodologies for establishing biological function: the antioxidant and anti-inflammatory effects of flavonoids on atherosclerosis, *Ann. Rev. Nutr.* 2004, 24, 511-538.
9. Gross, M., Flavonoids and cardiovascular disease, *Pharm. Biol.*, 2004, 42, 21–35.
10. Yochum L., Kushi L. H., Meyer K., Folsom A. R., Dietary flavonoid intake and risk of cardiovascular disease in postmenopausal women, *Am. J. Epidemiol.*, 1999, 149, 943–949.
11. Nichenametla S. N., Taruscio T. G., Barney D. L., Exon J. H., A review of the effects and mechanism of polyphenolics in cancer, *Crit. Rev. Food Sci.*, 2006, 46, 161–183.
12. Le Marchand L., Murphy S. P., Hankin J. H., Wilkens L. R., Kolonel L. N., Intake of flavonoids and lung cancer, *J. Natl. Cancer Inst.*, 2000, 92, 154–160.
13. Cushnie T. P. T., Lamb A. J., Antimicrobial activity of flavonoids, *Int. J. Antimicrob. Agent.*, 2005, 26, 343–356.
14. Kim H. P., Son K. H., Chang H. W., Kang S. S., Anti-inflammatory plant flavonoids and cellular action mechanisms, *J. Pharmacol. Sci.*, 2004, 96, 229–245.
15. Benavente-García O., Castillo J., Marín F. R., Ortuño A., Del Río J. A., Uses and properties of Citrus flavonoids, *J. Agric. Food Chem.*, 1997, 45, 4505–4515.
16. Borrelli F., Izzo A. A., The plant kingdom as a source of anti-ulcer remedies, *Phytother. Res.*, 2000, 14, 581–591.

17. Espín J. C., García-Conesa M. T, Tomás-Barberán F. A., Nutraceuticals: Facts and fiction, *Phytochemistry*, 2007, 68, 986–3008.
18. Nijveldt R. J., van Nood E., van Hoorn D. E. C., Boelens P. G., van Norren K., van Leeuwen P. A. M., Flavonoids: a review of probable mechanisms of action and potential applications. *Am. J. Clin. Nutr.* 2001, 74, 418–425.
19. Moufida S., Marzouk B., Biochemical characterization of blood orange, sweet orange, lemon, bergamot and bitter orange, *Phytochemistry*, 2003, 62, 1283–1289.
20. Hollman P. C. H., Arts I. C. W., Flavonols, flavones and flavanols – nature, occurrence and dietary burden, *J. Sci. Food Agr.*, 2000, 80, 1081–1093.
21. Tripoli E., La Guardia M., Giammanco S., Di Majo D., Giammanco M., *Food Chemistry*, 2007, 104, 466-479.
22. Gattuso G., Caristi C., Gargiulli C., Bellocco E., Toscano G., Leuzzi U., *J. Agric. Food Chem.*, 2006, 54, 3929-3935.
23. Franke A. A., Cooney R. V., Henning S. M., Custer L. J., Bioavailability and antioxidant effects of orange juice components in humans, *J. Agric. Food Chem.*, 2005, 53, 5170–5178.
24. Ross J. A., Kasum C. M., Dietary flavonoids: bioavailability, metabolic effects, and safety, *Ann. Rev. Nutr.*, 2002, 22, 19–34.
25. Miyake Y., Yamamoto K., Morimitsu Y., Osawa T., Isolation of C-glucosylflavone from lemon peel and antioxidative activity of flavonoid compounds in lemon fruit, *J. Agric. Food Chem.*, 1997, 45, 4619–4623.
26. Leuzzi U., Caristi C., Panzera V., Licandro G., Flavonoids in pigmented orange juice and second-pressure extracts, *J. Agric. Food Chem.*, 2000, 48, 5501–5506.
27. Pernice R., Borriello G., Ferracane R., Borrelli R. C., Cennamo F., Ritieni A., *Food Chemistry*, 2009, 112, 545-550.
28. Gattuso G., Barreca D., Caristi C., Gargiulli C., Leuzzi U., *J. Agric. Food Chem.*, 2007, 55 9921–9927.
29. Di Donna L., Dolce V., Sindona G., patent nr. CS2008A00019.
30. Di Donna L., De Luca G., Mazzotti F., Napoli A., Salerno R., Taverna D., Sindona G., *J. Nat. Prod.*, 2009, 72 1352–1354
31. Veloso D., W.W. Cleland, J.W. Porter, *Biochemistry*, 20 (1981) 887–894.
32. Wang B.G. Darnay, V.W. Rodwell, *J. Biol. Chem.*, 265 (1990) 21634–21641.
33. Frimpong K., Rodwell V.W., *J. Biol. Chem.*, 269 (1994) 11478–11483.
34. Eva S.Istvan, Maya Palnitkar, Susan K.Buchanan and Johann Deisenhofer, *The EMBO Journal*, 19, 5 (2000) 819–830.
35. Eva Istvan, Johann Deisenhofer, *Science*, 2001, 292 1160.

36. Balbisi E. A., Management of hyperlipidemia: new LDL-C targets for persons at high-risk for cardiovascular events. *Med. Sci. Monit.*, 2006, 12, RA34-39.
37. Miller J. P., Hyperlipidaemia and cardiovascular disease, *Curr. Opin. Lipidol.*, 1996, 7, U18-24.
38. Goldstein J. L., Brown M. S., Regulation of the mevalonate pathway, *Nature*, 1990, 343, 425-430.
39. Ross S. D., Allen I. E., Connelly J. E., Korenblat B. M., Smith M. E., Bishop D., Luo D., Clinical outcomes in statin treatment trials: a meta-analysis. *Arch. Intern. Med.*, 1999, 159, 1793-1802.
40. Brown M. S., Goldstein J. L., A receptor-mediated pathway for cholesterol homeostasis, *Science*, 1986, 232, 34-47.
41. Endres M., Laufs U., Huang Z., Nakamura T., Huang P., Moskowitz M. A., Liao J. K., Stroke protection by 3-hydroxy-3-methylglutaryl (HMG)-CoA reductase inhibitors mediated by endothelial nitric oxide synthase, *Proc. Natl. Acad. Sci. U S A*, 1998, 95, 8880-8885.
42. Farmer J. A., Gotto A. M. Jr., Antihyperlipidaemic agents. Drug interactions of clinical significance, *Drug Saf.*, 1994, 11, 301-309.
43. Steinberg D., Glass C. K., Witztum J. L., Evidence mandating earlier and more aggressive treatment of hypercholesterolemia, *Circulation*, 2008, 118, 672-677.
44. Giudetti A. M., Siculella L., Caputi Jambrenghi A. M., Ragni M., Vonghia G., Gnani G. V., Fatty acid chain elongation synthesis in eel (*Anguilla anguilla*) liver mitochondria, *Comp. Biochem. Physiol. B Biochem. Mol. Biol.*, 2001, 128, 11-18.
45. Rai S. K., Sharma M., Tiwari M., Inhibitory effect of novel diallyldisulfide analogs on HMG-CoA reductase expression in hypercholesterolemic rats: CREB as a potential upstream target, *Life Sci.*, 2009, 85, 211-219.
46. Scharnagl H., Schinker R., Gierens H., Nauck M., Wieland H., Marz W., Effect of atorvastatin, simvastatin, and lovastatin on the metabolism of cholesterol and triacylglycerides in HepG2 cells, *Biochem. Pharmacol.*, 2001, 62, 1545-1555.
47. Krause B. R., Newton R. S., Lipid-lowering activity of atorvastatin and lovastatin in rodent species: triglyceride-lowering in rats correlates with efficacy in LDL animal models, *Atherosclerosis*, 1995, 117, 237-244.

APPENDIX I

On the Inhibitor Effects of Bergamot Juice Flavonoids Binding to the 3-Hydroxy-3-methylglutaryl-CoA Reductase (HMGR) Enzyme

MONICA LEOPOLDINI, NAIM MALAJ, MARIROSA TOSCANO, GIOVANNI SINDONA, AND NINO RUSSO*

Dipartimento di Chimica, Università della Calabria, I-87036 Rende (CS), Italy

Density functional theory was applied to study the binding mode of new flavonoids as possible inhibitors of the 3-hydroxy-3-methylglutaryl-CoA reductase (HMGR), an enzyme that catalyzes the four-electron reduction of HMGCoA to mevalonate, the committed step in the biosynthesis of sterols. The investigated flavonoid conjugates brutieridin and melitidin were recently quantified in the bergamot fruit extracts and identified to be structural analogues of statins, lipids concentration lowering drugs that inhibit HMGR. Computations allowed us to perform a detailed analysis of the geometrical and electronic features affecting the binding of these compounds, as well as that of the excellent simvastatin drug, to the active site of the enzyme and to give better insight into the inhibition process.

KEYWORDS: HMGR; statin-like principles; enzyme inhibition; DFT

INTRODUCTION

Bergamot (*Citrus bergamia* Risso), a hybrid between orange and lemon plants, is a typical fruit of the southern provinces of Italy. It is mostly used for the extraction of its essential oil from the peel. Because of its unique fragrance and freshness, bergamot oil is widely used in the cosmetic and food industries (1). Furthermore, due to its antiseptic and antibacterial properties, the essence is also used in the pharmaceutical industry (2).

In the past few years, following the growing interest in antioxidant bioactive compounds and their dietary sources, bergamot juice, as well as its peel, has attracted some attention because of its remarkable content of flavonoids (3–9). In particular, it has been identified and quantified (10) that together with the most abundant neoeriocitrin, naringin and neohesperidin, also *C*-glucosides (lucenin-2, vicenin-2, stellarin-2, lucenin-2-4'-methyl ether, scoparin, and orientin 4'-methyl ether), flavone *O*-glycosides (rhoifolin 4'-*O*-glucoside, chrysoeriol 7-*O*-neohesperidoside-4'-*O*-glucoside, rhoifolin, chrysoeriol 7-*O*-neohesperidoside, and neodiosmin), and flavanone *O*-glycosides (eriocitrin) are present.

Many epidemiological and biochemical studies (11) have demonstrated flavonoids to possess beneficial effects on human health because of their established antioxidant activity in scavenging harmful free radicals. Recently (12), a detailed analysis of bergamot fruit extractions, carried out by LC-MS, MS/MS, and NMR techniques, has led to the isolation of two new flavonoid conjugates, named brutieridin (hesperetin 7-(2''- α -rhamnosyl-6'''-(3''''-hydroxy-3''''-methylglutaryl)- β -glucoside)) and melitidin (naringenin 7-(2''- α -rhamnosyl-6'''-(3''''-hydroxy-3''''-methylglutaryl)- β -glucoside)) (1 and 2 in Scheme 1). They are present in bergamot fruit in concentration ranges of approximately 300–500

and 150–300 ppm, respectively, and are found either in the juice or in the albedo and flavedo layers of bergamot.

Their structure resembles that of cholesterol inhibitor drugs statins (13). Like statins, the new active principles contain the hydroxyl mevalonate moiety. Mevalonate is a precursor of isoprenoids, a class of compounds involved in several cellular functions such as cholesterol synthesis and growth control. Within cells, the concentration of mevalonate and therefore that of its metabolic products is tightly controlled through the activity of 3-hydroxy-3-methylglutaryl-CoA reductase (HMGR), an enzyme that catalyzes the four-electron reduction of HMGCoA to mevalonate (14).

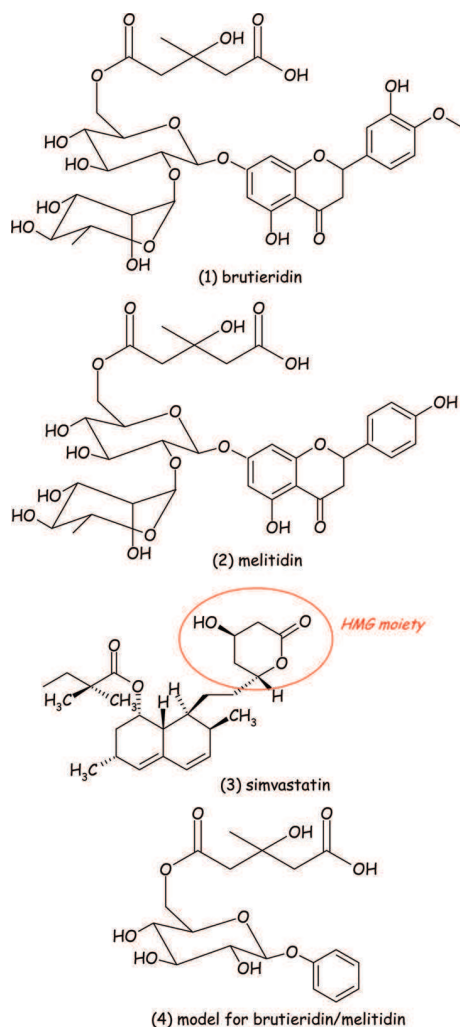
Elevated serum-blood cholesterol levels are associated with a high risk of heart coronary artery diseases (15). Inhibition of HMGR enzyme is reported to significantly decrease cholesterol levels and to reduce the risks of stroke (16). Statins are potent HMGR inhibitors since they bind to the active site where also the natural substrate HMG binds, and are prescribed widely in the treatment of hypercholesterolemia. They are thought to bind competitively with the natural substrate in the active site of HMGR (17, 18). However, adverse experiences have been associated with statins, both in monotherapy and in combination therapy with other agents (19, 20).

Both the wide variety of different types of flavonoids molecules and the fact that some of these compounds are present in good amounts (150–500 ppm) make possible the future applications of bergamot juice in health care, also considering the recommended statins dosage ranging from 5 mg to 80 mg, depending on the particular drug and cholesterol levels.

The aim of this computational study is to investigate the interaction of the two new compounds brutieridin and melitidin with the active site of the human HMGR enzyme in order to have insights on their possible inhibitory effect. For the purpose of

*To whom correspondence should be addressed. E-mail: nrusso@unical.it.

Scheme 1. Representation of (1) Brutieridin, (2) Melitidin, (3) Simvastatin, and (4) the Model Used for Brutieridin/Melitidin



comparison, the behavior of the excellent HMGR inhibitor simvastatin (3 in scheme 1) is also investigated.

MATERIALS AND METHODS

The model cluster used to simulate the active site of the HMGR enzyme was built starting from the 2.33 Å X-ray structure of human HMGR in complex with the simvastatin inhibitor (pdb code 1HW9) (21).

In the case of the simvastatin–enzyme complex, the cluster was built by simply cutting the active site with selected residues and the drug from the available X-ray structure. For the brutieridin/melitidin–HMGR complex, since no experimental X-ray structures exist, we rebuilt the 3D structure by deleting the non-HMG moiety of simvastatin and substituting it with the remaining part of the brutieridin/melitidin. To get the reasonable structure for quantum mechanical investigation, molecular dynamics (MD) calculations were performed. These computations were carried out by means of the Gromacs 3.2 program (22). The gromacs force field was applied, and the force field parameter of the brutieridin/melitidin drug was generated by the PRODRG server (23) to build a Gromacs 87 topology for the drug. The solvent SPC water model implemented in the Gromacs package and an octahedral box, setting the box edge at a distance of 5.0 nm from the target, were used. Na⁺ counterions were added to satisfy the electroneutrality condition.

First of all, the energy minimization was performed, applying the steepest descent method to remove local strain and bad van der Waals contacts. Then we ran a 20 ps position-restrained dynamics simulation, restraining the atom positions of the macromolecule while letting the solvent and the drug relax into the protein. The simulation was performed at constant temperature and pressure by coupling the system to a

Berendsen bath (22) at 300 K and 1 atm. Finally, a 100 ps MD simulation was performed for the system. Root-mean-square deviation (rmsd) time series (Figure S1 in the Supporting Information) suggest that the system was well equilibrated after about 50 ps.

Enzymes are proteins with a high molecular weight so that they cannot be entirely studied without introducing significant approximations or using chemical models to represent the active region of the enzymes. Results must be interpreted in light of the above-mentioned computational limitations.

The model cluster was reproduced by considering the 7 Glu559, Cys561, Leu562, Lys735, His752, Asn755, and Leu853 residues and the 10 Arg590, Asn658, Ser684, Gly685, Asn686, Cys688, Thr689, Asp690, Lys691, and Lys692 residues belonging to the chains A and B of the protein, respectively. Following a consolidated procedure (24–36), simple models for these amino acids were employed, i.e., CH₃COO[−] for Asp and Glu, CH₃NHC(NH₂)₂⁺ for Arg, CH₃NH₃⁺ for Lys, CH₃OH for Ser, CH₃CH₂CH₃ for Leu, CH₃CONH₂ for Asn, CH₃SH for Cys, methylimidazole for His, and CH₃CONH- for Gly and Thr residues. This practice is widely applied in the studies regarding enzymatic proteins and in many cases has given very reliable results (24–36). The built up cluster model for the enzyme active site resulted in having a total charge of +3 and to be made up by 150 atoms, all described at the quantum mechanical level. Another simple model (4 in Scheme 1) was used to simulate the brutieridin/melitidin statin-like molecule. It consists of a phenyl ring for the flavonone moiety and only one sugar molecule, so as to reduce the computational efforts. Simvastatin was considered as such. Both brutieridin/melitidin and simvastatin have a charge of −1.

An H atom of each amino acid residue coming from the protein was kept frozen at its crystallographic position in order to mimic the steric effects produced by the surrounding protein and to avoid an unrealistic expansion of the cluster during the optimization procedure (27, 28). No constraints were imposed to simvastatin and brutieridin/melitidin. All of the quantum chemical computations were performed with the Gaussian 03, revision C02, code (37).

The hybrid B3LYP functional was employed to perform geometry optimization, and the 6-31G* basis set was chosen to describe the C and H atoms, while for O and N atoms, the 6-31+G* orbital set was used, as implemented in Gaussian 03. Frequency calculations were performed at the B3LYP level on all of the stationary points so as to establish their character of minima. Zero point energy (ZPE) corrections, obtained by vibrational analysis, were then included in all relative energies. The basis set superposition error (BSSE), computed according to the counterpoise method of Boys and Bernardi, as implemented in Gaussian 03, was always less than 1 kcal/mol.

To account for the polarization effects caused by the part of the surrounding enzyme that is not explicitly included in the quantum model, solvent effects were introduced as B3LYP/6-311++G** single point computations on the optimized gas phase structures, in the framework of Self Consistent Reaction Field Polarizable Continuum Model (SCRFP-CM) using the IEF-PCM model, as implemented in Gaussian 03, in which the cavity is created via a series of overlapping spheres. This is a simple model for treating long-range solvent effects and considers the solvent as a macroscopic continuum with a dielectric constant and the solute as filling a cavity in this continuous medium. United Atom Topological (UA0) Model applied on atomic radii of the UFF force field was used to build the cavity, in the gas-phase equilibrium geometry. The dielectric constant of the protein is the main empirical parameter of the model, and it was chosen to be equal to 4, in line with previous suggestions for proteins (24–36). This value corresponds to a dielectric constant of about 3 for the protein itself and of 80 for the water medium surrounding the protein.

The binding energies (BE) were computed as in protein-like environment B3LYP/6-311++G** single point energy computations on the optimized geometries of the inhibitor (brutieridin/melitidin and simvastatin), of the model active site, and of both inhibitor–enzyme complexes:

$$BE = E(\text{complex}) - [E(\text{inhibitor}) + E(\text{active site})]$$

RESULTS AND DISCUSSION

Simvastatin–HMGR Complex. Crystal structures of HMGR in complex with statins show that the orientation and bonding

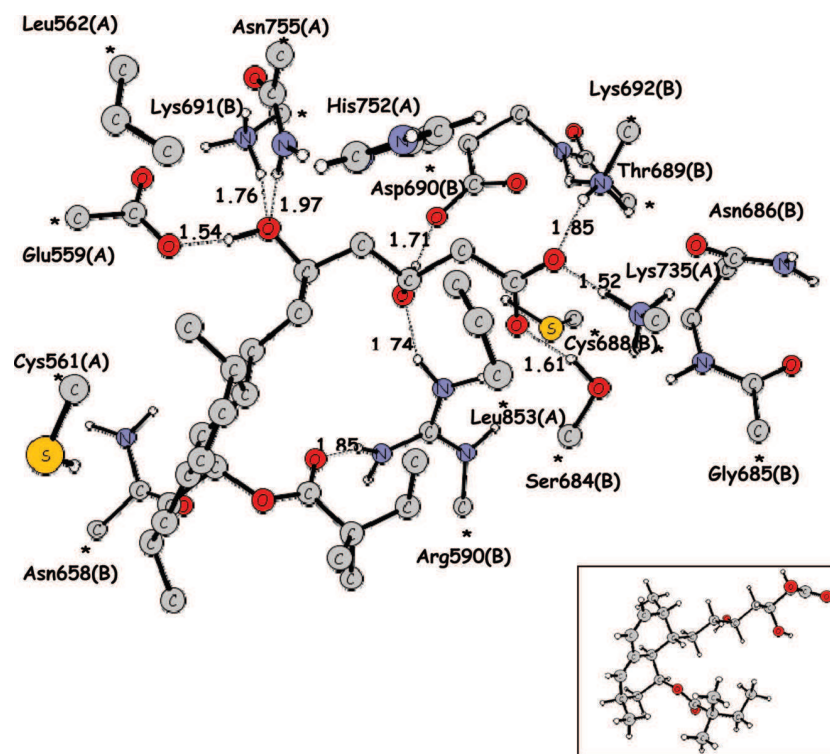


Figure 1. B3LYP optimized geometry of the simvastatin–HMGR complex. For clarity, unimportant hydrogen atoms are omitted. Inset: the geometry of simvastatin.

interactions of the HMG moieties of the inhibitors resemble those of the HMGCoA substrate (38). Crystal structures clearly indicate that the linear forms of statins are predisposed to bind to the enzyme. The hydroxy acid side chain is the most flexible part of the drug molecules. Because of the structural similarity to the HMG moiety, it is mainly responsible for the competitive inhibition of human HMGR.

Several dipole/dipole interactions and hydrogen bonds are used by statins to bind to the active site of the enzyme, focusing on residues in the cis loop (Ser684, Asp690, Lys691, and Lys692), with minimal involvement of the hydrophobic interactions. Lys691 is suggested to be involved in a hydrogen bond with the O5-hydroxyl of the statins, while the terminal carboxylate of the HMG moiety seems to establish a salt bridge to Lys735. Hydrophobic side chains of the enzyme involved in contact with statins were identified to be Leu562, Val683, Leu853, Ala856, and Leu857 residues (38).

The B3LYP optimized structure of the complex between simvastatin and the HMGR active site model cluster is illustrated in the **Figure 1**. The minimum energy structure is characterized by several hydrogen bonds as well as hydrophobic interactions.

The rigid hydrophobic naphthalene ring of simvastatin rearranges to maximize nonpolar interactions which are established with Cys561 and Leu562, and with Leu853 also through the methyl butyrate ester moiety. The binding mode of this portion of the molecule is also characterized by the presence of a H-bond (1.85 Å) between the positive NH₂ group of Arg590 and the carbonyl oxygen atom of the simvastatin ester moiety.

The terminal carboxylic group of simvastatin gives rise to strong hydrogen bonds. One carboxylic oxygen of the drug is involved in a H-bond with the –OH of Ser684 (1.61 Å). The other oxygen establishes two strong hydrogen bonds, with the amino groups from Lys735 (1.52 Å) and Lys692 (1.85 Å). The original salt bridge (21) involving the negative COO[–] of simvastatin and the NH₃⁺ of the lysine residue is retained during the optimization procedure.

The hydroxyl attached on C₃ in simvastatin forms two hydrogen bonds with the oxygen atom coming from Asp690 (1.71 Å) and with the NH₂ group of Arg590 (1.74 Å). The C₅-OH, replacing the thio-ester oxygen atom found in the HMG-CoA substrate, acts as a H-bond donor with Glu559 (1.54 Å) and as an acceptor with Lys691 (1.76 Å) and Asn755 (1.97 Å).

This bonding network obtained through B3LYP computations is in good agreement with that observed in the experimental crystal structure of the simvastatin–HMGR adduct (21). The statin is positioned approximately in the HMG-CoA binding site, thus not occupying the NADP(H) binding pocket. In particular, the H-bonds involving the hydroxyls attached to C₃ and C₅ as well as those involving the carboxylic moiety in simvastatin are quite well reproduced, with a deviation of ~0.3 Å.

The interactions between the HMG-like moieties of the simvastatin and the active site of the enzyme are mainly electrostatic involving numerous hydrogen binding connections similar to those formed with the HMG-CoA substrate. The bulky hydrophobic part, indeed, occupies the HMG-binding pocket and part of the binding surface for CoA so that the access of the substrate HMG-CoA to HMGR is blocked when the statin is bound.

The binding energy in a protein-like environment is computed to be 101.1 kcal/mol, indicating that the binding of the drug is thermodynamically favored, further contributing to the inhibition process.

Brutieridin/Melitidin–HMGR Complex. The B3LYP optimized structure of the complex between brutieridin/melitidin and the HMGR active site model cluster is depicted in **Figure 2**. Most of the noncovalent bonds found for the binding of simvastatin to the HMGR active site are involved in the formation of the complex between brutieridin/melitidin and the HMGR enzyme. However, the starting geometry of the brutieridin/melitidin–HMGR complex for the QM computations is slightly different with respect to the simvastatin–enzyme one as far as the Ser684 residue is concerned. Particularly, upon MD simulations, the

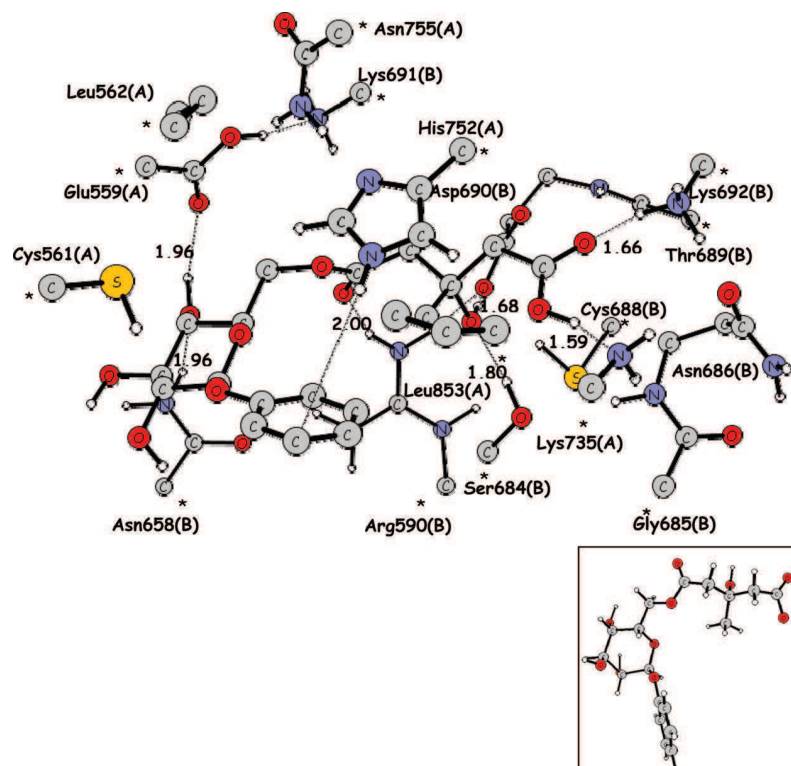


Figure 2. B3LYP optimized geometry of the brutieridin/melitidin–HMGR complex. For clarity, unimportant hydrogen atoms are omitted. Inset: the geometry of brutieridin/melitidin.

Ser684 OH points toward the hydroxyl at the C3 and not to the carboxylic moiety of the statin-like molecule. This will cause some differences in the binding of the brutieridin/melitidin molecule in the HMGR active site when compared to the behavior of simvastatin.

Lys735 and Lys692 form two H-bonds with the terminal carboxylic group of the brutieridin/melitidin molecule (1.59 and 1.66 Å, respectively). It is worth noting that during the optimization procedure, the salt bridge involving the negative COO^- of brutieridin/melitidin and the NH_3^+ of Lys735 is removed, leading to both neutral COOH and NH_2 groups. It is possible, however, that this proton transfer from Lys735 is an artifact of the relative smallness of the employed HMGR model and that it might not occur when more parts are included that can provide proper solvation to the COO^- – Lys^+ ion pair. In the former simvastatin–enzyme complex, the COO^- – Lys^+ couple remains unprotonated probably because of the presence of the Ser684 hydroxyl that stabilizes the negative charge on the carboxylate. The C_3 -OH interacts with the oxygen coming from Asp690 (1.68 Å) and with the OH group coming from Ser684 (1.80 Å).

The ester moiety of brutieridin/melitidin, which replaces the C_5 -OH of simvastatin, is responsible for a different arrangement of this compound with respect to simvastatin. The carbonyl oxygen receives an H-bond from Arg590 (2.00 Å), but no interaction with Glu559 occurs. The latter in fact establishes a strong polar interaction with the amino group of Lys691 so that a spontaneous proton shift from the positive NH_3^+ to the negative COO^- takes place.

The sugar moiety rearranges itself to establish H-bonds through its hydroxyl groups with polar residues in the active site. Particularly, the hydroxyl attached to the C_3' in the sugar ring donates a H-bond to the oxygen of Glu559 (1.96 Å) while receiving one from the side chain of Asn658 (1.96 Å).

The aromatic ring of brutieridin/melitidin establishes van der Waals interactions with the nonpolar Leu562 and Leu853. The

imidazole ring of His752 approaches the phenyl ring of the brutieridin/melitidin molecule in such a way that one hydrogen of the imidazole ring points toward the π electrons of the aromatic ring (see Figure 2).

One has to remember that the phenyl ring is just a crude representation of the flavanone moiety of brutieridin/melitidin, which thanks to the presence of multiple OH groups could establish H-bonds with the active site of the enzyme. This binding mode is absent in statins, which possess rigid hydrophobic substituents that presumably should mimic the nicotinamide ring of NADP(H) (39).

The B3LYP binding energy in the protein-like medium is computed to be 90.8 kcal/mol. This value is comparable to the one exhibited by simvastatin and may indicate that brutieridin/melitidin is a good candidate in performing the binding to the active site of HMGR.

Brutieridin/melitidin seems to invade the HMG-binding site and partially occupies the site accommodating the CoA part of the substrate, like that occurring in the simvastatin binding mode. Electrostatic interactions are predominant in brutieridin/melitidin binding to the HMGR active site, while in the case of the simvastatin–HMGR complex, a certain amount of van der Waals bonds is also present as far as the hydrophobic decalin ring is concerned.

In conclusion, we have investigated by means of density functional theory the binding of new bergamot fruit containing flavonoids conjugates, brutieridin and melitidin, to a simplified model of the active site of 3-hydroxy-3-methylglutaryl-CoA reductase (HMGR). Their structure closely resembles that of cholesterol inhibitor drugs, statins. The calculations have allowed us to investigate the geometrical features affecting the bond to the active site and to compute the protein-like binding energy. The behavior of the excellent HMGR inhibitor simvastatin has been also studied.

The binding mode of the bergamot fruit containing statin-like molecules to the HMGR active site involves the Arg590, Ser684, Asp690, Lys692, and Lys735 residues, as well as the nonpolar aminoacids. The terminal carboxylic group of the brutieridin/melitidin molecule is involved in two H-bonds with the amino groups of Lys735 and Lys692. The C₃-OH interacts with the oxygen coming from Asp690 and with the OH group coming from Ser684 (1.80 Å).

The ester moiety of brutieridin/melitidin, which replaces the C₅-OH of simvastatin and resembles the thio-ester of the CoA substrate, receives an H-bond from Arg590, while no interactions with Glu559 are found. The aromatic ring of brutieridin/melitidin establishes van der Waals interactions with the nonpolar Leu562 and Leu553, and a H-bond-like interaction with the hydrogen atom coming from the imidazole ring of His752. This binding mode is absent in statins, which possess rigid hydrophobic substituents.

Consistent with the presence of the HMG-like moiety, brutieridin and melitidin compounds seem to be competitive inhibitors of HMG-CoA reductase with respect to the binding of HMG-CoA. Computations of binding energies in the protein-like medium indicate that brutieridin and melitidin compounds are good candidates to perform the inhibition of HMG-CoA reductase in vivo.

These findings support the experienced anticholesterolemic activity of the new drug candidates (40) and also the recent results about the in vitro inhibition of HMG-CoA reductase performed by isoflavones (41). Light on the prescription of local folk medicine indicating bergamot juice as a natural product that lowers blood cholesterol levels is thrown. This study may be the starting point for bergamot exploitation in drug industry applications.

ACKNOWLEDGMENT

The University of Calabria, the Food Science & Engineering Interdepartmental Center of University of Calabria, L.I.P.A.C., and QUASIORA Laboratories (Regione Calabria APQ- Ricerca Scientifica e Innovazione Tecnologica I atto integrativo, Azione 2 laboratori pubblici di ricerca mission oriented interfiliere) are gratefully acknowledged.

Supporting Information Available: Root-mean-square deviation (rmsd) of the protein structure during MD simulation. This material is available free of charge via the Internet at <http://pubs.acs.org>.

LITERATURE CITED

- Verzera, A.; Trozzi, A.; Gazea, F.; Ciccirello, G.; Cotroneo, A. Effects of rootstock on the composition of bergamot (*Citrus bergamia* Risso et Poiteau) essential oil. *J. Agric. Food Chem.* **2003**, *51*, 206–210.
- Mandalari, G.; Bennett, R. N.; Bisignano, G.; Saija, A.; Dugo, G.; Lo Curto, R. B.; Faulds, C. B.; Waldron, K. W. Characterization of flavonoids and pectins from bergamot (*Citrus bergamia* Risso) peel, a major by-product of essential oil extraction. *J. Agric. Food Chem.* **2006**, *54*, 197–203.
- Gattuso, G.; Barreca, D.; Gargiulli, C.; Leuzzi, U.; Caristi, C. Flavonoid composition of *Citrus* juices. *Molecules* **2007**, *12*, 1641–1673.
- Leuzzi, U.; Caristi, C.; Panzera, V.; Licandro, G. Flavonoids in pigmented orange juice and second pressure extracts. *J. Agric. Food Chem.* **2000**, *48*, 5501–5506.
- Nogata, Y.; Sagamoto, K.; Shiratsuchi, H.; Ishii, T.; Yano, M.; Ohta, H. Flavonoid composition of fruit tissues of citrus species. *Biosci. Biotechnol. Biochem.* **2006**, *70*, 178–192.
- Berhow, M.; Tisserat, B.; Kaness, K.; Vandercook, C. Survey of phenolic compounds produced in *Citrus*. *USDA ARS Tech. Bull.* **1998**, *1856*, 1–154. Available from United States Department of Agriculture, Agricultural Research Service. <http://www.ars.usda.gov/is/np/phenolics/title.htm> (accessed 7/9/07).
- Kawaii, S.; Tomono, Y.; Katase, E.; Ogawa, K.; Yano, M. HL-60 differentiating activity and flavonoid content of the readily extractable fraction prepared from *Citrus* juices. *J. Agric. Food Chem.* **1999**, *47*, 128–135.
- Caristi, C.; Bellocco, E.; Panzera, V.; Toscano, G.; Vadalà, R.; Leuzzi, U. Flavonoids detection by HPLC-DAD-MS-MS in lemon juice from Sicilian cultivars. *J. Agric. Food Chem.* **2003**, *51*, 3528–3534.
- Caristi, C.; Bellocco, E.; Gargiulli, C.; Toscano, G.; Leuzzi, U. Flavone-di-C-glycosides in *Citrus* juices from southern Italy. *Food Chem.* **2006**, *95*, 431–437.
- Gattuso, G.; Caristi, C.; Gargiulli, C.; Bellocco, E.; Toscano, G.; Leuzzi, U. Flavonoid glycosides in bergamot juice (*Citrus bergamia* Risso). *J. Agric. Food Chem.* **2006**, *54*, 3929–3935.
- Nijveldt, R. J.; van Nood, E.; van Hoorn, D. E. C.; Boelens, P. G.; van Norren, K.; van Leeuwen, P. A. M. Flavonoids: a review of probable mechanisms of action and potential application. *Am. J. Clin. Nutr.* **2001**, *74*, 418–425 and references therein.
- Di Donna, L.; De Luca, G.; Mazzotti, F.; Napoli, A.; Salerno, R.; Taverna, D.; Sindona, G. Statin-like principles of bergamot fruit (*Citrus bergamia*): Isolation of 3-hydroxymethylglutaryl flavonoid glycosides. *J. Nat. Prod.* **2009**, *72*, 1352–1354.
- Corsini, A.; Maggi, F. M.; Catapano, A. L. Pharmacology of competitive inhibitors of HMG-CoA reductase. *Pharmacol. Res.* **1995**, *31*, 9–27.
- Edwards, P. A.; Ericsson, J. Sterols and isoprenoids: signalling molecules derived from the cholesterol biosynthetic pathway. *Annu. Rev. Biochem.* **1999**, *68*, 157–185.
- Eisenberg, D. A. Cholesterol lowering in the management of coronary artery disease: the clinical implications of recent trials. *Am. J. Med.* **1998**, *104*, 2S–5S.
- Hebert, P. R.; Gaziano, J. M.; Chan, K. S.; Hennekens, C. H. Cholesterol lowering with statin drugs, risk of stroke and total mortality. An overview of randomized trials. *J. Am. Med. Assoc.* **1997**, *278*, 313–321.
- Endo, A. Compactin (ML-236B) and related compounds as potential cholesterol-lowering agents that inhibit HMG-CoA reductase. *J. Med. Chem.* **1985**, *28*, 401–405.
- Gotto, A. M., Jr. Results of recent large cholesterol-lowering trials and implications for clinical management. *Am. J. Cardiol.* **1997**, *79*, 1663–1666.
- Bays, H. Statin safety an overview and assessment of the data: 2005. *Am. J. Cardiol.* **2006**, *97*, 6C–26C.
- Jacobson, T. A. Statin safety: lessons from new drug applications for marketed statins. *Am. J. Cardiol.* **2006**, *97*, 44C–51C.
- Istvan, E. S.; Deisenhofer, J. Structural mechanism for statin inhibition of HMG-CoA reductase. *Science* **2001**, *292*, 1160–1164.
- Lindahl, E.; Hess, B.; Spoel, D. v. d. GROMACS 3.0: A package for molecular simulation and trajectory analysis. *J. Mol. Model.* **2001**, *7*, 306–317.
- Schuettelkopf, A. W.; van Aalten, D. M. F. PRODRG: a tool for high-throughput crystallography of protein-ligand complexes. *Acta Crystallogr.* **2004**, 1355–1363.
- Leopoldini, M.; Russo, N.; Toscano, M. Role of the metal ion in formyl-peptide bond hydrolysis by a peptide deformylase active site model. *J. Phys. Chem. B* **2006**, *110*, 1063–1072.
- Marino, T.; Russo, N.; Toscano, M. A comparative study of the catalytic mechanisms of the zinc and cadmium containing carbonic anhydrase. *J. Am. Chem. Soc.* **2005**, *127*, 4242–4253.
- Leopoldini, M.; Russo, N.; Toscano, M. Which one among Zn(II), Co(II), Mn(II), and Fe(II) is the most efficient ion for the methionine aminopeptidase catalyzed reaction? *J. Am. Chem. Soc.* **2007**, *129*, 7776–7784.
- Siegbahn, P. E. M.; Blomberg, M. R. A. Transition metal systems in biological studied by high-accuracy quantum chemical methods. *Chem. Rev.* **2000**, *100*, 421–437.
- Noodleman, L.; Lovell, T.; Han, W. G.; Li, J.; Himo, F. Quantum chemical studies of intermediates and reaction pathways in selected

- enzymes and catalytic synthetic systems. *Chem. Rev.* **2004**, *104*, 459–508.
- (29) Leopoldini, M.; Russo, N.; Toscano, M.; Dulak, M.; Wesoloski, A. T Mechanism of nitrate reduction by *Desulfovibrio desulfuricans* nitrate reductase: A theoretical investigation. *Chem.—Eur. J.* **2006**, *12*, 2532–2541.
- (30) Leopoldini, M.; Russo, N.; Toscano, M. The preferred reaction path for the oxidation of methanol by PQQ-containing methanol dehydrogenase: Addition–elimination versus hydride-transfer mechanism. *Chem.—Eur. J.* **2007**, *13*, 2109–2117.
- (31) Leopoldini, M.; Marino, T.; Michelini, M. C.; Rivalta, I.; Russo, N.; Sicilia, E.; Toscano, M. The role of quantum chemistry in the elucidation of the elementary mechanisms of catalytic processes. From atoms, to surfaces, to enzymes. *Theor. Chem. Acc.* **2007**, *117*, 765–779.
- (32) Leopoldini, M.; Marino, T.; Russo, N.; Toscano, M. On the binding mode of urease active site inhibitors. A density functional study. *Int. J. Quantum Chem.* **2008**, *108*, 2023–2029.
- (33) Leopoldini, M.; Marino, T.; Toscano, M. How much can a theoretical investigation contribute to the knowledge of the catalytic mechanism of an enzyme: the case of Protein arginine deiminase 4. *Theor. Chem. Acc.* **2008**, *120*, 459–466.
- (34) Leopoldini, M.; Chiodo, S. G.; Russo, N.; Toscano, M. The reaction mechanism of molybdoenzyme formate dehydrogenase. *Chem.—Eur. J.* **2008**, *14*, 8674–8681.
- (35) Leopoldini, M.; Russo, N.; Toscano, M. The determination of the catalytic pathway of manganese arginase enzyme throughout density functional investigation *Chem.—Eur. J.* **2009**, in press.
- (36) Leopoldini, M.; Marino, T.; Russo, N.; Toscano, M. Potential Energy Surfaces for Reaction Catalyzed by Metalloenzymes from Quantum Chemical Computations. In *Self-Organization of Molecular Systems*; Russo, N., Antonchenko, V., Kryachko, E., Eds.; Springer: New York, 2009; pp 275–314.
- (37) Frisch, M. J.; Trucks, G. W.; Schlegel, H. B.; Scuseria, G. E.; Robb, M. A.; Cheeseman, J. R.; Montgomery, J. A. Jr.; Vreven, T.; Kudin, K. N.; Burant, J. C.; Millam, J. M.; Iyengar, S. S.; Tomasi, J.; Barone, V.; Mennucci, B.; Cossi, M.; Scalmani, G.; Rega, N.; Petersson, G. A.; Nakatsuji, H.; Hada, M.; Ehara, M.; Toyota, K.; Fukuda, R.; Hasegawa, J.; Ishida, M.; Nakajima, T.; Honda, Y.; Kitao, O.; Nakai, H.; Klene, M.; Li, X.; Knox, J. E.; Hratchian, H. P.; Cross, J. B.; Adamo, C.; Jaramillo, J.; Gomperts, R.; Stratmann, R. E.; Yazyev, O.; Austin, A. J.; Cammi, R.; Pomelli, C.; Ochterski, J. W.; Ayala, P. Y.; Morokuma, K.; Voth, G. A.; Salvador, P.; Dannenberg, J. J.; Zakrzewski, V. G.; Dapprich, S.; Daniels, A. D.; Strain, M. C.; Farkas, O.; Malick, D. K.; Rabuck, A. D.; Raghavachari, K.; Foresman, J. B.; Ortiz, J. V.; Cui, Q.; Baboul, A. G.; Clifford, S.; Cioslowski, J.; Stefanov, B. B.; Liu, G.; Liashenko, A.; Piskorz, P.; Komaromi, I.; Martin, R. L.; Fox, D. J.; Keith, T.; Al-Laham, M. A.; Peng, C. Y.; Nanayakkara, A.; Challacombe, M.; Gill, P. M. W.; Johnson, B.; Chen, W.; Wong, M. W.; Gonzalez, C.; Pople, J. A. *Gaussian 03*, revision C02; Gaussian, Inc.: Pittsburgh, PA, 2003.
- (38) Istvan, E. Statin inhibition of HMG-CoA reductase: a 3-dimensional view. *Atheroscler. Suppl.* **2003**, *4*, 3–8.
- (39) Istvan, E.; Palnitkar, M.; Buchanan, S. K.; Deisenhofer, J. Crystal structure of the catalytic portion of human HMG-CoA reductase: insights into regulation of activity and catalysis. *EMBO J.* **2000**, *19*, 819–830.
- (40) Di Donna, L.; Dolce, V.; Sindona, G. patent nr. CS2008A00019.
- (41) Sung, J. H.; Lee, S.-J.; Park, K. H.; Moon, T. W. Isoflavones inhibit 3-hydroxy-3-methylglutaryl coenzyme A reductase in vitro. *Biosci. Biotechnol. Biochem.* **2004**, *68*, 428–432.

Received for review July 2, 2010. Revised manuscript received September 3, 2010. Accepted September 3, 2010.

CHAPTER IV

4 Functional Food from Bergamot Waste Tissues

4.1 Introduction

In the last decades consumer demands in the field of food production has changed considerably. While in the past foods were intended to only satisfy hunger and to provide necessary nutrients for humans, today food is intended also to improve physical and mental well-being of the consumers contributing directly to their health [1-2]. Foods that fulfils this role are called “functional foods” and are consumed as part of the usual diet but provide health effects that go beyond traditional nutritional effects.

The term “functional food” itself was first used in Japan, in the 1980s, for food products fortified with particular constituents that possess advantageous physiological effects [3]. Soon the interest on functional food was diffused in Europe and United States. Experts in these countries realized that besides being able to ameliorate the health, functional food might also give a commercial potential for the food industry.

Although the term “functional food” has already been defined several times [5], so far there is no unitary accepted definition for this group of food [6]. In most countries there is no legislative definition of the term and drawing a border line between conventional and functional foods is challenging even for nutrition and food experts [7]. To date, a number of national authorities, academic bodies and the industry have proposed definitions for functional foods. These ranges from the very simple to the more complex: “foods that may provide health benefits beyond basic nutrition” or “food similar in appearance to conventional food that is intended to be consumed as part of a normal diet, but has been modified to subserve physiological roles beyond the provision of simple nutrient requirements” are just two examples . The European Commission’s Concerted Action on Functional Food Science in Europe, coordinated by International Life Science Institute (ILSI) Europe defined functional food as follows: “a food product can only be considered functional if together with the basic nutritional impact it has beneficial effects on one or more functions of the human organism thus either improving the general and physical conditions or/and decreasing the risk of the evolution of diseases. The amount of intake and form of the functional food should be as it is normally expected for dietary purposes. Therefore, it could not be in the form of pill or capsule just as normal food form” [9]. On the contrary to this latter statement,

since 2001 in Japan a functional food can also take the form of capsules and tablets. For the EU, instead, a functional food can be a natural food or can be made functional by using any of the following approaches:

- 1) Eliminating a component known to cause or identified as causing a deleterious effect when consumed (e.g. an allergenic protein).
- 2) Increasing the concentration of a component naturally present in food to a point at which it will induce predicted effects (e.g. fortification with a micronutrient to reach a daily intake higher than the recommended daily intake but compatible with the dietary guidelines for reducing risk of disease), or increasing the concentration of a nonnutritive component to a level known to produce a beneficial effect.
- 3) Adding a component that is not normally present in most foods and is not necessarily a macronutrient or a micronutrient but for which beneficial effects have been shown (e.g. nonvitamin antioxidant or prebiotic fructans).
- 4) Replacing a component, usually a macronutrient (e.g. fats), whose intake is usually excessive and thus a cause of deleterious effects.
- 5) 5) Increasing bioavailability or stability of a component known to produce a functional effect or to reduce the disease-risk potential of the food.

A functional food might be functional for all members of a population or for particular groups of the population, which might be defined, for example, by age or by genetic constitution.

Apart from the term “functional food” there are more terms for dietary products that explicitly link nutrition with health, for example “food supplements” (or “dietary supplements”) and nutraceuticals (or “nutriceuticals”). According to the Directive 2002/46/EC of the EU “food supplements” are defined as “foodstuffs the purpose of which is to supplement the normal diet and which are concentrated sources of nutrients or other substances with a nutritional or physiological effect, alone or in combination, marketed in dose form, namely forms such as capsules, pastilles, tablets, pills and other similar forms, sachets of ampoules of liquids, drop dispensing bottles, and other similar forms of liquids and powders designed to be taken in measured small unit quantities”[8]. Hence, the main difference between functional food and food supplements is that the former “are similar in appearance to conventional foods and are consumed as part of a normal diet”, whereas the latter are not considered to be proper “food”. A nutraceutical, on the other hand, is defined as “substances which are not traditionally recognised nutrients but which have positive physiological effects on the human body”. They are generally marketed in the context of health promotion/disease prevention rather than disease management. There is no legal definition of the term 'nutraceutical' nor are they currently regulated on a European-wide basis leaving each

member state free to apply its own regulatory framework. This has led to confusion with such products being available in some countries and not in others as well as being categorized differently between countries.

The development of functional foods is currently one of the most intensive areas of food product development worldwide [10]. Interest in functional foods has been prompted by a rapid expansion of scientific knowledge of the importance of a healthy diet and the technical advances in the food industry [11]. The lack of an agreed terminology seems not to be a direct obstacle to the development of a mature market since consumers are more attracted by a health message rather than the use of a particular legal term. In fact, a large number of functional foods in various forms have already been introduced into the market. Many of them contain a number of characteristic functional ingredients such as fibre, oligosaccharides, peptides and proteins, prebiotics and probiotics, phytochemicals and antioxidants, polyunsaturated fatty acids etc.

The classification of functional food can be done according to several principles: the food group it belongs to (e.g. dairy products, beverages, cereal products, confectionary, oils and fats), the diseases it is expected to prevent or alleviate (e.g. diabetes, osteoporosis, colon cancer), its physiological effects (e.g. immunology, digestibility, anti-tumor activity), the category of its specific biologically active ingredients (e.g. minerals, antioxidants, lipids, probiotics), its physico-chemical and organoleptic properties (e.g. colour, solubility, texture), or the processes that are used in its production (e.g. chromatography, encapsulation, freezing) [12]. Although there is no unified classification of food, in the literature various of the above topical groups are used to classify functional foods.

In the following sections will be presented some results which show the possibility to extract the anticholesterolemic active principles (brutieridin and melitidin) from bergamot albedo, actually a waste of essential oil industries, without making use of toxic solvents. The possibility to extract these active principles using only water as solvent open the door to applications of bergamot albedo for functional food preparations. Therefore, in sections 4.3-4.4 we will see some examples of functional foods with anticholesterolemic proprieties prepared by addition of bergamot albedo containing brutieridin and melitidin as active ingredients. Then will be shown a chromatographic method that we developed to isolate brutieridin and melitidin from bergamot juice, the other bergamot waste tissue. The latter isolated compounds, purified with a food-compatible procedure, may be used for functional food preparation purposes as well.

4.2 Recycling of industrial essential oil waste: brutieridin and melitidin, two anticholesterolaemic active principles from bergamot albedo

As was mentioned in chapter III paragraph 3.3, what remains after the extraction of the volatile fraction present in flavedo layer, the albedo and the bergamot juice, are considered waste for essential oil industries. The albedo layer, rich in pectin and several flavonoids, has never been investigated in details to see whether it could provide value-added compounds, such as active ingredients. Typically, juice and albedo of members of Citrus have very similar chemical composition. Therefore, we examined the flavonoid profile of bergamot juice which was compared with that of the same fruit albedo tissue. In fact, as can be seen in figure 4.1 chromatograms of bergamot juice and albedo are practically identical, where brutieridin and melitidin (amongst the other flavonoids) other than in bergamot juice are present in good amounts in albedo tissue.

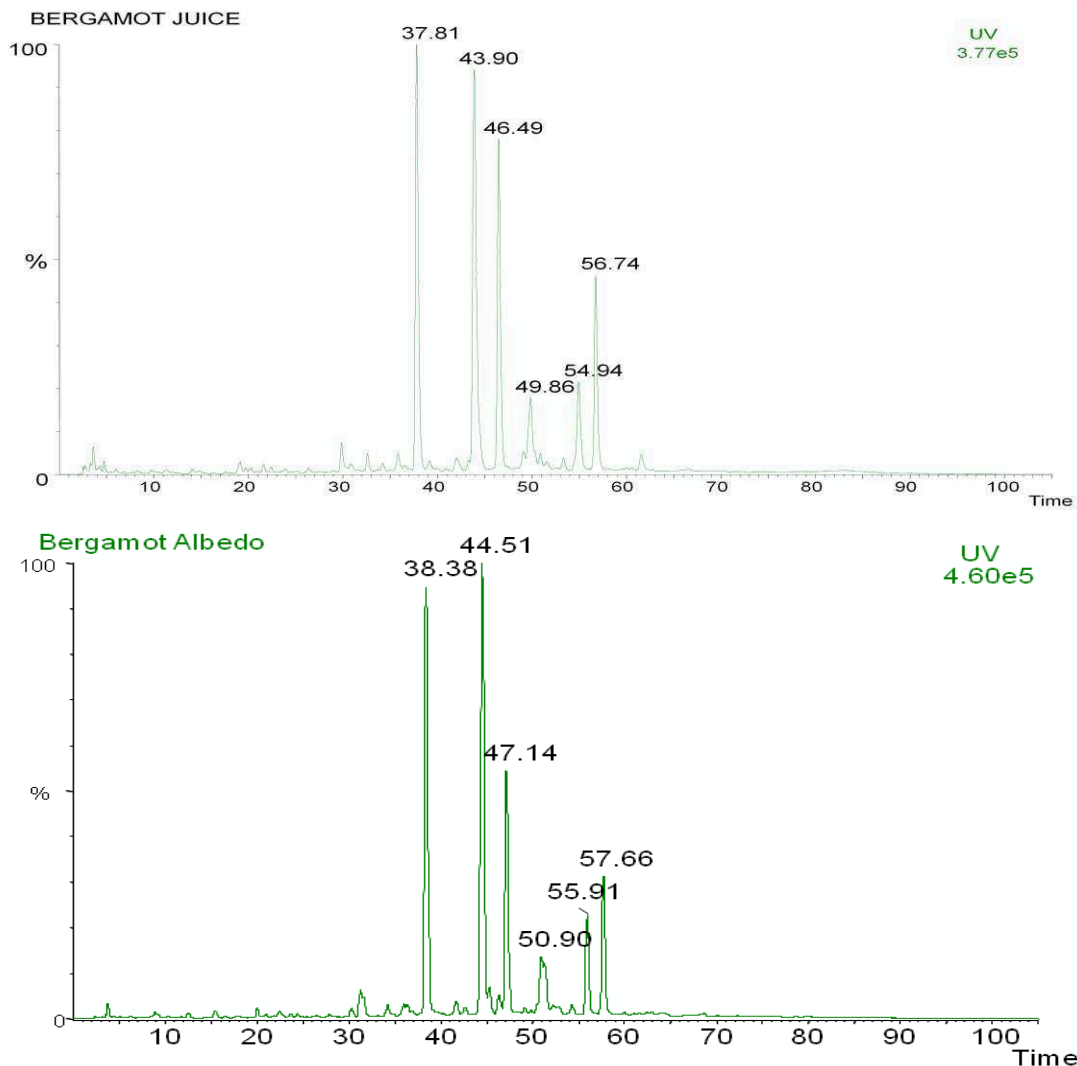


Figure 4.1 Top: UV Chromatogram of bergamot juice: neoeriocitrin (rt 37,81), naringin (rt 43,90), neohesperidin (rt 46,49), neodiosmin (rt 49,86), melitidin (rt 54,94),

brutieridin (rt 56,74). Bottom: UV chromatogram of methanol extract of bergamot albedo (peak identity as in bergamot juice).

Therefore, it was examined the possibility of finding a method to extract these two statin-like flavonoids from albedo tissue without using toxic solvents. Different procedures were used aiming at optimizing the yields of the two active principles present in albedo tissues with a particular attention on the implementation of safety procedures matching food directives issued by European and International bodies [13]. The optimization of the extraction procedure was exploited in different conditions (i) water in a microwave (MW) oven operated at 500W or (ii) by simple extraction with warm-to-hot water. Water extracts taken at different time/temperature of the MW procedure were analyzed by LC/UV-MS and the content of brutieridin and melitidin was evaluated by UV (280 nm), using the same purified analytes as external standards ($R=0.9999$). The run time was 105 min, the flow rate 1 ml/min, and the gradient was built using 0.1% HCOOH in H₂O (solvent A) and CH₃OH (solvent B) as mobile phases. The elution gradient was composed of the following steps: isocratic elution 80% A for 10 min; linear gradient from 80% A to 74% A in 2 min; linear gradient from 74% A to 31% A in 65 min; linear gradient from 31% A to 80% A in 18 min; equilibration of the column for 10 min. The results are shown in figure 4.2A and the temperatures of each MW experiment are reported in the table 4.1.

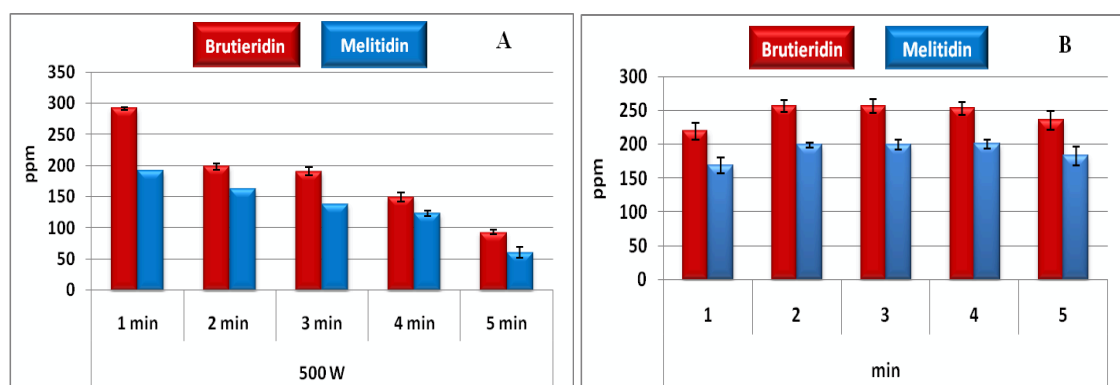


Figure 4.2 Brutieridin and melitidin content (ppm) after five independent experiments (1-5 min) by (A) microwave extraction and (B) warm-to-hot water extraction. The mean values and the standard deviations were calculated out of three measurements.

In the MW extraction the temperature of water experienced a steadily increasing from 48°C to 82°C from 1 to five minutes exposure (table 4. 1), whereas the absolute amount of extracted species decreases almost linearly with the increasing of the exposition time and solvent temperature. Therefore the best conditions are those corresponding to 1 min exposure of albedo in water at 500 W microwave oven. The damage caused by

prolonging the extraction time could be ascribed either to radiation or temperature effect on the active principles brutieridin and melitidin. It was, therefore, important to verify the behavior of albedo under water extraction at temperatures equal to those experienced in the MW procedures. The results shown in figure 4.2B allows to conclude that there is no thermal instability in the conventional extraction of the two statin-like molecules, indicating that what was observed in MW measurements is due to the molecule-MW radiation interactions.

Table 4.1. Temperatures reached in MW extraction and successively used in warm/hot water extraction method.

Time (min)	1	2	3	4	5
Temperature (°C)	48	58	68	75	82

In other analysis we have investigated the behavior of whole albedo versus dried albedo in water extracts. 93.0 g of homogenized albedo were dried in oven in two successive steps: at 30°C for 16 hours and at 40°C for 12 hours. 23.2 g of dried tissue were obtained, corresponding to the reduction to one-fourth of the original weight. The same quantity of whole and dried albedo was left, under gentle swirling, for four minutes in 100 ml of boiling water (100°C); both extracts, submitted to conventional LC/UV-MS analysis showed that the relative yields of brutieridin and melitidin do not change during drying process and are unaffected by the presence of water in the tissue. More details can be found in appendix II at the end of this chapter.

The thermal stability of brutieridin and melitidin in water medium, examined up to 100°C, promise new applications of bergamot albedo, which can be used as whole or dried, for anticholesterolemic infusion preparations.

4.3 Functional food from bergamot albedo*

Bergamot albedo was investigated for its use as a source of active principles for functional food preparation. The thermal stability of brutiridin and melitidin (tested up to 100 °C) in water indicate that both of them may be easily available by simple extraction ways amenable to domestic cooking procedures. Thus, we have examined the possibility of preparing infusions submitting albedo to the commercially tea bags and following domestic procedures for tea preparation. 503 mg of dried albedo, (or 2,012 g of whole albedo) was added to commercial tea bags (Lipton tea) containing circa 1,5 g of black tea. The prototypal tea bags were left, under weak agitation, for four minutes in a tea cup containing 200 ml of boiling water (100°C). The same procedure was followed

* Manuscript in preparation

for tea bags containing whole albedo. In both cases 20 µl of the so prepared infusions, previously filtered using a 0,45 µm Teflon syringe filter, were injected into LC/UV-MS. The results reported in table 4.2 and figure 4.3 confirm the relative amount of extracted active principles and that the two statin-like molecules brutieridin and melitidin can be extracted easily by household procedures.

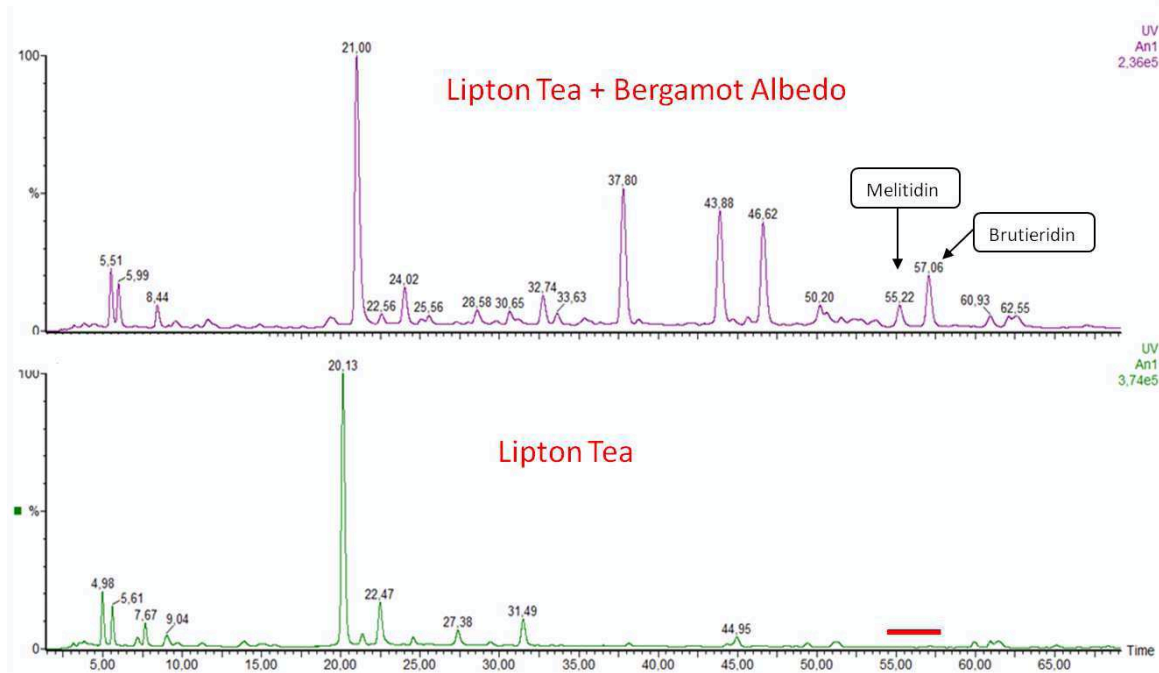


Figure 4.3. Bottom: UV profile of commercial black tea (Lipton). Top: UV profile of commercial black tea (Lipton) after addition of dry bergamot albedo.

Table 4.2. Absolute content of brutieridin and melitidin in tea infusions*.

Sample	Brutieridin (ppm)	Melitidin (ppm)
Dried albedo in black tea	10,1 ± 0,2	7,0 ± 0,1
Whole albedo in black tea	10,6 ± 0,8	6,6 ± 0,3

*The mean values and the standard deviations were calculated over three measurements.

Analog experiments were carried out following the procedures for coffee preparation (Italian espresso). Espresso coffee samples were prepared by using medium roasted and ground coffee arabica (geographical origin: Ethiopia) and packed into iperespresso capsules. Each capsule contained 6,7± 0,1 g of coffee. To this iperespresso capsules were added 100, 300 and 500 mg of lyophilized albedo (obtaining the espresso samples L100, L300, L500, respectively) while the espresso samples F100, F300, F500, F800 were prepared by addition of 100, 300, 500 and 800 mg of oven-dried bergamot albedo,

respectively. The espresso coffee using the above prototypal samples were prepared by using a professional iperespresso coffee machine (mod. X2, Illycaffè S.p.A.). Brutieridin and melitidin were quantified by HPLC (1100 Agilent) using the external calibration method (pure standards, brutieridin and mlitidin, purified in our lab by semi-preparative HPLC), as reported in section 4.2 (for MW and hot water extraction of albedo). Results are summarized in table 4. 3.

Espresso coffee sample	Melitidin (ppm)	Brutieridin (ppm)
L100	ND	ND
L300	16	49
L500	38	117
F100	nd	nd
F300	11	36
F500	43	125
F800	52	155
S100*	236	1774

Table 4.3. Content of melitidin and brutieridin in espresso coffee samples. nd - not detected. *Sample S100 was prepared by adding to iperespresso capsules 100 mg of brutieridin purified by VersaFlash chromatography (see next section).

The above data allow to conclude that bergamot albedo can be used also for coffee preparations with anticholesterolemic proprieties.

In other experiments it was investigated the use of bergamot albedo for preparation of milk and its derivatives. To 500 ml of UHT milk (Parmalat) were added 7 g of dried albedo, left under weak agitation for 10 min at 75°C and then filtered (to remove the albedo). 0,5 ml of milk were then extracted according the method of Nagy et al. [14] and analyzed by LC-MS/UV, as for tea and coffee cases. After the confirmation of the presence of both active principles, the milk was cooled to 40°C, added lactic ferments (*Lactobacillus bulgaricus* & *Streptococcus thermophilus*) and incubated for 8 hours at 40°C. The yogurt obtained was analyzed every 3 days (for a total of three weeks) to follow the stability of brutieridin and melitidin during the fermentation process and its conservation at 4°C (3 weeks monitoring). The profiles shown in figure 4.4 indicate that brutieridin and melitidin are unaffected by the fermentation process and were stable for whole monitoring period. In fact, even at the 21st day of yogurt

conservation at 4°C, the amounts of brutieridin and melitidin were found to be invariable.

The thermal stability of brutieridin and melitidin at higher temperatures was tested using whole bergamot albedo for biscuit preparation which were cooked at 180°C for 20 min. Biscuits then were analyzed and both intact brutieridin and melitidin were found.

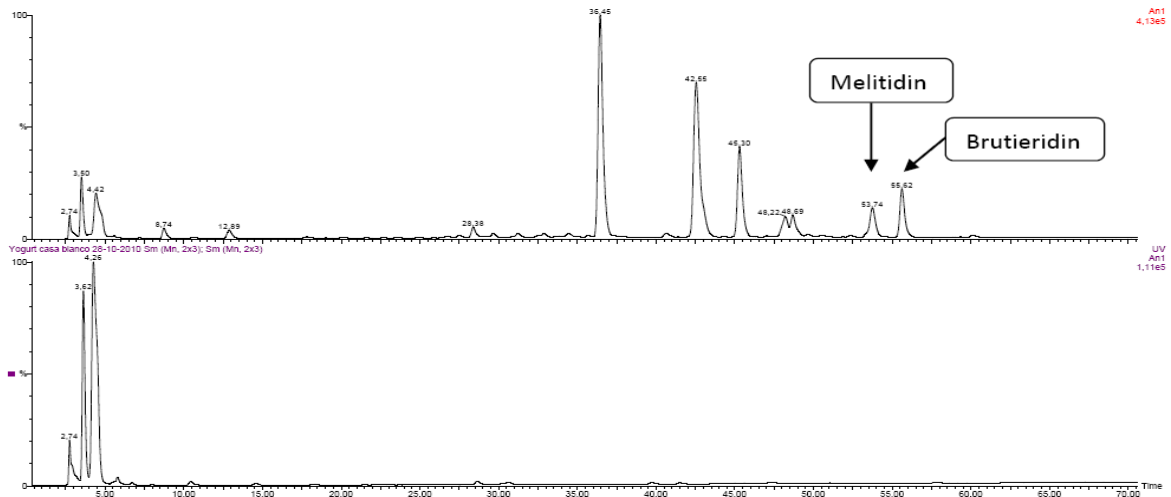


Figure 4.4. UV profiles obtained from LC/UV-MS of yogurt (after 21 days) obtained from milk containing albedo (top) and yogurt made from milk without albedo addition (bottom).

The above results clearly support the use of albedo as a source of active principles for preparation of different functional foods and beverages such as tea, coffee, infusions, milk, yogurt, biscuits etc., with anticholesterolemic proprieties.

4.4. Isolation of brutieridin and melitidin from bergamot juice by VersaFlash chromatography

Bergamot juice contain circa 500 mg/L of brutieridin and about 300 mg/L of meltidin other than several other flavonoids (mostly neoeriocitrin, neoesperidin, naringin and neodiosmin) [15]. Although all this compounds are known for their beneficial effects on health, the juice is not used for food purposes due to its bitter taste and is still considered a waste product. The pervious semi-preparative HPLC method developed from our group [15], although useful to purify



small quantities with high purity (>99%) grade, makes use of toxic solvents (acetonitrile, methanol) therefore the purified compounds can not be used for food purposes. Thus, we have performed several experiments aiming the isolation of brutieridin and melitidin from bergamot juice by means of a simpler, less expensive chromatographic system, called VersaFlash (Supelco). This relatively cheap chromatographic system permits the use of cartridges with high loading capacity. In the present case was used a cartridge with dimensions 40 x 75 mm, which was packed with 70 g of C18 stationary phase. The elution was optimized in order to obtain brutieridin and melitidin as pure as possible, using only food grade solvents (water and ethanol). The following method gave the best results for brutieridin in terms of purity and solvent consumption: isocratic elution water/ethanol 92:8 (table 4.4). In figure 4.5 can be appreciated the purity of the fractions of our interest.

Table 4.4. Elution and isolated fractions of bergamot juice flavonoids by VersaFlash chromatography.

Volume (ml)	Elution (H ₂ O/EtOH)	Fractions isolated	Flow (ml/min)
0-2300	92:8	Neoeriocitrin/neoesperidin/naringin	40
2350-3100		Brutieridin/melitidin/neoesperidin	
3150-4200		Brutieridin/melitidin	
4250-5200		Brutieridin	

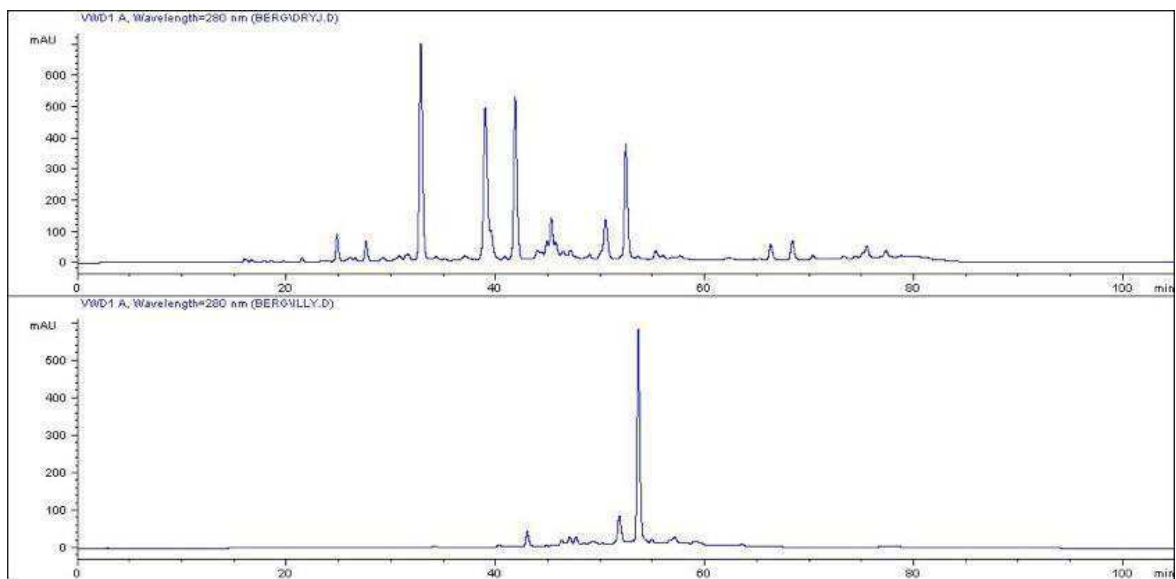


Figure 4.5. UV profile (HPLC) of a dry extract of bergamot juice before (top) and after (bottom) VersaFlash purification. The purified fraction was used to prepare the espresso coffee sample S100.

It is evident the high purity of the brutieridin isolated (figure 4.5 bottom). 100 mg of this fraction were added to the iperespresso coffee capsules to prepare the sample S100 (table 4.3). In figure 4.6 can be observed the profiles of coffee before and after addition of purified brutieridin.

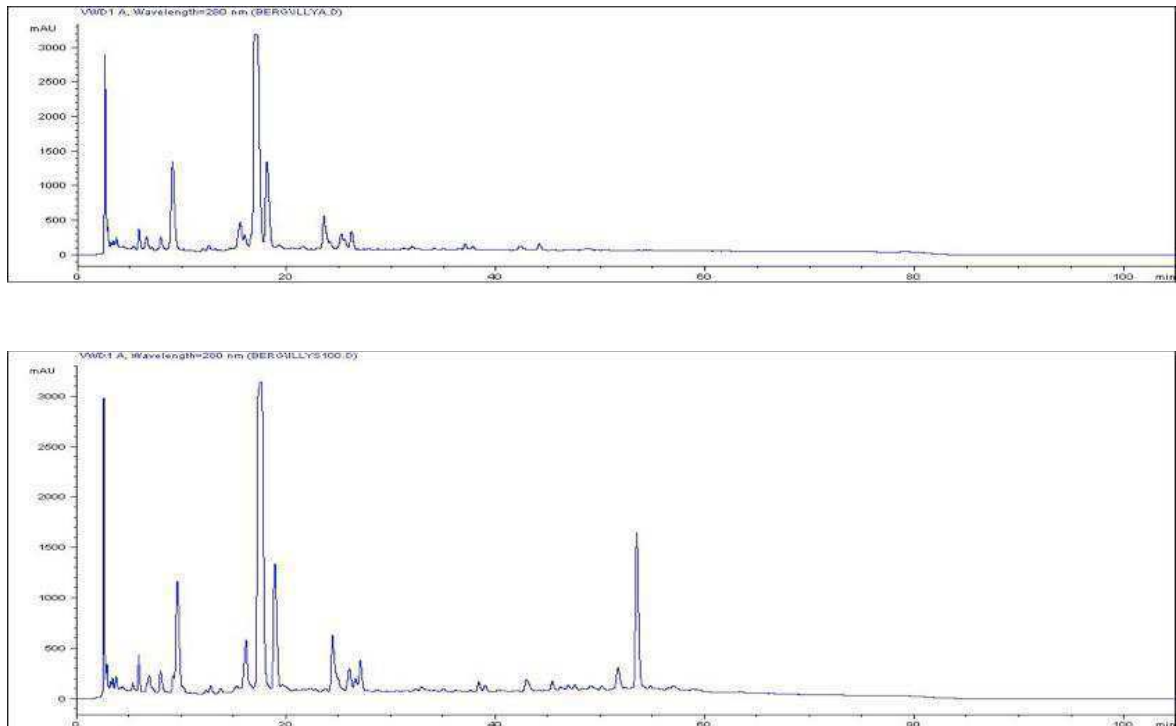


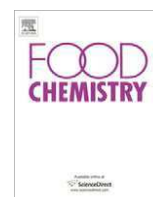
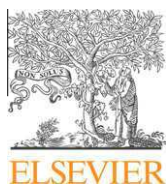
Figure 4.6 UV profile (HPLC) of an espresso coffee obtained from an iperespresso capsule containing 6,7 g of a medium roasted and ground coffee arabica (top) and (bottom) profile of the same iperespresso capsule enriched with 100 mg of a purified brutieridin (sample S100).

It remains for the future to perform the scale-up of the Versaflash method in order to extend its application to industrial scale. The pure fractions obtained may then be used as active ingredients for anticholesterolemic functional food production.

References

1. Mollet B., Rowland I., Functional foods: at the frontier between food and pharma, *Current Opinion in Biotechnology*, 2002, 13, 483–485.
2. Roberfroid M. B., An European consensus of scientific concepts of functional foods, *Nutrition*, 2000b, 16, 689–691.
3. Farr D. R., Functional foods, *Cancer Letters*, 1997, 114, 59-63.
4. Niva M., Makela J., Finns and functional foods: Sociodemographics, health efforts, notions of technology and the acceptability of health-promoting foods, *International Journal of Consumer Studies*, 2007, 31, 34–45.
5. Roberfroid M. B., Global view on functional foods: European perspectives, *British Journal of Nutrition*, 2002, 88, S133–S138.
6. Alzamora S. M., Salvatori D., Tapia S. M., López-Malo A., Welti-Chanes J., Fito P., Novel functional foods from vegetable matrices impregnated with biologically active compounds. *Journal of Food Engineering*, 2005, 67, 205–214.
7. Niva M., ‘All foods affect health’: Understandings of functional foods and healthy eating among health-oriented Finns, *Appetite*, 2007, 48, 384–393.
8. DIRECTIVE 2002/46/EC OF THE EUROPEAN PARLIAMENT AND OF THE COUNCIL, 10 June 2002.
9. Diplock A.T., Aggett P.J., Ashwell M., Bornet F., Fern E.B., Roberfroid M.B., Scientific concepts of functional foods in Europe-consensus document, *Br. J. Nutr.*, 1999, 81, S1–S27.
10. Menrad K., Market and marketing of functional food in Europe, *Journal of Food Engineering*, 2003, 56, 181–188.
11. Biström M., Nordström K., Identification of key success factors of functional dairy foods product development, *Trends in Food Science & Technology*, 2003, 13, 372–379.
12. Juvan S., Bartol T., Boh B., Design and development of a relational database for functional foods, *Acta Agriculturae Slovenica*, 2005, 86, 3-15.
13. ICH, Guideline for residual solvents Q3C(R4), 2009.
14. Nagy K., Redeuil K., Bertholet R., Steiling H., Kussmann M., Quantification of Anthocyanins and Flavonols in Milk-Based Food Products by Ultra Performance Liquid Chromatography-Tandem Mass Spectrometry, *Anal. Chem.* 2009, 81, 6347–6356.
15. Di Donna L., De Luca G., Mazzotti F., Napoli A., Salerno R., Taverna D., Sindona G., *J. Nat. Prod.*, 2009, 72 1352–1354.

APPENDIX II



Recycling of industrial essential oil waste: *Brutieridin* and *Melitidin*, two anticholesterolaemic active principles from bergamot albedo

Leonardo Di Donna, Giselda Gallucci, Naim Malaj, Elvira Romano, Antonio Tagarelli, Giovanni Sindona*

Dipartimento di Chimica, Università della Calabria, I-87030 Arcavacata di Rende, CS, Italy

ARTICLE INFO

Article history:

Received 1 July 2010

Received in revised form 3 September 2010

Accepted 7 September 2010

Keywords:

Bergamot waste

Albedo

Brutieridin

Melitidin

ABSTRACT

Bergamot albedo, the white tissues between the skin and the pulp, is a polluting waste in the production of the renowned fragrance and is easily available by simple industrial processes. Brutieridin and melitidin are found in bergamot albedo and possess statin-like activity. Their anticholesterolaemic effect has been proved *in vitro*. Different procedures were exploited to assay the presence of brutieridin and melitidin and to evaluate their availability in water extracts. The best results in terms of simplicity and accessibility of the method were obtained with hot water at 65 °C. Interestingly, tea beverages enriched with the two active principles have been obtained by simple addition of dried albedo into commercial tea bags. This is the first report on the availability of methodologies to extract active principles from citrus albedo wastes.

© 2010 Elsevier Ltd. All rights reserved.

1. Introduction

Bergamot (*Citrus bergamia* Risso) is the common name of the fruit of the genus *Citrus* belonging to the family Rutaceae, subfamily Esperidea, which is a very delicate plant that has its natural habitat in a narrow zone in the province of Reggio Calabria (Italy). The essential oil from the fruit flavedo is widely used in the cosmetics industry. However, bergamot juice and albedo, the white tissue between the skin and the pulp, have no important industrial applications, in evident disparity with other citrus fruits. The albedo layer, rich in pectin and several flavonoids, has never been investigated in detail, to see if it could provide value-added compounds, such as nutraceuticals. What remains after the extraction of the volatile fraction is considered, in fact, industrial waste with its relative economic and environmental disadvantages. Recently, our research group has identified, in the whole fruit juice, the presence of two new statin-like flavonoids brutieridin (**1**) and melitidin (**2**).

The inhibitory effect on HMG-CoA reductase of these new flavonoids, bearing the 3-hydroxy-3-methyl-glutaric acid (HMG) moiety, was compared, *in vitro*, against commercial statin drugs with excellent results (Di Donna, Dolce, & Sindona, 2008). Preliminary results from animal testing against the commercial drug pravastatin have shown that the new natural molecules **1** and **2** (Fig. 1) can play an important role as natural active principles lowering blood

cholesterol level (Sindona et al., unpublished results). Moreover, computational studies based on density functional theory have demonstrated that both molecules bind efficiently to the catalytic site of HMG-CoA reductase (Leopoldini, Malaj, Toscano, Sindona, & Russo, in press). Calabrian folk medicine has considered, since the introduction of the plant in the middle of the 18th century, bergamot juice as a natural answer to the control of cholesterol level in blood. These important properties have always been associated with the effect of flavonoids, such as naringin, neoeriocitrin and neohesperidin, present in the order of several hundreds of ppm and to other minor species such as rhoifolin, neodiosmin, and chrysoeriol present at lower concentrations (Dugo et al., 2005; Gattuso, Barreca, Caristi, Gargiulli, & Luezzi, 2007; Gattuso et al., 2006). The association of anticholesterolaemic activity to flavonoid content lacks any scientific support. It cannot explain why other citrus fruits, containing the same species, do not exhibit the healing effect traditionally associated with bergamot.

Recycling of waste from the citrus industry is limited to the transformation of the entire raw material into fertiliser (Van Heerden, Cronjé, Swart, & Kotzé, 2002) or animal fodder (Tripodo, Lanzetta, Micali, Coppolino, & Nucita, 2004). Considering that the cost of the albedo industrial waste is lower than the cost of the transportation to manufacturing plants, it is worthwhile to exploit its possible use as a source of anticholesterolaemic food supplements. Different procedures, therefore, are now presented aiming at optimising the yields of those active principles present in properly treated albedo tissues. Safety procedures matching food supplements directives issued by European and International bodies were implemented (ICH, 2009).

* Corresponding author. Tel.: +39 0984 49 2083; fax: +39 0984 49 3307.

E-mail address: sindona@unical.it (G. Sindona).

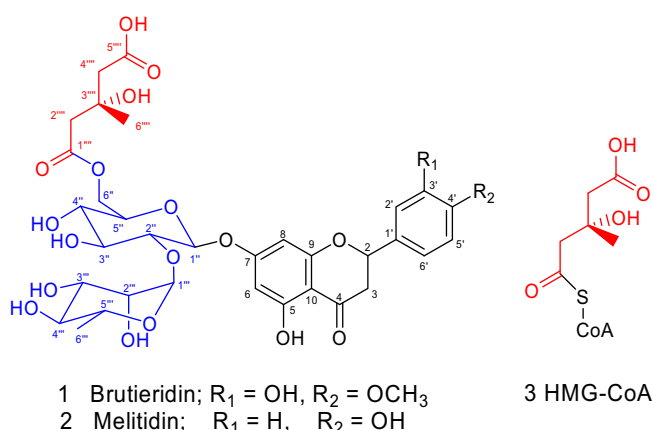


Fig. 1. Structures of brutieridin (1), melitidin (2) and HMG-CoA.

2. Materials and methods

2.1. Chemicals

HPLC-grade methanol and 99% formic acid were purchased from Carlo Erba (Milan, Italy). Aqueous solutions were prepared using ultrapure water, with a resistivity of 18.2 M Ω cm, obtained from a Milli-Q plus system (Millipore, Bedford, MA). Brutieridin and melitidin used as calibration standards were purified in our laboratory.

2.2. Plant material

Frozen bergamot albedo was furnished by Goiasucchi s.r.l. (Gioia Tauro, Italy). Commercial Yellow Label Tea (Lipton) was used for the preparation of prototype albedo-containing tea bags.

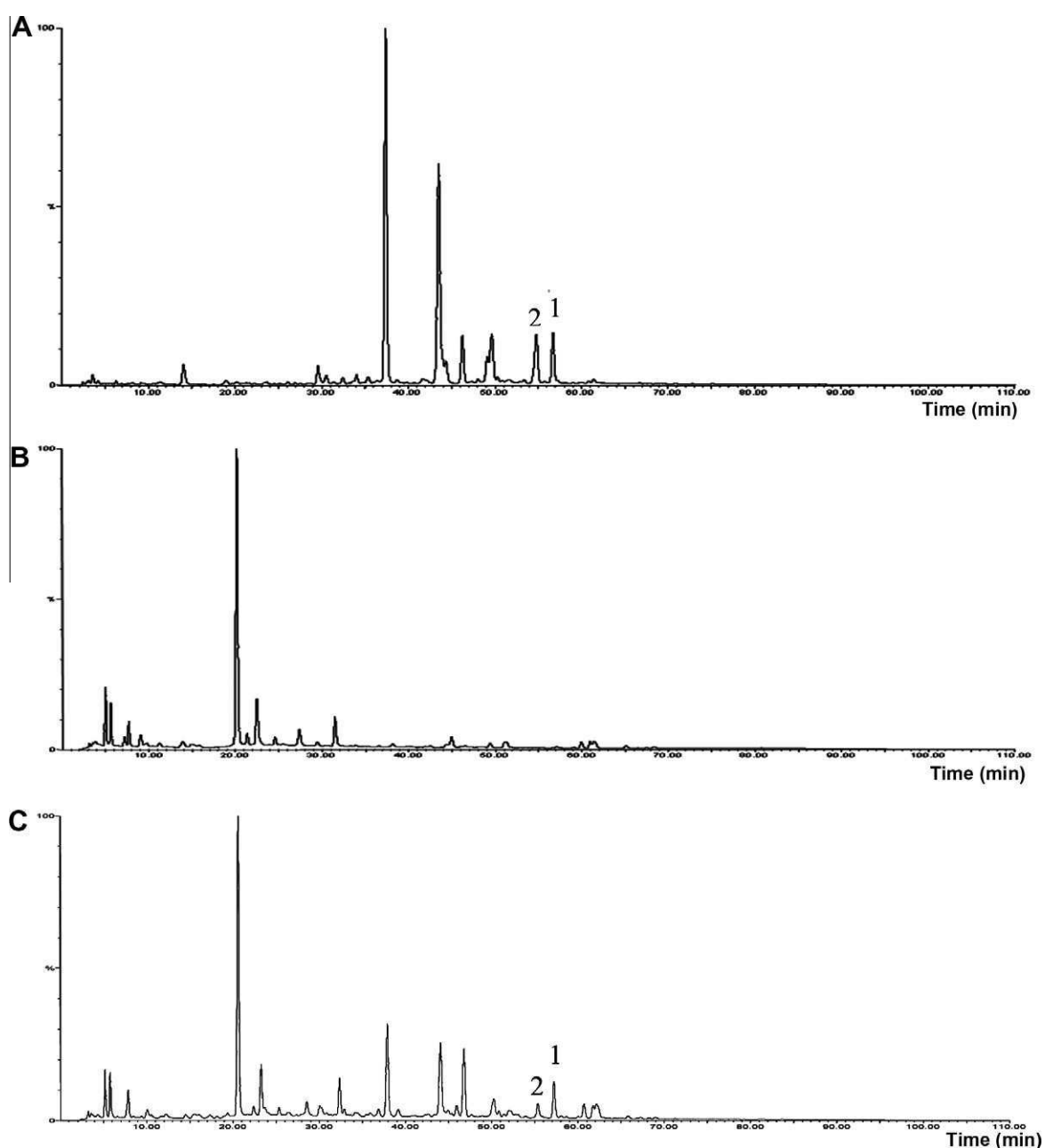


Fig. 2. UV profiles obtained from LC/UV/MS of albedo (A) water extract, (B) commercial tea and (C) dried albedo in commercial tea bag.

2.3. Instrumentations and conditions

Microwave-assisted extraction was carried out using an Anton Paar Multiwave 3000 with programmable power control (maximum power 1400 W) and rotor XF100 (operating pressure up to 120 bar maximum; operating temperature 260 °C maximum; construction material PTFE-TFM for the vessel). In every vessel were put 3 g of homogenised whole albedo and 20 ml of water (4 vessels were used for each analysis) and a potential of 500 W was applied for different duration times (1–5 min). This matrix/solvent ratio was maintained constant for warm/hot water extraction method. All water extracts were centrifuged at 4500 rpm for 5 min and filtered before instrumental analysis.

LC-ESI-MS/UV analysis was performed using a Waters Fraction-Lynx system (Milford, MA) equipped with a ZMD mass spectrometer and a 486 UV detector. The column used for all our analyses was a Luna C18 (2) (250 × 4.6 mm; Phenomenex, Torrance, CA). The UV detector was set at 280 nm.

The run time was 105 min, the flow rate was 1 ml/min, and the gradient was built using 0.1% HCOOH in H₂O (solvent A) and CH₃OH (solvent B) as mobile phases. The elution gradient was composed of the following steps: isocratic elution 80% A for 10 min; linear gradient from 80% A to 74% A in 2 min; linear gradient from 74% A to 31% A in 65 min; linear gradient from 31% A to 80% A in 18 min; equilibration of the column for 10 min. The calibration curve was constructed from the following solutions of brutieridin in methanol/water (1:1): 25, 12.5, 6.25 and 3.125 ppm.

3. Results and discussion

The peculiarity of bergamot lies in the presence of two new statin-like molecules **1** and **2** that are esters of 3-hydroxy-3-methylglutaric (HMG) acid which, when linked to CoA (**3**, Fig. 1), represents the key intermediate in cholesterol biosynthesis. The action of NADPH in the presence of HMG-CoA reductase is the accepted mechanism, which brings about the reduction of the thioester function to the corresponding alcohol and provides the biochemical tools to investigate the inhibitory effects of commercial statin drugs (Istvan & Deisenhofer, 2000, 2001; Istvan, Planitkar, Buchanan, & Deisenhofer, 2000; Taberner, Bochar, Rodwell, & Stauffacher, 1999). Compounds **1** and **2** show an acceptable degree of inhibition against the same reduction system (Sindona et al., unpublished results). In this case in fact the ester function between positions 6' of the glucose and 1''' of the HMG moieties should be stable to the action of the NADPH reducing agent.

3.1. The content of active principles in the bergamot albedo

Mass spectrometric and UV analysis of the water extract (see Section 2.3) of bergamot albedo (Fig. 2A) displays a profile similar to that obtained with the juice, where the two active principles are present. The optimisation of the extraction procedure was exploited under different conditions: (i) water in a microwave (MW) oven operated at 500 W or (ii) by simple extraction with warm-to-hot water. Water extracts taken at different time/temperature of the MW procedure were analysed by LC/UV-MS (Di Donna et al., 2009) and the content of **1** and **2** was evaluated by UV (280 nm), using the same purified analytes (Di Donna et al., 2009) as external standard ($r=0.9999$; Fig. 3). The results are shown in Fig. 4A and the temperatures of each MW experiment are reported in Table 1.

In the MW extraction the temperature of water ranged from 48 °C to 82 °C with 1–5 min exposure (Table 1); however, the absolute amount of extracted species decreased almost linearly with

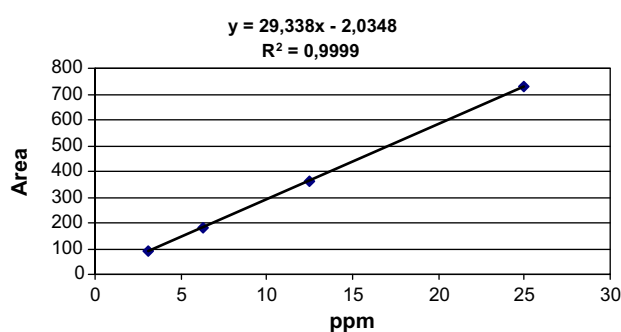


Fig. 3. Calibration curve for brutieridin standard.

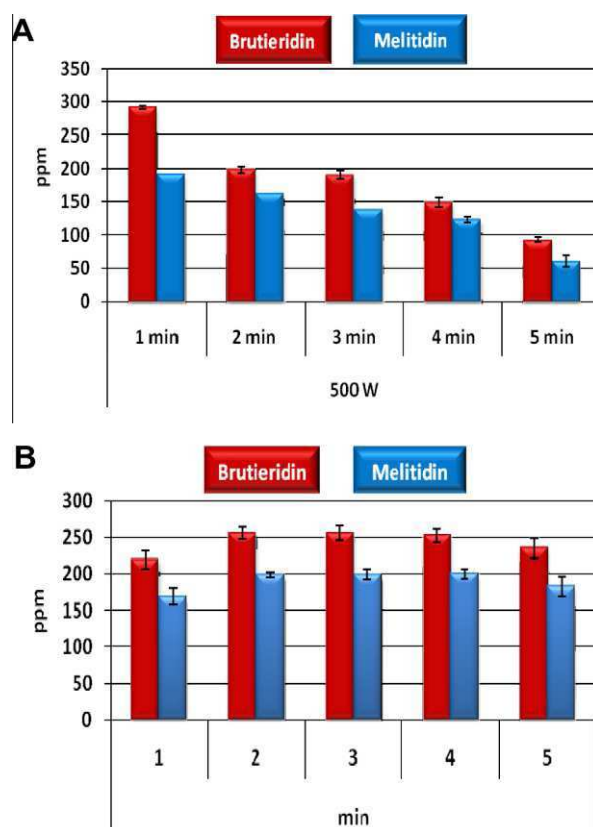


Fig. 4. Brutieridin (**1**) and melitidin (**2**) content (ppm) after five independent experiments (1–5) by (A) microwave extraction and (B) warm-to-hot water extraction. The mean values and the standard deviations were calculated from three measurements.

Table 1

Temperatures reached in microwave extraction and successively used in warm/hot water extraction method.

Time (min)	1	2	3	4	5
Temperature (°C)	48	58	68	75	82

increasing extraction time and solvent temperature. Therefore the best conditions are those corresponding to 1 min exposure of albedo in water in a 500-W microwave oven. The losses caused by prolonging the extraction time could be ascribed either to radiation or temperature effect on the active principles **1** and **2**. It was, therefore, important to verify the behaviour of albedo under water extraction at temperatures equal to those experienced in the MW procedures. The results shown in Fig. 4B suggest that there is no

Table 2
Absolute content of brutieridin and melitidin in tea infusions.^a

Sample	Brutieridin (ppm)	Melitidin (ppm)
Dried albedo in black tea	10.12 ± 0.16	7.01 ± 0.08
Whole albedo in black tea	10.56 ± 0.81	6.62 ± 0.34

^a The mean values and the standard deviations were calculated over three measurements.

thermal effect on the conventional extraction of the two statin-like molecules.

What was observed in MW conditions may result from the exposure to microwaves, which probably degrade the compounds of interest, acting on the sugar or on the glutaric moieties. Actually, the amount of statin-like molecules in water extracts seems almost independent from the temperature, which can be conveniently set at a value of 65 °C in order to optimise the yields.

3.2. The content of active principles in whole albedo vs. dried albedo

Homogenised albedo (93.0 g) was oven-dried in two successive steps: at 30 °C for 16 h and then at 40 °C for 12 h. Dried tissue (23.2 g) was obtained, corresponding to a reduction to one-quarter of the original weight. The same quantity of whole and dried albedo was left, under gentle swirling, for four minutes in 100 ml of boiling water (100 °C); both extracts, submitted to conventional LC/UV/MS analysis showed that the relative yields of **1** and **2** were unaffected by the presence of water in the tissue. When dried matter is used, the absolute recovery of the natural statins is four times higher than that from whole albedo.

Finally, a recovery test was performed, submitting albedo to the domestic procedure for preparing infusions from commercial tea bags. Dried albedo (0.503 g or 2.012 g of whole albedo) was added to commercial tea bags containing ca. 1.5 g black tea. The prototype tea bags were left, under weak agitation, for four minutes in a tea cup containing 200 ml of boiling water (100 °C). The same procedure was followed for bags containing whole albedo. In both cases 20 µl of the so prepared infusions, previously filtered using a 0.45-µm Teflon syringe filter, were injected into an LC/UV/MS.

The results reported in Table 2 confirm the relative amount of extracted active principles does not depend on the presence of water and that the two statin-like molecules brutieridin and melitidin can be extracted easily by household procedures.

4. Conclusions

The results here presented throw light onto the possible use of an industrial waste as a natural resource in the control of blood cholesterol level. The active principles **1** and **2** can be easily obtained by simple extraction procedures.

Acknowledgments

This project was funded by the Calabrian APQ-RAC network, QUASIORA project, and by IRIDEA S.R.L. company.

References

- Di Donna, L., De Luca, G., Mazzotti, F., Napoli, A., Salerno, R., Taverna, D., et al. (2009). Statin-like principles of bergamot fruit (*Citrus bergamia*): Isolation of 3-hydroxymethylglutaryl flavonoid glycosides. *Journal of Natural Products*, 72, 1352–1354.
- Di Donna, L., Dolce, V., & Sindona, G. (2008). Patent Nr. CS2008A00019.
- Dugo, P., Lo Presti, M., Ohman, M., Fazio, A., Dugo, G., & Mondello, L. (2005). Determination of flavonoids in citrus juices by micro-HPLC-ESI/MS. *Journal of Separation Science*, 28, 1149–1156.
- Gattuso, G., Barreca, D., Caristi, C., Gargiulli, C., & Leuzzi, U. (2007). Distribution of flavonoids and furocoumarins in juices from cultivars of *Citrus bergamia* Risso. *Journal of Agricultural and Food Chemistry*, 55, 9921–9927.
- Gattuso, G., Caristi, C., Gargiulli, C., Bellocco, E., Toscano, G., & Leuzzi, U. (2006). Flavonoid glycosides in bergamot juice (*Citrus bergamia* Risso). *Journal of Agricultural and Food Chemistry*, 54, 3929–3935.
- ICH. (2009). *Guideline for residual solvents Q3C(R4)*.
- Istvan, E., & Deisenhofer, J. (2000). The structure of the catalytic portion of human HMG-CoA reductase. *Biochimica et Biophysica Acta*, 1529, 9–18.
- Istvan, E., & Deisenhofer, J. (2001). Structural mechanism for statin inhibition of HMG-CoA reductase. *Science*, 292, 1160–1164.
- Istvan, E. S., Planitkar, M., Buchanan, S. K., & Deisenhofer, J. (2000). Crystal structure of the catalytic portion of human HMG-CoA reductase: Insights into regulation of activity and catalysis. *The EMBO Journal*, 19, 819–830.
- Leopoldini, M., Malaj, N., Toscano, M., Sindona, G., & Russo, N. (in press). On the inhibitor effects of Bergamot juice flavonoids binding to 3-hydroxy-3-methylglutaryl-CoA reductase (HMGR) enzyme. *Journal of Agricultural and Food Chemistry*.
- Sindona et al., unpublished results from our laboratory.
- Taberero, L., Bochar, D. A., Rodwell, V. W., & Stauffacher, C. V. (1999). Substrate-induced closure of the flap domain in the ternary complex structures provides insights into the mechanism of catalysis by 3-hydroxy-3-methylglutaryl-CoA reductase. *Proceedings of the National Academy of Sciences of the United States of America*, 96, 7167–7171.
- Tripodo, M. M., Lanuzza, F., Micali, G., Coppolino, R., & Nucita, F. (2004). Citrus waste recovery: A new environmentally friendly procedure to obtain animal feed. *Bioresource Technology*, 91, 111–115.
- Van Heerden, I., Cronjé, C., Swart, S. H., & Kotzé, J. M. (2002). Microbial, chemical and physical aspects of citrus composting. *Bioresource Technology*, 81, 71–76.

CHAPTER V

5 Analysis of Citrus Flavonoids by Paper Spray and Leaf Spray Mass Spectrometry

5.1 PS-MS determination of flavonoids from Citrus juices

Paper spray (PS) is a recently developed ambient ionization method that has been shown to be effective for fast, qualitative, and quantitative analysis of complex mixtures, including complex biological fluids such as whole blood and raw urine (paragraph 2.2, chapter II). It is a very simple method which consist of a paper (or other porous substrates) cut into a triangular shape with typical height 10 mm and base 5 mm (dimensions can be changed in function of sample amount) and then the sample is loaded. When solvent is applied and a high voltage is supplied to the paper, a spray of charged droplets is induced at the tip of the paper triangle. One of the principal advantages of PS is that the analyte can be loaded without any pretreatment and sprayed directly as the voltage is applied or it may be preloaded on paper, allow to dry and successive solvent addition and voltage application generate the spray. The experiments are done in the open lab environment and the distance between the tip of the paper triangle and the inlet to the mass spectrometer is >3 mm.

Although it is a recent method, it has been used for several applications (see chapter II, paragraph 2.2 for further details), especially those of biomedical field. The good performance of paper spray, its simplicity of use (respect the consolidated ionization techniques), non necessity of sample pretreatment, rapidity, low volumes of solvent needed etc. make it a potential ionization method to apply in almost all the fields of science.

One unexplored field of PS application is that of food analysis. Therefore, it was particularly interesting to examine the performance of PS for the analysis of liquid food samples. For this purpose, flavonoids of Citrus juices were selected as a target class of compounds to be determined. In particular, it was investigated the possibility of detection of flavonoids in different Citrus juices without or with some simple and fast sample pretreatment. It is known that Citrus juices are complex mixtures of organic

acids, sugars, flavonoids, aminoacids etc. This high complexity of Citrus juices may pose problems of ion suppression even to the well consolidated ionization methods (like ESI and APCI). For this reason, citrus juices were: (i) diluted in different organic solvents (methanol, ethanol, isopropanol) at different ratios and (ii) purified by a C18 SPE (solid phase extraction) cartridge (Supelco Discovery DSC-18 SPE tube 6ml, Sigma Aldrich).

Target flavonoids investigated in each citrus juice are reported in table 5.1. The identification of flavonoids was performed comparing the MSⁿ fragmentation pattern with literature data and with pure compounds, where possible. In most of the cases the MS/MS (MS²) was sufficient to identify each flavonoid, confirmed further by MS³ and MS⁴. It is worth to be mentioned that operating in this experimental conditions, neohesperidoside and rutinoid isomers can not be distinguished in juices where both isomers are present.

5.1.1 Sample Preparation

Juices of orange, lemon, mandarin and bergamot were obtained by hand squeezing the respective fruits purchased from the local market (Lafayette, IN, USA). For the group (i) analysis, 1 ml of each juice was centrifuged (6500 rpm x 5 min) and then diluted in different solvents (methanol, ethanol, isopropanol) at diverse mixing ratios: 99:1, 95:5, 90:10, 80:20, 70:30 solvent/juice (v/v). For group (ii) experiments, after the centrifugation of the juices, the SPE purification was performed as follows: equilibration of the cartridge with 4 ml of methanol (or ethanol, isopropanol) followed by 4 ml of water; 2 ml of juice were loaded and the eluate was collected (labeled "fraction 1"). The retained fraction was washed 2 x 2 ml of water, collecting each fraction separately (labeled as "fraction 2 and 3" respectively). Finally, the retained fraction was recovered with 2 ml of methanol (or ethanol, isopropanol) and labeled "fraction 4". Note that the volume of juice loaded and the volume of methanol used to recover the retained fraction were the same, so no pre-concentration operations occurred during this SPE purification procedure. 2 µl of each sample were loaded on a triangle (5 mm long and 2,5 mm base-width) of printer paper (Xerox).

5.1.2 Instrumentation

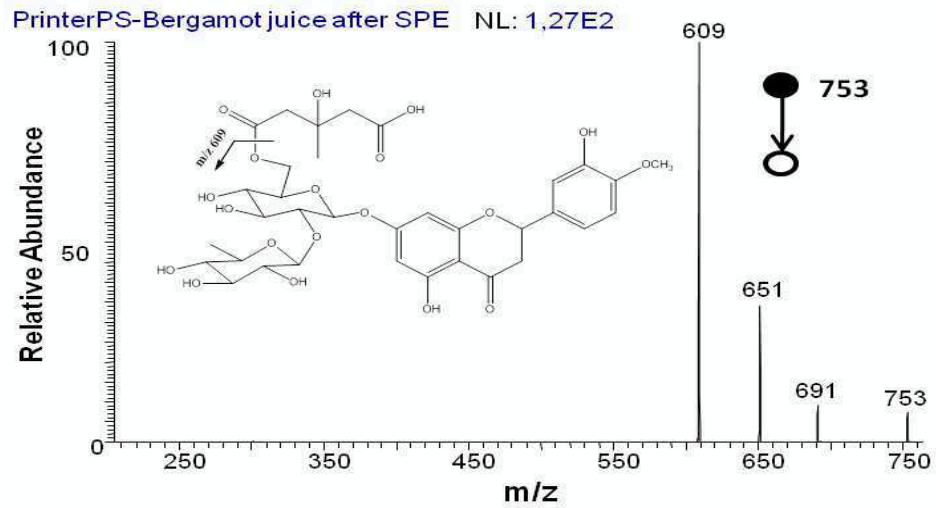
All the measurements reported herein were carried out on Finnigan LTQ mass spectrometer (Thermo Finnigan San José, CA, USA) tuned for optimum detection via the Xcalibur software. The voltage of 4,5 kV was applied to the base of paper triangle through a copper clip. Full scan and MSⁿ mass spectra were recorded in negative

ionization mode and using automatic gain control mode with a maximum ion trap injection time of 300 ms and 3 microscans per spectrum. The main experimental parameters used were as follows: capillary temperature 200 °C; tube lens (V): -65 V; capillary voltage: -15 V. Tandem mass spectrometry experiments were performed using collision-induced dissociation (CID). All experiments were performed using an isolation window of 1.4 (m/z units) and 15–30% collision energy (manufacturer's unit).

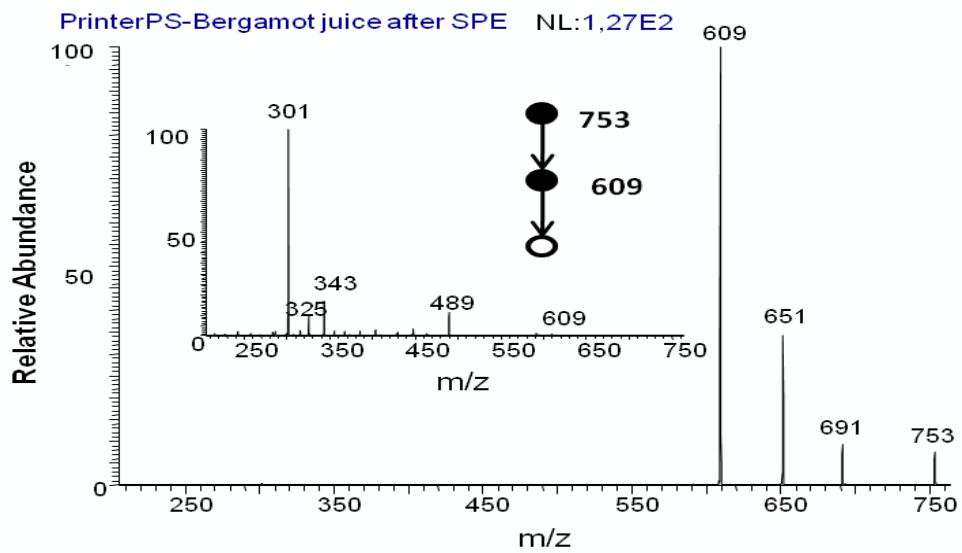
5.1.3 Results and discussion

Initially, for group (i) experiments 2 µl of the most diluted sample were loaded on a printer paper triangle (5 mm long and 2,5 mm base-width). The application of the voltage, in negative ion mode, didn't produce any signal attributable to flavonoids, except for bergamot juice which showed very low but characteristic signals of flavonoids under investigation. Different voltages (2-5 kV), for both polarities, were tried for all the samples of group (i) but no characteristic flavonoids' signal was observed. Changing the type of paper, for example chromatographic (Whatman International Ltd., Maidstone, England) and Teflon papers were used instead of printer one, or changing the solvent didn't resolve the problem. The absence of flavonoids' signal in some extent was expected due to the complex composition of Citrus juices. It is probably due to the ion suppression caused by the non volatile portion of Citrus juices or because of the presence of compounds with higher ionization efficiencies than those of our analytes. The most diluted samples (99:1 and 95:5) showed some low intensity signals of flavonoids under examination and this may indicate that flavonoids' signal absence may be caused by the non volatile fraction.

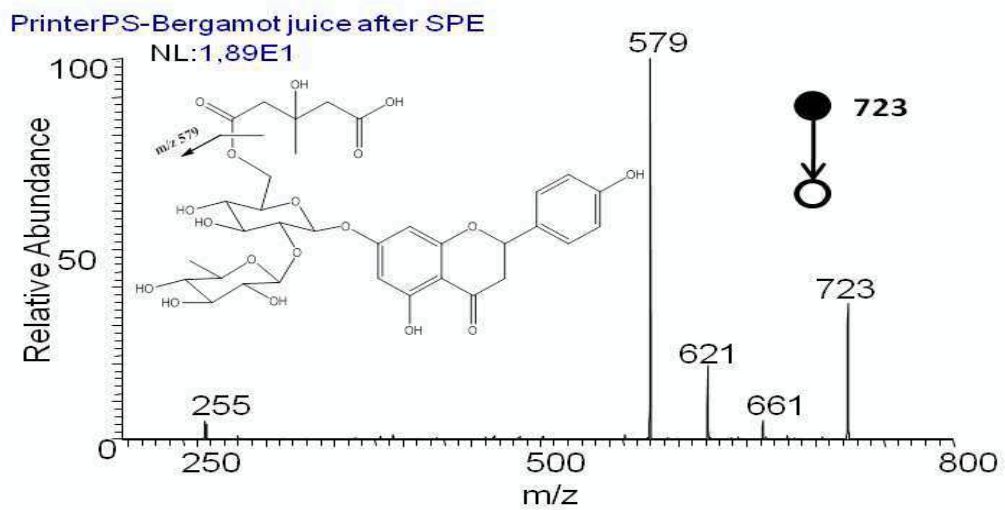
To overcome the above inconvenience, a simple SPE purification of juices was performed (group (ii) experiments) as reported in section 5.1.1. Now, when 2 µL of the purified "fraction 4" were added to printer paper triangle, in negative mode, all the flavonoids reported in table 5.1 were observed and easily identified in most cases only by MS² and MS³. Hence, it's clear the role of the polar fraction removed (fractions 1-3) by SPE purification on the ion suppression. During the optimization experiments, printer paper and isopropanol solvent (amongst those tested) furnished the best results in terms of signal intensity, signal duration and stability, therefore were selected and used for all the experiments. In figures 5.1A-G are reported some of the spectra of flavonoids acquired by PS-MS after SPE juice purification, while in table 5.1 are summarized all the flavonoids identified in Citrus juices.



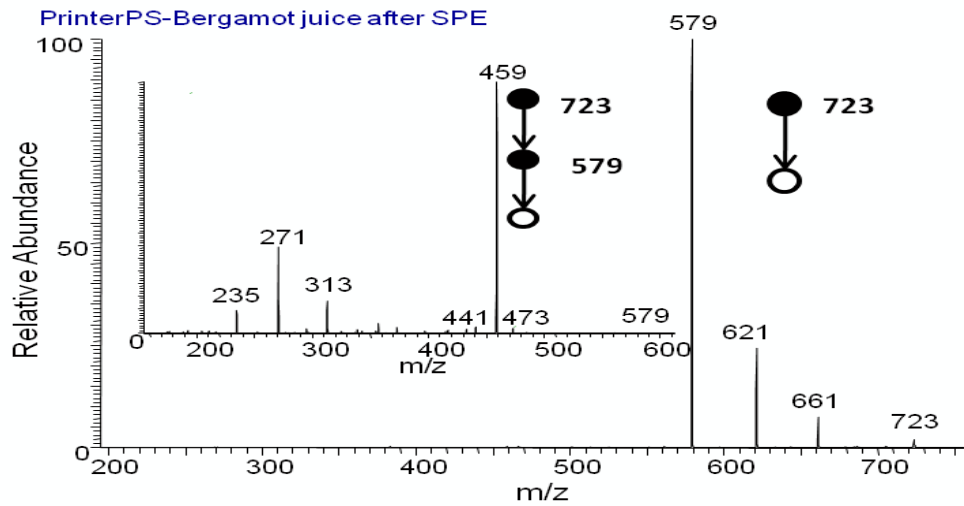
A)



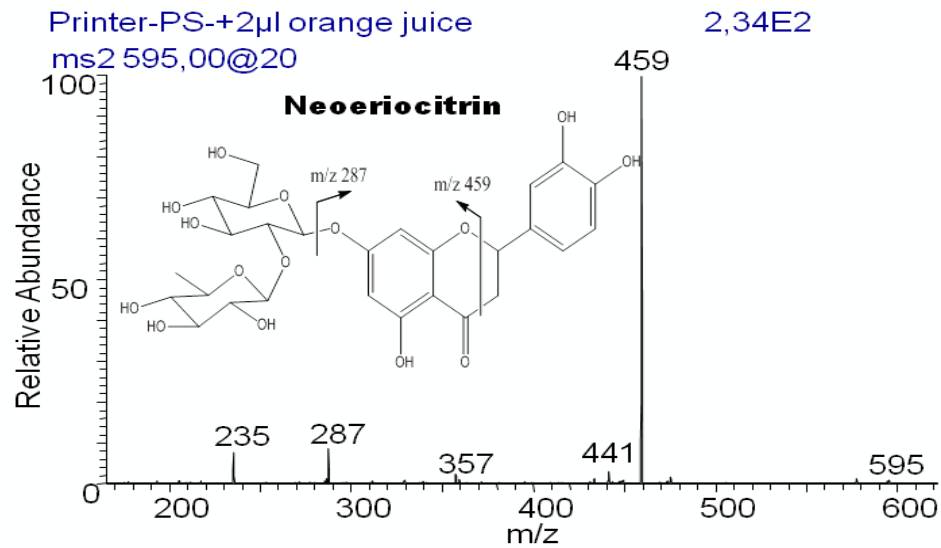
B)



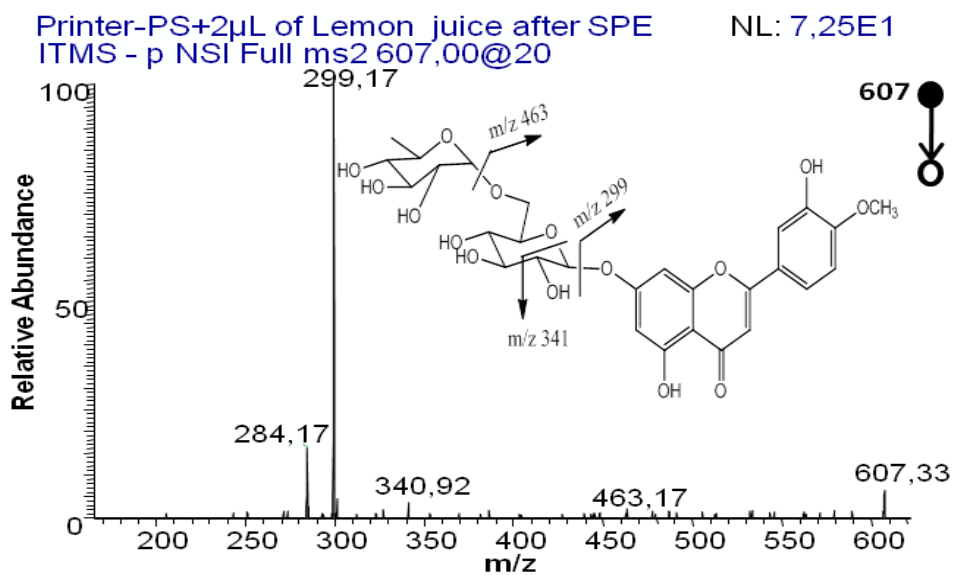
C)



D)



E)



F)

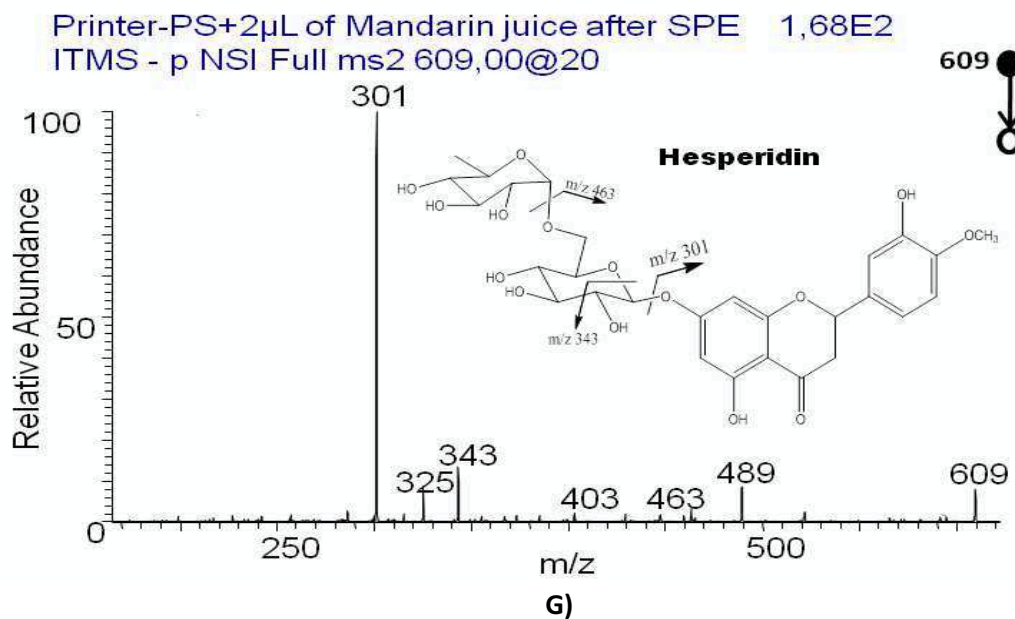


Figure 5.1A-G. Some examples of flavonoids detected and identified by PS-MS after SPE juice purification: (A) and (B) MS² and MS³(insert) of brutieridin in bergamot juice; (C) and (D) MS² and MS³(insert) of melitidin; (E) MS² of neoeriocitrin in orange juice; (F) MS² of diosmin in lemon juice; (G) MS² of hesperidin in mandarin juice. The other flavonoids are summarized in table 5.1.

Valencia Orange juice/albedo	
Compound name	[M-H] ⁻
Eriocitrin/neoeriocitrin	595
Hesperidin	609
Narirutin/naringin	579
Vicenin-2/Poncirin	593
Stellarin	623
Rhoifolin	577
Mandarin juice/albedo	
Compound name	[M-H] ⁻
Eriocitrin/neoeriocitrin	595
Hesperidin	609
Narirutin	579
Dydimin	593

Lemon juice/albedo	
Compound name	[M-H] ⁻
Eriocitrin	595
Hesperidin	609
Vicenin-2/	593
Diosmin	607
lucenin-2 4'-methyl ether	623
Rhoifolin	577
Bergamot juice/albedo	
Compound name	[M-H] ⁻
Neoeriocitrin	595
Neohesperidin	609
Naringin	579
Poncirin/vicenin-2	593
Melitidin	723
Brutieridin	753
Neodiosmin/Diosmin	607
Rhoifolin	577
Stellarin-2/lucenin-2 4'-methyl ether	623

Table 5.1. Flavonoids detected by PS-MS (and albedo Leaf Spray, see section 5.3.2).

To make an estimation of the ion suppression induced by the removed polar “fractions 1-3”, “fraction 4” was spiked with “fractions 1-3”, separately, in the following ratios: 9:1, 8:2 and the intensities of the signals were compared with those of “fraction 4” spiked at the same ratio with pure water and with the relative juices. In figure 5.2, as an illustrative example is reported a histogram showing the extent of hesperidin signal suppression induced by polar components of the lemon juice (“fraction 1” reported only). Analog behavior was observed for all other juices and related flavonoids.

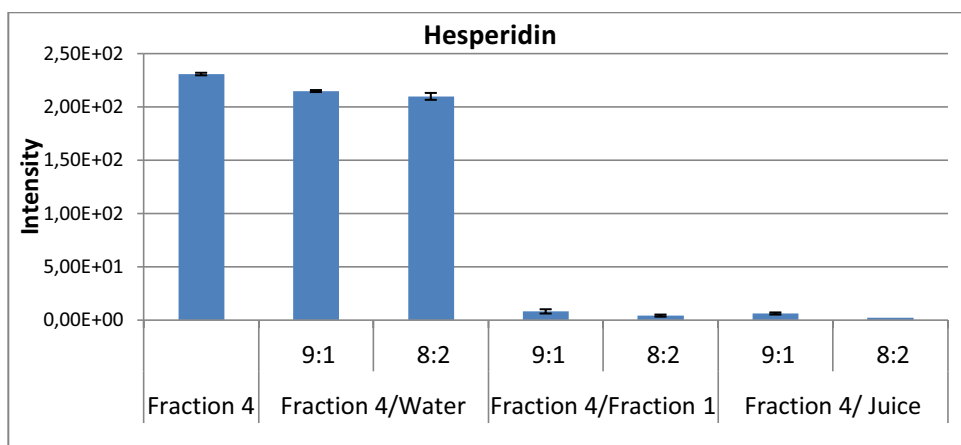


Figure 5.2. Effect of polar fraction (“fraction1”) of lemon juice on signal intensity of hesperidin.

5.2 Detection of Fraudulent Adulteration of Bergamot Juice

In addition to the identification of flavonoids from citrus juices, we examined the use of PS to reveal the fraudulent addition of bergamot juice to the lemon juice. Frauds regarding fruit juices include several aspects, such as the false declaration of the geographic origin of the product, undeclared sugar addition, water addition in “not from concentrate” juices, use of technologies not allowed by legislation (for example, in the case of citrus juices, the addition of peel and/or pulpwash fraction), and the addition of other not declared compounds (such as organic acids, coloring agents, etc.) [1]. Another common fraud regarding fruit juices is the undeclared addition of different juices from botanic-related fruits [2-4]. It has been reported that this is a very common practice with bergamot juice, a waste of essential oil industries, which has no market. Thus, fraudulent operators use bergamot juice, with or without any treatment, to adulterate

other citrus juices that have a wider market, in particular, lemon juice which has organoleptic proprieties very similar to bergamot juice.

The use of minor components of juices as markers, in particular way flavonoids, has been indicated as a choice approach to assess the authenticity of fruit juices [5-7]. Cautela et al. developed an HPLC method, based on the abundance of neohesperidin, naringin and neoeriocitrin, to detect and quantify the fraudulent addition of bergamot to the lemon juice [1]. That approach may overestimate or give false positives because the compounds used as markers (naringin, neohesperidin, and neoeriocitrin) are present in small amounts in lemon juice as well.

Here, instead, we propose the use of brutieridin and melitidin as specific markers to detect and evaluate the fraudulent addition of bergamot juice to that of lemon. To reach this goal, once again, we used PS-MS. Lemon juice was spiked with bergamot at different levels: 1%, 10%, 20%, 40%. Lemon spiked juices were purified by SPE, as described in paragraph 5.1.1, and the flavonoid-containing fraction was checked by PS-MS for brutieridin and melitidin presence.

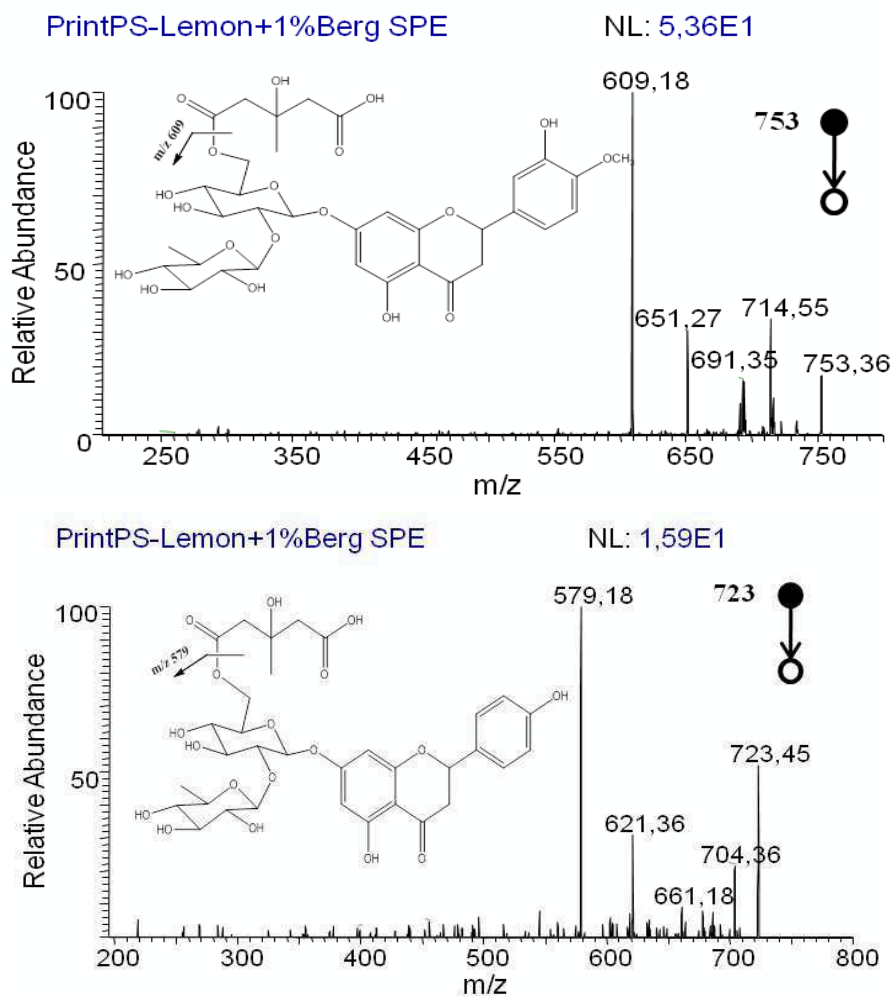


Figure 5.3. Brutiridin (top) and melitidin (bottom) detected in adulterated lemon juice with 1% of bergamot one.

Both markers were detected even at the lowest mixed level (1% of bergamot juice added to lemon juice) when operating in MS/MS mode (figure 5.3). When operating in fullscan mode, signals of brutieridin and melitidin were detectable starting from 2,5 % (for brutieridin) and 5% (for melitidin) of bergamot juice addition to the lemon juice. These findings indicate that this fast method can be used to detect the illegal addition of bergamot juice to the lemon juice at levels as low as 1%, when brutieridin and melitidin are used as makers. Additional experiments are needed to make an estimation of the amount of bergamot juice added to the lemon one.

5.3 Analysis of Flavonoids from Citrus Albedo by Leaf Spray-Mass Spectrometry

5.3.1 Introduction

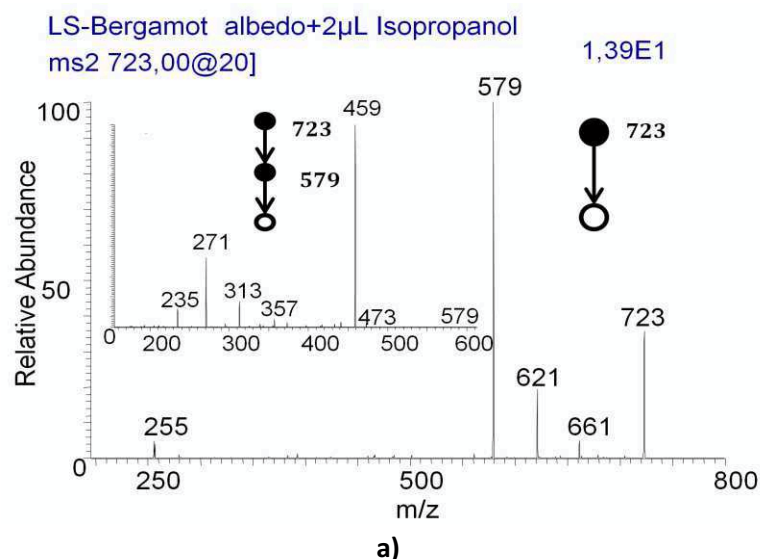
Leaf spray (LS) is the newest reported ionization method for mass spectrometry which consist in direct plant tissue spray (see further details in chapter II, paragraph 2.3). In this ionization method the vegetal tissue is used to generate charged gas phase ions for mass spectrometry, hence, no other ionization device or support is needed since the vegetal tissue acts simultaneously as an ionization source and as the sample. In analogy with paper spray, from which LS derives, the vegetal tissues are cut to a sharp triangular tip (<1 cm base width, 1-3 cm long, and < 5mm of thickness). It should be pointed out that any other geometry containing a sharp tip work well and the choice of triangular shape is only due to the easiness of sharp tip formation. The voltage is applied at the centre of the base with the tissue tip held 0,3-1 cm from mass spectrometer inlet. As the voltage is applied signals appear in the mass spectrum, the confirmation of charged ions generation. The spray duration goes from 1 to several minutes depending on the juiciness of the vegetal tissue. However, small volumes of solvent added (1-2 μ L) to the tissue triangle resulted in a higher signal intensities, better S/N ratios and sometimes in richer signal mass spectra. Citrus albedo of orange, mandarin, lemon and bergamot were examined for the same flavonoids detected in their juices by PS-MS (previous sections) and keeping the same instrumental conditions (see section 5.1.2) .

5.3.2 Flavonoids of Citrus albedo by LS-MS

Liquid chromatography coupled with mass spectrometry (LC-MS) is the analytical technique of choice for both qualitative and quantitative determinations of flavonoids in fruits and vegetables. Although its incontestable qualitative and quantitative advantages, LC-MS technique requires a long sample pretreatment which is time and chemical consuming. The most commune procedures for sample preparation include: 1) sample homogenization (chopping, milling); 2) extraction of the homogenized material by

methanol (or other solvents) often under stirring or mild warming; 3) centrifugation/filtration; 4) removal of non polar compounds from the previous filtrated fraction using petroleum ether, n-hexane (or other non polar solvents); 5) additional purification by SPE; 6) concentration (rotary evaporator or nitrogen gas flow). Therefore, developing a reliable method that do not require all these sample preparation steps seems of remarkable environmental, time and economic impact.

Therefore, here we examine the performance of LS as an alternative ambient ionization method for the analysis of flavonoids contained in plant tissues. In particular, albedo tissue of citrus fruits (lemon, orange, mandarin and bergamot) was cut to a sharp triangular tip (< 1 cm base width, 1-3 cm long, and < 5 mm of thickness) and sprayed without any further sample treatment. 2 μ L of isopropanol were used as a spray solvent and a voltage of 4,5 kV was applied to the base of tissue triangle by means of a copper clip (in analogy with PS). All the measurements were carried out on Finnigan LTQ mass spectrometer. Full scan and MS^n mass spectra were acquired in negative ionization mode. Flavonoids under investigation are listed in table 5.1 and comprise O-glycosylated and C-glycosylated flavanones and flavones. The identification was performed comparing the MS^n fragmentation pattern with literature data and, where possible, with pure compounds (as for PS). It is well known that flavonoids are distributed mostly in juice and albedo layer and at smaller extent in flavedo of citrus fruits. In fact, when flavedo was used, MS/MS characteristic but very low intensity signals were observed, in agreement with previous literature reports which indicate lower flavonoid abundance in this tissue. In albedo tissue, on the other hand, were detected and identified all the compounds reported in table 5.1. In figure 5.4 are reported the MS^2 mass spectra of one flavonoid for each Citrus fruit albedo examined: (a) melitidin from bergamot albedo; (b) diosmetin 6,8-di-C-glucoside from lemon albedo; (c) narirutin from orange albedo and (d) diosmin from mandarin albedo.



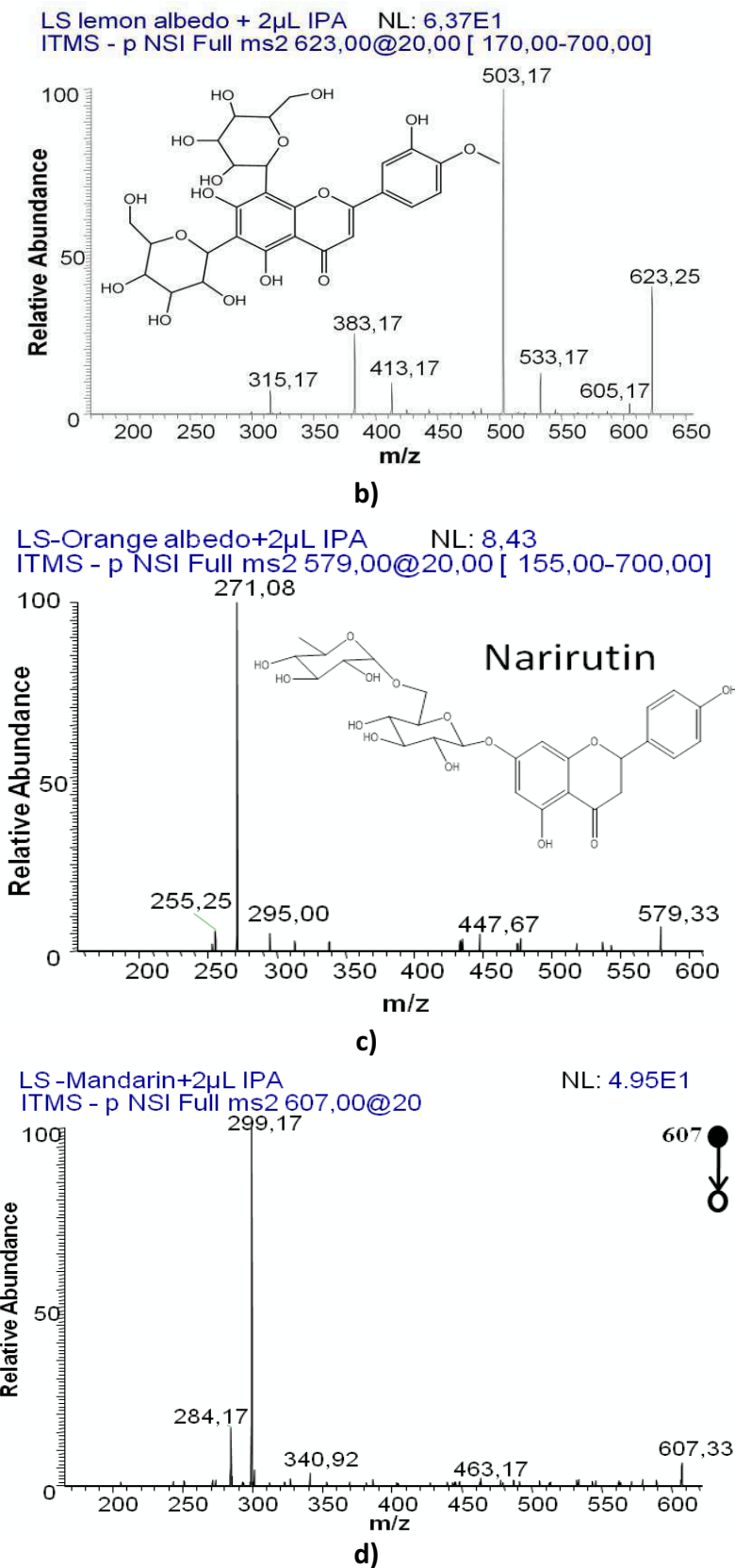


Figure 5.4. MS/MS (and MS³ inserts) of a) melitidin from bergamot albedo; b) diosmetin 6,8-di-C-glucoside from lemon albedo; c) narirutin from orange albedo; d) diosmin from mandarin albedo.

It was, therefore, demonstrated that LS-MS is a fast, cheap and very convenient approach to study flavonoids (and other secondary plant metabolites and chemicals) in fruits and in general in plants, without laborious time and chemical-consuming sample preparations. We are hopeful that this new approach will be applied in several other fields and for a wide range of chemicals (e.g., to monitor seasonal variations of chemicals during plant/fruit development; to obtain biosynthetic information etc.).

References

1. Cautela D., Laratta B., Santelli F., Trifirò A., Servillo L., Castaldo D., *J. Agric. Food Chem.* 2008, 56, 5407–5414.
2. Ooghe W., Detavernier M. J., Flavonoids as authenticity markers of *Citrus sinensis* juice, *Fruit Process.* 1999, 8, 308–313.
3. Thavarajah P., Low N. H., *J. Agric. Food Chem.* 2006, 54, 4861–4867.
4. Mouly P. P., Gaydou E. M., *J. Chromatogr., A*, 1993, 634, 129–134.
5. Grandi R., Trifirò, A., Gherardi S., Calza M., Saccani G., *Fruit Process*, 1994, 11, 335–359.
6. Mouly P. P., Azzouyan C. R., Gaydan E. G., Estienare J. M., *J. Agric. Food Chem.*, 1994, 42, 70–79.
7. Mouly P. P., Gaydou E. M., Faure R., Estienne J. M., *J. Agric. Food Chem.* 1997, 45, 373–377.

CHAPTER VI**6 Analysis of Agrochemicals by Leaf Spray Mass Spectrometry****6.1 Introduction**

Pesticides are substances widely used at different stages of crop cultivation or post-harvest storage to prevent, destroy, repel or mitigate any pest or fungi. Their use provide higher product yields, storage and longevity. Residues of pesticides may end up in the final commodities or processed foods posing risks for human health. The legislation of different countries (European Union, USA and Japan) is continuously updated with the maximum residue limits (MRLs) allowed before product commercialization, in order avoid adverse effects in public health. For most of the pesticides the MRLs in fruits and vegetables are low (ppb order) which means that highly sensitive and accurate analytical techniques are required for their detection and quantitative determination. Traditionally, agrochemical determinations in food are performed by highly sensitive techniques such as gas chromatography coupled to mass spectrometry (GC-MS) and liquid chromatography-mass spectrometry (LC-MS). GC-MS has been widely used for simultaneous determination and confirmation of pesticide residues in fruits and vegetables, processed foods, water, soil, serum etc. [1-2]. The sensitivity of GC-MS and its specificity, especially when operating in multiple reaction monitoring (MRM) mode, rendered it an important tool for thermally stable pesticide determinations in last two decades. On the other hand, liquid chromatography-mass spectrometry (LC-MS) methods have been successfully reported for several simultaneous pesticide determinations since the introduction of electrospray ionization (ESI) and atmospheric pressure chemical ionization (APCI) methods [3-10]. Although GC-MS/MS and LC-MS/MS have shown excellent analytical performance, both require several chemical-consuming steps for sample preparation prior to instrumental injection, a clear disadvantage in terms of time and analysis cost. Since its introduction, the sample preparation method known as the quick, easy, cheap, effective, rugged, and

safe (QuEChERS) is the most used for both GC- and LC-MS pesticide determinations [11].

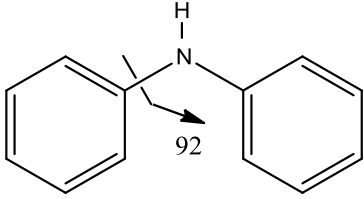
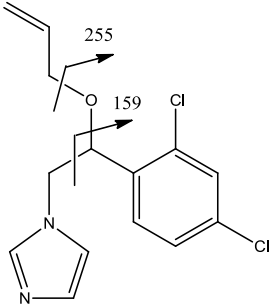
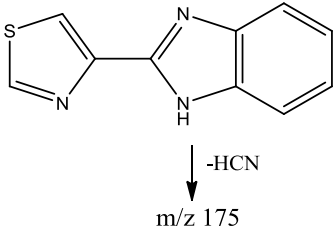
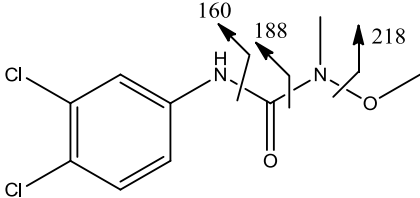
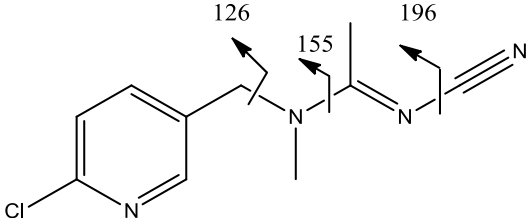
Direct analysis of foodstuffs without any kind of sample treatment is an interesting challenge for several research groups worldwide. In fact, in literature there are several papers reporting different ambient ionization methods which permits the direct pesticide determinations in foodstuffs in their native environment, without sample preparation or pre-separation [12-14]. The introduction of desorption electrospray (DESI) allowed in situ analysis of a wide range of samples, in their native environment, by creating ions from surfaces outside the mass spectrometer [15-16]. In fact, DESI has been used for the determination of sixteen agrochemicals from different classes with excellent performance without sample treatment [17]. Wiley et al. [18] used low temperature plasma (LTP) for fast agrochemical screening in fruit and vegetable peels as well as in their extracts.

In the present work we report the application of leaf spray (see more details in chapter II, paragraph 2.3) as a novel approach for mass spectrometric determination of agrochemicals in fruit and vegetable tissues [19-20]. LS performance was examined for fast screening and discrimination of organic and non organic fruit and vegetable tissues without any sample pre-treatment. In particular, peels and pulps of non organic apples (red delicious, gold and green apples) were screened for the presence of diphenylamine and thiabendazole, as two most diffused post-harvested fungicides by apple producers. Both tissues of potatoes (peel and pulp) and pear peel were examined for thiabendazole presence. Carrot (peel and pulp) was examined for linuron whereas eggplant and cucumber were screened for acetamiprid presence in both tissues (peel and pulp). Flavedo and albedo of orange and lemon were checked for the presence of thiabendazole and imazalil. To evaluate the analytical performance of LS-MS, external calibration curves of the above mentioned pesticides were built on the relative organic fruit tissues. The structures of agrochemicals included in this study together with their principal fragmentations are reported in table 6.1.

6.2 Samples

Organic and non organic fruits and vegetables were purchased from the local markets (Lafayette, IN, USA). Peels and pulps (flavedo and albedo for Citrus fruits) were cut to a sharp triangular tip (~0,5 cm base width, ~1 cm long, and < 3 mm in thickness) and used for spray generation without any further treatment.

Table 6.1. Agrochemicals involved in LS-MS analysis.

Agrochemical	[M+H] ⁺	Principal fragmentations
Diphenylamine	170	
Imazalil	297	
Thiabendazole	202	
Linuron	249	
Acetamiprid	223	

6.3 Chemicals

Pesticide analytical standards were purchased from Chem Service Inc. (West Chester, PA). HPLC-grade methanol and isopropyl alcohol were obtained from Mallinckrodt Baker Inc. (Phillipsburg, NJ, USA). Stock solutions of each pesticide were prepared

dissolving 10 mg in 10 ml of methanol and stored at -20 °C. Working solutions were prepared by appropriate dilution with isopropyl alcohol.

6.4 Instrumental conditions

Experiments were performed using a Thermo LTQ linear ion trap mass spectrometer (Thermo Finnigan San José, CA, USA). Instrumental conditions were optimized by adding known amounts of pesticides on organic fruit and vegetable tissues under investigation. All LS-MS analyses were performed applying a voltage of 3.5 kV in the positive ion mode and spectra were acquired using automatic gain control mode with a maximum ion trap injection time of 300 ms and 3 micro-scans per spectrum. The other experimental parameters used were as follows: capillary temperature: 200 °C; tube lens (V): -65 V; capillary voltage: -15 V. Tandem mass spectrometry experiments (MS/MS) were performed using collision-induced dissociation (CID) experiments in order to confirm the presence of particular agrochemicals in the studied samples and an average of five spectra at highest intensity peak was used for quantitative measurements. All experiments were performed using an isolation window of 1.4 (m/z units) and 25–45% collision energy (manufacturer's unit).

6.5 Results and discussion

Screening experiments were performed simply by comparing the instrumental response of organic and respective non organic tissues. Pesticide identification was performed comparing the mass spectra with pure standards and literature data. In figure 6.1a-b are reported the full-scan spectra of organic and non organic orange flavedo, respectively, after addition of 2 μ L of isopropyl alcohol (IPA). The mass spectrum of non organic orange flavedo, figure 6.1b, shows the presence of two signals, at m/z 202 and 297, which are absent in the mass spectrum of the relative organic tissue, figure 6.1a. Product ion (MS/MS) mass spectra of m/z 202 and 297, figures 6.2a-b, show typical fragmentation patterns of thiabendazole and imazalil, respectively. Thiabendazole and imazalil are the most diffused post-harvested fungicides utilized in citrus fruits. Both, thiabendazole and imazalil, were also detected in non organic lemon flavedo. Albedo layer of the same fruits, orange and lemon, was examined in the same way and the full-scan spectra, figure 6.3a-b show the presence of only imazalil in this tissue. Although the signal intensity of thiabendazole was found to be very intense (base peak) in flavedo layer of the same fruits, it is absent in albedo indicating its total accumulation in flavedo. This latter result is in agreement with previous literature data reporting

imazalil migration from the external layer of peel (flavedo) toward the inner layers and reaching the juice.

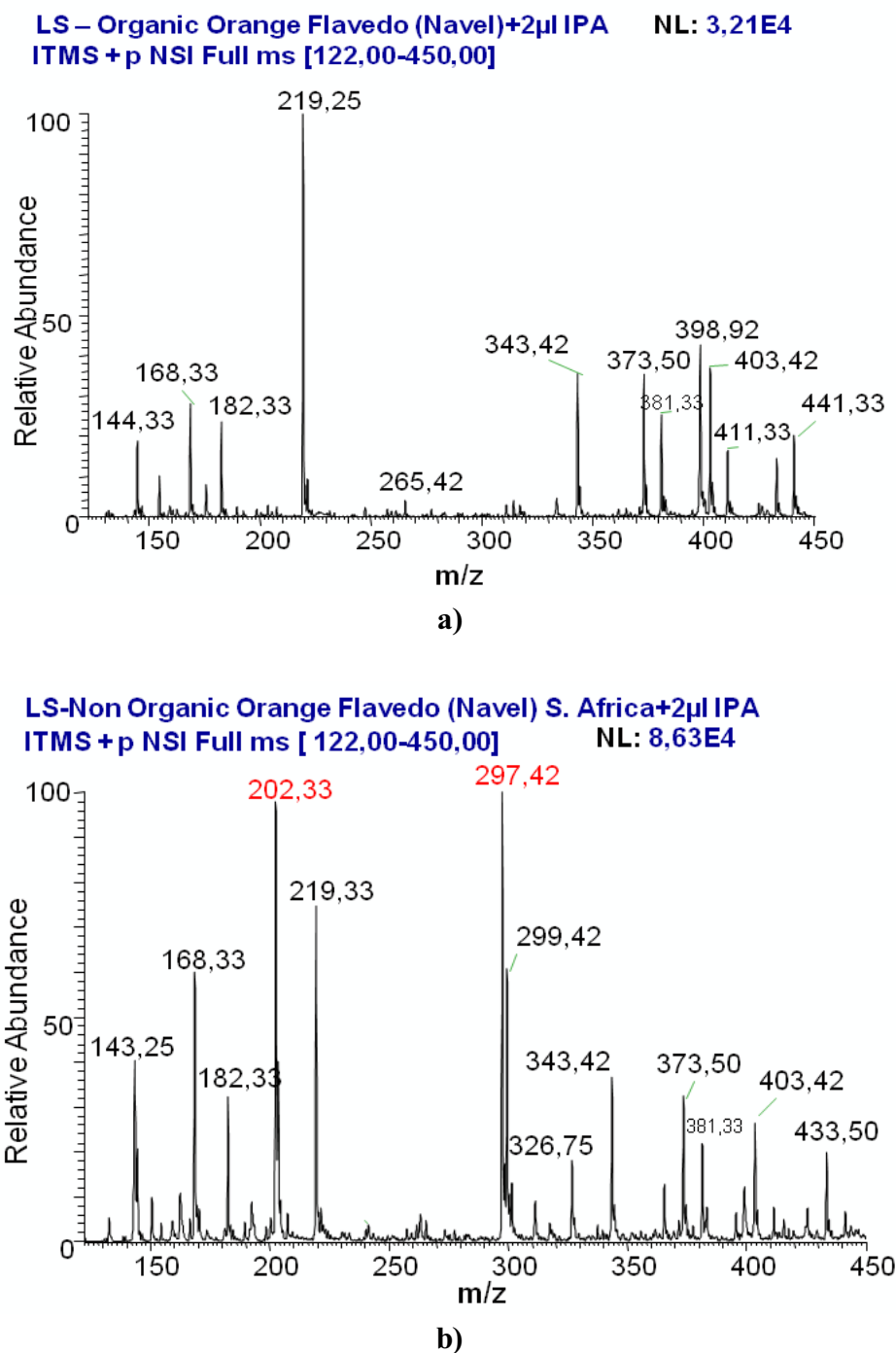


Figure 6.1. a) Full-scan mass spectrum of organic orange flavedo and b) Full-scan mass spectrum of non organic orange flavedo. Both spectra were obtained by LS using 2 μ L of isopropanol as a spraying solvent. Thiabendazole (m/z 202) and imazalil (m/z 297), present only in non organic orange flavedo, are reported in red.

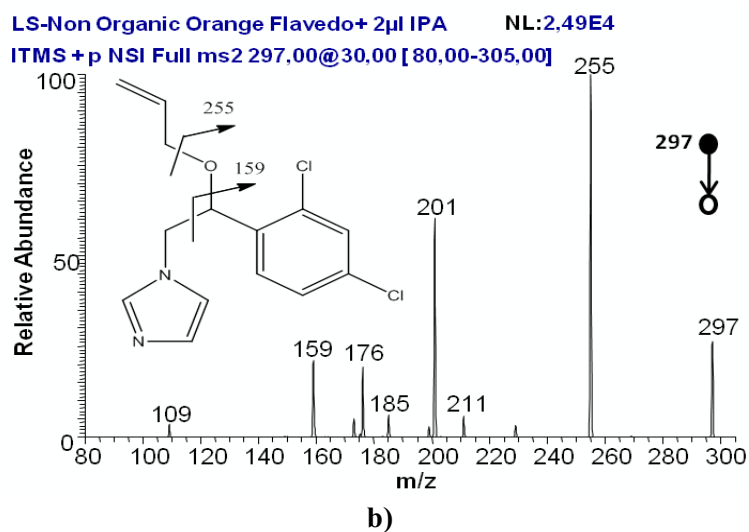
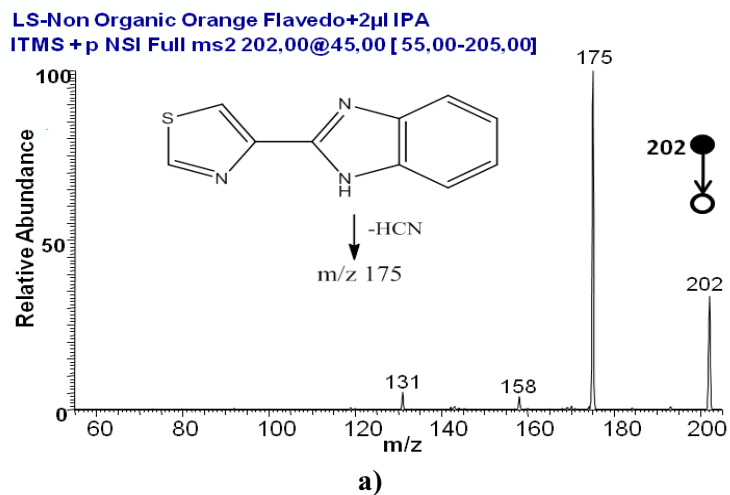


Figure 6.2. a) MS/MS (product ion) of thiabendazole (m/z 202) and b) imazalil (m/z 297) detected in non organic orange flavedo.

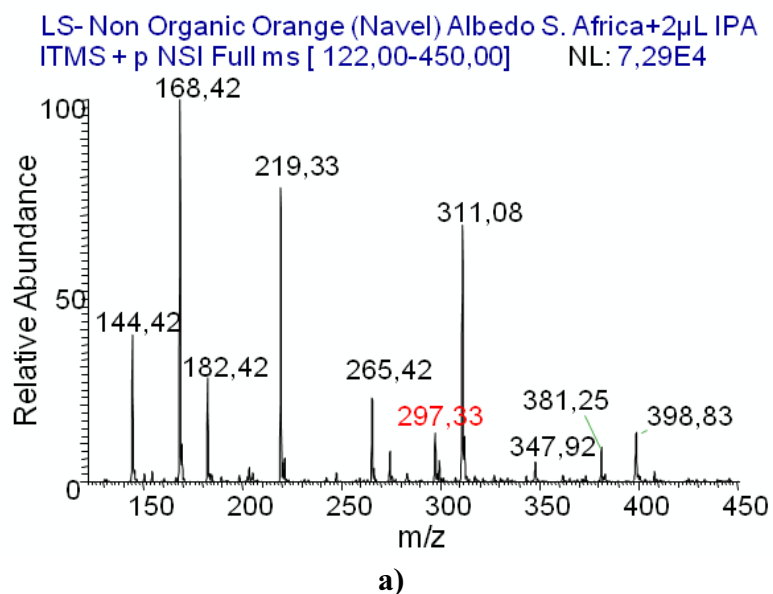


Figure 6.3 (continue).

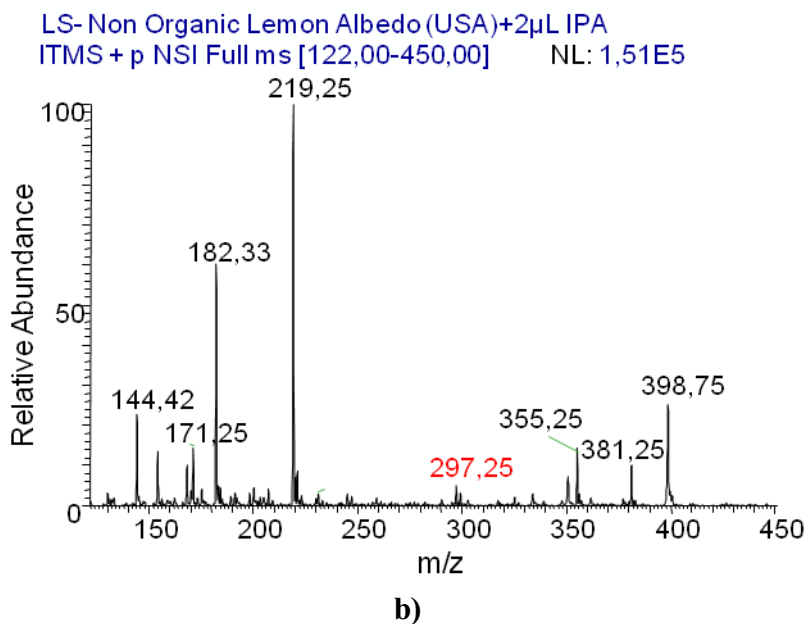


Figure 6.3. Full-scan mass spectra of non organic orange (a) and lemon (b) albedo showing the absence of thiabendazole on these tissues.

In table 6.2 is reported the list of non organic tissues where the pesticides under examination were detected. Higher sensitive MS/MS mode was necessary for the detection of some of the pesticides which were present in examined tissues at low concentrations.

The present data obtained from direct plant tissue spray (without any sample pretreatment) confirm that this novel and very simple ionization method is appropriate for fast screening and discrimination of organic from non organic fruits and vegetables. Nowadays, the demand for organic food is raising due to the health risk associated with pesticide residues in foods and with that the necessity of fast and inexpensive methods of analysis capable to discriminate between organic and non organic fruits and vegetables. The approach reported here, therefore, offers the possibility to operate under ambient conditions, in a very simple, fast and convenient manner. In fact, this method is applicable at any location (lab, outdoor, market etc.) and when portable mass spectrometers become commercially available it may be used for on site analysis. It remains for the future to extend its application to many other pesticides and tissues.

In addition to the screening experiments we investigated the analytical performance of LS for semi-quantitative measurements. For this purpose, external calibration curves were built for each organic tissue sample adding 2 μ L of increasing amounts of pesticides directly on the tissue triangle. As illustrative example in figure 6.4a is reported the product ion mass spectrum of linuron and in 6.4b its calibration curve, both on carrot peel and pulp (overlapped).

Agrochemical	Product	Tissue	Detected
Thiabendazole	Apple	Peel	Y
		Pulp	Y
	Potato	Peel	N
		Pulp	N
	Orange	Flavedo	Y
		Albedo	N
	Pear	Peel	Y
Diphenylamine	Apple	Peel	Y
		Pulp	Y
Linuron	Carrot	Peel	N
		Pulp	N
Imazalil	Orange	Flavedo	Y
		Albedo	Y
Acetamiprid	Eggplant	Peel	N
		Pulp	N
	Cucumber	Peel	N
		Pulp	N

Y = yes, detected.

N = not detected.

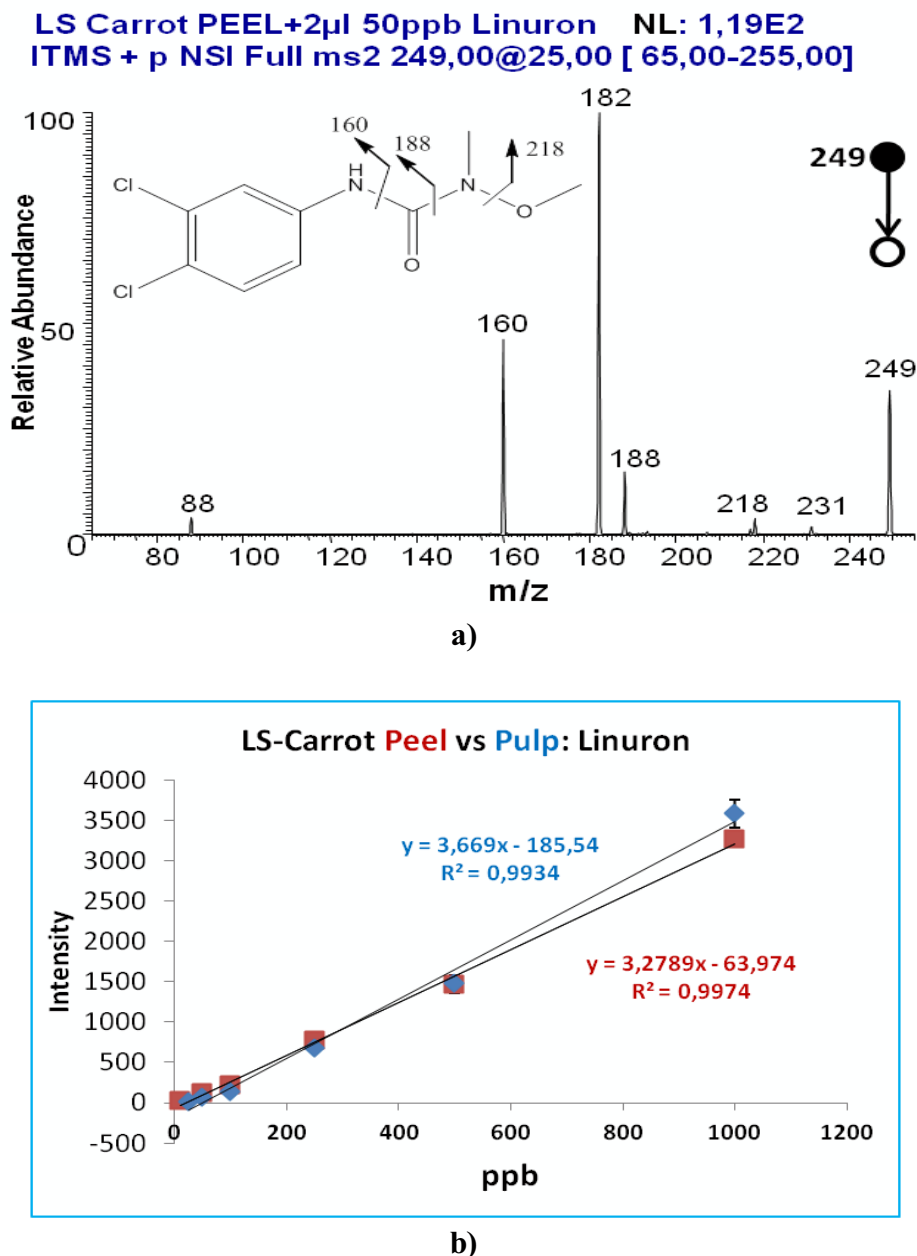
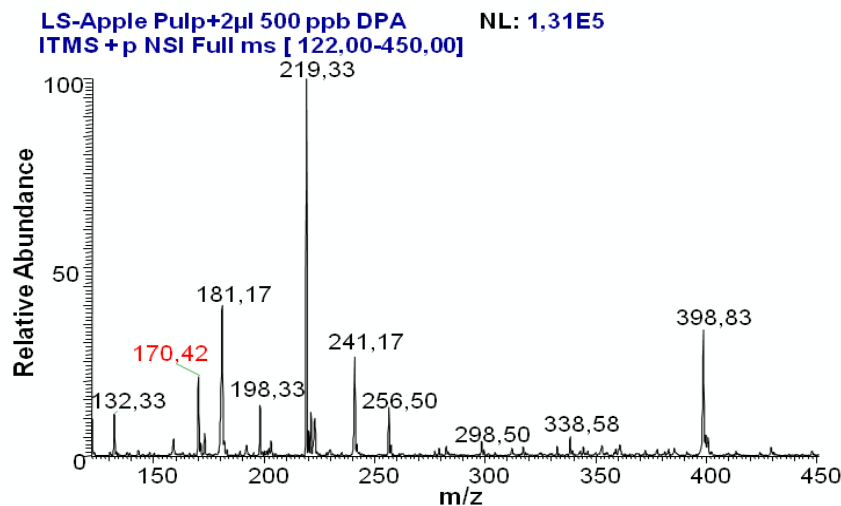
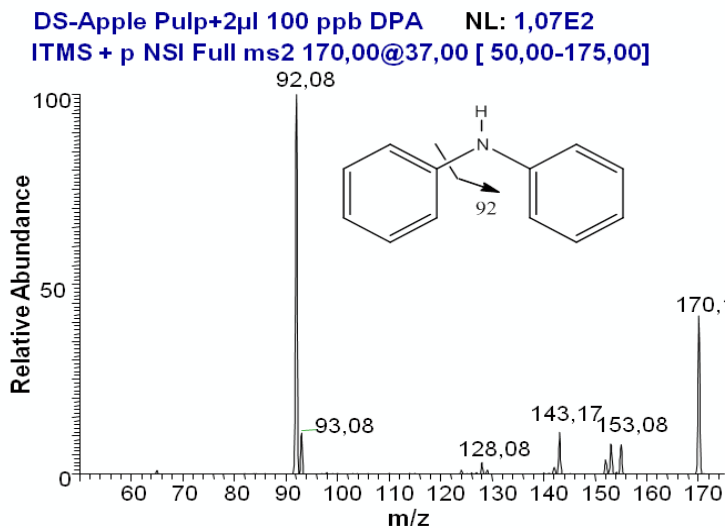


Figure 6.4. a) Product ion mass spectrum obtained by LS of organic carrot peel (pulp is not reported) after addition of 2 μ L of linuron (50 ppb) standard solution; (b) Calibration curve of linuron (m/z 249) on carrot peel and pulp.

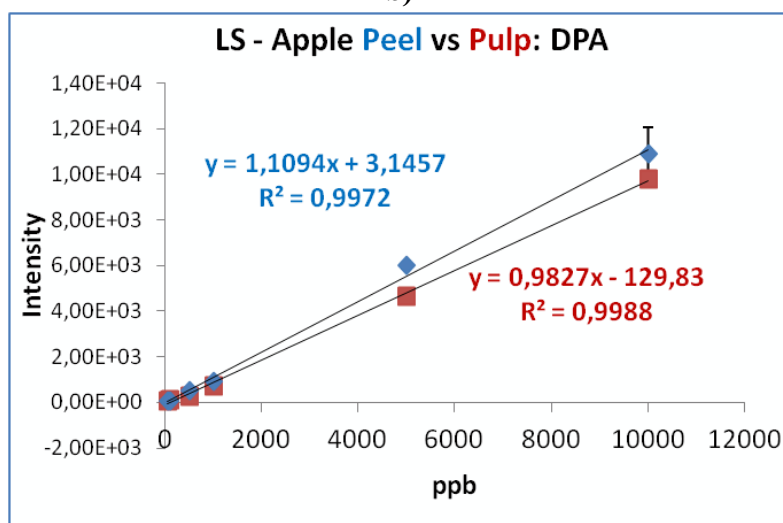
Full-scan and product ion scan mass spectra of diphenylamine on apple pulp and its calibration curve built on (red delicious) organic apple peel and pulp are reported in figure 6.5a-c. The data of all the other pesticides are summarized in table 6.3 which shows also the analytical parameters (linear ranges, correlation coefficients (R^2) and LODs) for each pesticide/tissue examined.



a)



b)



c)

Figure 6.5. a) Full mass spectrum and b) MS/MS spectrum of diphenylamine (m/z 170) in red delicious organic apple pulp; c) diphenylamine calibration curve on apple peel and pulp.

Table 6.3. Analytical performance of LS for agrochemical determination in fruit and vegetable tissues.

Agrochemical	Product	Tissue	Conc. range tested ($\mu\text{g L}^{-1}$)	Calibration equation	Correl. Coeff. (r^2)	LOD ($\mu\text{g L}^{-1}$)	EU MRLs (mg Kg^{-1})
Thiabendazole	Apple	Peel	10-10000	$y = 4,3372x - 274,92$	0,9945	10	5
		Pulp	50-10000	$y = 3,028x + 105,9$	0,9983	50	
	Potato	Peel	5-15000	$y = 1,8355x + 372,29$	0,9947	5	15
		Pulp	25-15000	$y = 2,2385x - 217,63$	0,9996	25	
	Orange	Flavedo	50-10000	$y = 0,1408x + 19,128$	0,9989	25	5
		Albedo	50-10000	$y = 1,3028x - 90,964$	0,9996	25	
Pear	Peel	50-10000	$y = 5,0955x - 546,79$	0,994	35	5	
Diphenylamine	Apple	Peel	10-10000	$y = 1,1097x + 1,0223$	0,9974	10	5
		Pulp	25-10000	$y = 0,9791x - 102,21$	0,9987	25	
Linuron	Carrot	Peel	10-1000	$y = 3,2789x - 63,974$	0,9974	10	0,2
		Pulp	25-1000	$y = 3,669x - 185,54$	0,9934	25	
Imazalil	Orange	Flavedo	10-10000	$y = 0,4243x + 113,25$	0,9936	10	5
		Albedo	10-10000	$y = 76,959x - 7531,5$	0,9979	10	
Acetamiprid	Eggplant	Peel	10-5000	$y = 4,917x + 164,06$	0,9932	10	0,1
		Pulp	50-5000	$y = 1,1188x - 64,433$	0,9988	50	
	Cucumber	Peel	5-5000	$y = 2,2647x + 49,285$	0,9997	5	0,3
		Pulp	25-5000	$y = 0,8457x + 58,057$	0,9982	25	

Thiabendazole showed a wide linear range (i.e. 5-15000 $\mu\text{g L}^{-1}$ for potato peel), low LODs in the range of 5-50 $\mu\text{g L}^{-1}$, and very good correlation coefficients ($R^2 > 0,99$), for all the sample matrixes examined. The low LODs, well below the MRLs set up by EU, observed for each commodity tissue indicate that this approach is enough sensitive and suitable for thiabendazole determination in both tissues of apples, potatoes, pears (peel only) and Citrus fruits.

Diphenylamine is a post-harvested fungicide widely used to treat and enhance the storage period of apples. Its limit of detection in peel and pulp was found to be respectively 10 and 25 $\mu\text{g L}^{-1}$ which is well below the MRL imposed by European regulations and together with the wide linear range (10-10000 and 25-10000 $\mu\text{g L}^{-1}$, respectively for peel and pulp) and the excellent correlation coefficient ($R^2 = 0,9974$ and 0,9987 respectively for peel and pulp curves) are very good analytical indicators of this approach. Linuron calibration curves were built on organic carrot peel and pulp. All the analytical parameters reported in table 6.3 are similar for both tissues, with slightly higher LOD for pulp tissue. The range of linearity obtained for linuron, 10-1000 and 25-1000 $\mu\text{g L}^{-1}$ respectively for peel and pulp tissue, covers perfectly the EU MRL (0,2 mg kg^{-1}). Low limit of detection (10 $\mu\text{g L}^{-1}$), wide linear range (10-10000 $\mu\text{g L}^{-1}$) and good

correlation coefficients ($R^2=0,9936$ and $0,9979$ for flavedo and albedo respectively) were observed for imazalil on organic orange flavedo and albedo. Imazalil is used to treat also the other Citrus fruits (lemon, mandarin, bergamot, lime etc.). Being the morphological similarities between members of Citrus flavedo and albedo tissues, the above findings may be extended to the other members as well.

Acetamiprid calibration curves were built on peels and pulps of organic eggplant and cucumber. The LODs of this pesticide in both tissues of eggplant and cucumber are below the MRLs of acetamiprid allowed in these commodities ($0,1$ and $0,3 \text{ mg kg}^{-1}$, respectively in eggplant and cucumber); the linear ranges and correlation coefficients, promise application of LS even for determinations of pesticides with such a low MRLs. Finally, in table 6.3 a general trend can be observed: LOD values are usually higher for pulps (and albedo) tissues than peel (and flavedo) ones. This behavior may be due to the higher matrix effect caused by superior complexity attributed to high juice content of pulps (and albedo for Citrus members) respect to peel (and flavedo) tissues.

6.6 Conclusions

The present data obtained from direct plant tissue spray confirms that this novel and very simple ionization method is appropriate for different analytical measurements. In fact, the fast discrimination between organic and non organic fruits and vegetables reported here, for the first time, indicate that LS-MS approach is appropriate for fast screening experiments by cutting simply fruit/vegetable tissues to a small triangular tip and without any further sample preparation. Moreover, the good performance for semi-quantitative determinations of pesticides in fruit and vegetable tissues demonstrated here, confirms the validity of this approach. The introduction of LS-MS, therefore, promise new scenario in analytical-thinking as well as challenges to well-consolidated analytical techniques. The method do not require any ionization device, it can be conveniently used at ambient conditions at any location (lab, open field, market etc.) and without any sample pretreatment. The very low solvent and chemical consumption is another strong point of LS method. Of course, it remains for the future to extend its use to a wider range of compounds and applications.

References

1. Martinez Vidal J. L., Arrebola F. J., Mateu-Sanchez M., *Rapid Commun. Mass Spectrom.*, 2002, 16, 1106.
2. Moreno Frías M., Garrido Frenich A., Martínez Vidal J.L., Mateu Sánchez M., *Journal of Chromatography B*, 2001, 760, 1–15.
3. Ortelli D., Edder P., Corvi C, Multiresidue analysis of 74 pesticides in fruits and vegetables by liquid chromatography–electrospray–tandem mass spectrometry, *Analytica Chimica Acta*, 2004, 520, 33–45.
4. Wang J., Cheung W., Grant D., Determination of Pesticides in Apple-Based Infant Foods Using Liquid Chromatography Electrospray Ionization Tandem Mass Spectrometry, *J. Agric. Food Chem.*, 2005, 53, 528–537.
5. Blasco C., Font G., Picó Y., Analysis of pesticides in fruits by pressurized liquid extraction and liquid chromatography–ion trap–triple stage mass spectrometry, *Journal of Chromatography A*, 2005, 1098, 37–43.
6. García-Reyes J. F., Hernando D. M., Ferrer C., Molina-Díaz A., Fernández-Alba A. R., *Anal. Chem.* 2007, 79, 7308–7323.
7. Wang J., LEUNG D., CHOW W., Applications of LC/ESI-MS/MS and UHPLC QqTOF MS for the Determination of 148 Pesticides in Berries, *J. Agric. Food Chem.*, 2010, 58, 5904–5925.
8. Ferrer C., Martínez-Bueno M. J., Lozano A., Fernández-Alba A. R., Pesticide residue analysis of fruit juices by LC–MS/MS direct injection. One year pilot survey, *Talanta* , 2011, 83, 1552–1561.
9. Pareja L., Martínez-Bueno M. J., Cesio V., Heinzen H., Fernández-Alba A. R., Trace analysis of pesticides in paddy field water by direct injection using liquid chromatography–quadrupole-linear ion trap-mass spectrometry, *Journal of Chromatography A*, 2011, in press.
10. Dulaurent S., Moesch C., Marquet P., Gaulier J. M., Lachâtre G, Screening of pesticides in blood with liquid chromatography–linear ion trap mass spectrometry, *Anal. Bioanal. Chem.*, 2010, 396, 2235–2249.
11. Anastassiades M., Lehotay, S.J., Štajnbaher, D., & Schenck, F.J., *Journal of AOAC International*, 2003, 86, 412–431.
12. Chen H. W., Sun Y. P., Wortmann A., Gu H. W., Zenobi R., *Anal. Chem.*, 2007, 79, 1447–1455.
13. Jecklin M. C., Gamez G., Touboul D., Zenobi R., *Rapid Commun. Mass Spectrom.*, 2008, 22, 2791–2798.

14. Schurek J., Vaclavik L., Hooijerink H., Lacina O., Poustka J., Sharman M., Caldwell M., Nielen M. W. F., Hajslova J., *Anal. Chem.*, 2008, 80, 9567–9575.
15. Takats Z., Wiseman J. M., Gologan B., Cooks R. G., *Science*, 2004, 306, 471–473.
16. Takats Z., Wiseman J. M., Cooks R. G., *J. Mass Spectrom.*, 2005, 40, 1261–1275.
17. Garcia-Reyes J. F., Jackson A. U, Molina-Diaz A., Cooks R. G., *Anal. Chem.* 2009, 81, 820-829.
18. Wiley J. S., Garcia-Reyes J. F., Harper J. D., Charipar N. A., Ouyang Z., Cooks R. G., *Analyst*, 2010, 135, 971–979.
19. Liu J., Wang H, Cooks R. G., Ouyang Z., Leaf Spray: Direct Chemical Analysis of Plant Material and Living Plants by Mass Spectrometry, *Anal. Chem.* 2011, 83, 7608–7613.
20. Malaj N., Ouyang Z., Sindona G., Cooks R.G., Analysis of agrochemicals by direct vegetable tissue spray mass spectrometry, Turkey Run Analytical Chemistry Conference, Marshall, IN, USA, 30/9/2011-1/10/2011.
21. http://ec.europa.eu/sanco_pesticides/public/index.cfm

ACKNOWLEDGMENTS

I would like to express my gratitude to all those people who helped me to complete this marvelous journey. First of all, I want to thank my first teacher, “mësuesin Hasan Gashi”, and all my successive teachers ...their extraordinary contribution in the education of the young generations to which a ferocious occupation denied the instruction right, will be remembered as the best lecture ever! To all of them my heartfelt gratitude.

I would like to thank my supervisor, Professor Giovanni Sindona. I was privileged to work with him and to receive his professional support as well as that of all his group members. I wish to express my appreciation also to Professor Nino Russo and all his team. All my colleagues, my Professors of Dipartimento di Chimica, are heartily acknowledged. I am deeply grateful to the “Università della Calabria” and to those people (Prof. F. Altimari, Prof. P. Brandmayr etc.), who worked hard to realize the project that brought me in Calabria.

I want to express my heartfelt gratitude to Professor Graham Cooks and all his wonderful team members for the hospitality and professional support during my visiting period at Purdue University.

I would like to thank cordially my “flatmates” (Francesco & Riccardo) and my “kalabro-kosovar band”: Alfred, Arben&Antigona&Aurora, Giovanna, Giuseppe, f.lli Oliva, Fito&Vera, Arsim, Rushit&Ardita, Musa, Bardh, Elbasan, Elvira, and particularly the new entry Kifi.

Special thanks go to a special person, Nadia, for her immense support.

Finally, I would like to thank the most important persons that made this dream possible: my parents, my sisters, my brothers and my little nieces (Diellza, Vetii, and Hana), as well as the rest of my family. This thesis is dedicated to them.